AMERICAN UNIVERSITY OF BEIRUT

Modeling and Control of a Hybrid Autonomous Underwater Vehicle

by
Abed AlRahman Milad Al Makdah

A thesis
submitted in partial fulfillment of the requirements
for the degree of Master of Engineering
to the Department of Mechanical Engineering
of the Faculty of Engineering and Architecture
at the American University of Beirut

Beirut, Lebanon
September 2016
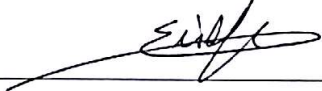
AMERICAN UNIVERSITY OF BEIRUT

Modeling and Control of a Hybrid Autonomous Underwater Vehicle

by
Abed AlRahman Milad Al Makdah

Approved by:

_____

Dr. Elie Shammas, Assistant Professor   Advisor

Mechanical Engineering

_____

Dr. Naseem Daher, Assistant Professor   Co-Advisor

Electrical and Computer Engineering

_____

Dr. Daniel Asmar, Associate Professor   Member of Committee

Mechanical Engineering

Date of thesis defense: September 16, 2016

AMERICAN UNIVERSITY OF BEIRUT

THESIS, DISSERTATION, PROJECT RELEASE FORM

Student Name: _AL MaKdah_____ _Abed AlRahman_____ _Milad_____
                  Last   First   Middle

☑ Master's Thesis   ◯ Master's Project   ◯ Doctoral Dissertation

☑   I authorize the American University of Beirut to: (a) reproduce hard or electronic copies of my thesis, dissertation, or project; (b) include such copies in the archives and digital repositories of the University; and (c) make freely available such copies to third parties for research or educational purposes.

☐   I authorize the American University of Beirut, **three years after the date of submitting my thesis, dissertation, or project,** to: (a) reproduce hard or electronic copies of it; (b) include such copies in the archives and digital repositories of the University; and (c) make freely available such copies to third parties for research or educational purposes.

_Abed AlRahman_____   _23-Sept-2016_____
Signature   Date

Acknowledgements

Through out this thesis, this was the most difficult part to write, as I was afraid of ruining this opportunity to thank all of those whom without their support this work would have been difficult to accomplish, if not impossible.

First and foremost, I would like to express my sincere gratitude to my advisor Dr. Elie Shammas for his continuous support and guidance through out my master study and research, for his immense knowledge, enthusiasm, and motivation. He was my greatest influence throughout my academic career at AUB. I am very proud and honored to be the student of such an intelligent, humble, and great person.

I owe my deepest gratitude to my co-advisor Dr. Naseem Daher whom without his encouragement, enthusiasm, support, and counseling this work would have hardly been accomplished. It was an honor for me to work with such a bright, humble, knowledgeable, and motivational person through out my master study and research.

I would like to thank my committee member Dr. Daniel Asmar for his generous support and feedback, and his insightful comments.

It is a pleasure to thank to my colleagues at the Vision and Robotics lab: Bilal Hamoud, Ali Harakeh, Salah Bazzi, Mohammad AlSalman, Bilal Wehbe, Mohammad Jawad Lakkis, Mahmoud Hamandi, Rahaf Rahal, and Sivag Babikian, for the stimulating discussions, for the sleepless nights we spent working together before deadlines, and for all the fun we had.

Also, I would like to thank Munib and Angela Masri Institute of Energy and Natural Resources, the University Research Board at the American University of Beirut, and the Lebanese National Council for Scientific Research for funding this project.

I am greatly indebted to my parents: Hala and Milad for supporting me at each step I am taking since the beginning, for being my light during my sleepless nights, and for being the support I lean on at each time I fall. Special and profound thanks to my brothers: Amer, Adnan, and AbdelHameed; and my little sister Rawaa who offered invaluable support and humor over the years.

An Abstract of the Thesis of

Abed ALRahman Milad Al Makdah   for   Master of Engineering
Major: Mechanical Engineering

Title: Modeling and Control of a Hybrid Autonomous Underwater Vehicle

In this work a six degrees of freedom (6DOF) dynamic model of a Hybrid Autonomous Underwater Vehicle (H-AUV) is developed. A new approach for designing a simplified control law is introduced to command the vehicle to track a given three-dimensional trajectory.

To get a linear time variant (LTV) state space model, the 6 DOF dynamics and kinematics models of the AUV are linearized about a given desired three-dimensional trajectory. A linear quadratic regulator (LQR) is designed based on the linearized model and is applied to the nonlinear model for validation purposes. The designed control law is robust enough to autonomously switch modes between propulsive and gliding dynamics to ensure minimal tracking error with respect to the desired trajectory.

Simulation results show that the linear control law provides satisfactory results when applied to the nonlinear model for tracking basic trajectory maneuvers: helix, saw-tooth trajectory, and 3D Dubin's trajectory. The robustness of the designed controller is investigated in the presence of underwater currents. Simulation shows that the controller is robust enough to command the vehicle to track the desired trajectory in the presence of underwater currents, in the case of thrust mode.

However, for the gliding mode, the designed controller gave unsatisfactory tracking performance in the presence of underwater currents. To mitigate this, a disturbance observer is designed based on the linearized model and is applied along with the designed control law which improved the tracking performance.

Contents

List of Figures

List of Tables

Chapter 1

Introduction

Rapid development in the field of marine robotics in the recent years provided scientists with advanced tools for ocean explorations. For marine robots to be able to roam the oceans freely and gather scientific information, the robots must be equipped with control systems that accurately navigate them to the desired destination. Therefore, considerable interest is concentrated on developing advanced control systems for underwater vehicles in the areas of trajectory tracking, path following, and point stabilization.

Trajectory tracking control allows the vehicle to track a certain parameterized curve with respect to time. Path following requires the vehicle to follow a desired path without any temporal constraints. Point stabilization control aims to steer the vehicle to a final desired target and a desired orientation.

The control design for an autonomous underwater vehicles (AUV) is very challenging because the dynamic model of marine vehicles is highly nonlinear and highly coupled, and the system is underactuated and nonholonomic.

In this work, a nonlinear six degrees of freedom dynamics model of a Hybrid Autonomous Underwater Vehicle (H-AUV), designed and manufactured at the American University of Beirut shown in Fig. 1.1, is derived. The H-AUV combines the features of a propelled vehicle and those of an underwater glider. Propelled AUV is a vehicle driven by a propeller that is attached to it. Examples of AUV's can be seen in [3], [4], [5], and [6]. Underwater glider is an AUV that is driven by controlling its buoyancy. The mass of the glider is changed by pumping water into or out of the vehicle and thus changing its buoyancy. When high speed and high maneuvering are required, the vehicle switches to the propeller mode, and when conserving energy and extending the battery life are required, the vehicle switches to the gliding mode. Examples of underwater gliders can be seen in [7], [8], [9], [10], and [11]. The aim of this work is to design a single controller, for both modes of operation, that commands the vehicle to track a trajectory in three dimensional
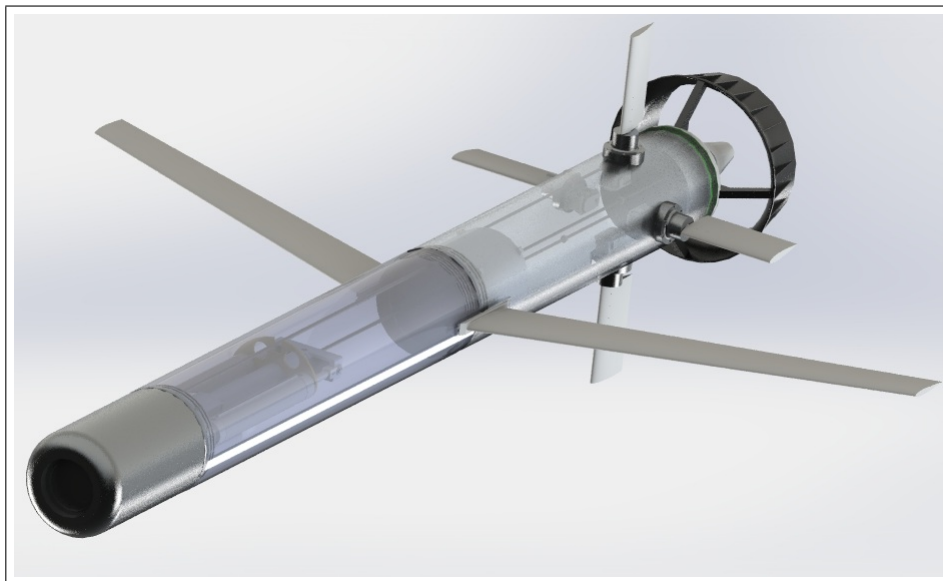
Figure 1.1: CAD model for the H-AUV

space parameterized with respect to time in the presence of disturbance. Also, the controller needs to decide when to use the propeller during gliding mode in the presence of disturbance. To simplify the control design problem, the model is linearized about a given optimal 3D Dubin's trajectory parameterized with respect to time, and a multi-input multi-output (MIMO) linear time variant (LTV) state space model is obtained. A linear quadratic regulator (LQR) is designed based on this linearized model and is applied to the nonlinear model to control the vehicle to track the given Dubin's trajectory.

One option to simplify the control design problem for the AUV, is to decouple the nonlinear 6DOF model into three independent and non-interacting subsystems: steering, diving, and speed control. Each subsystem can be linearized about constant operating points, as was done in [12], where a control law for each single-input multi-output (SIMO) subsystem was derived. However, these control laws give unsatisfactory results when applied to the highly coupled nonlinear model. Because decoupling the system assumes that the states related to the steering plane do not affect the states related to the diving plane, the control inputs will be conflicting. In this work, the 6DOF model is linearized about a given equilibrium 3D trajectory without decoupling. A single control law is derived taking into account the coupling between the states, and the conflict between the control inputs is avoided, while keeping the control design problem simplified.

The problem of trajectory tracking for underwater and air vehicles was introduced in [13], where the authors used gain scheduled controllers to control the vehicle to track the desired trajectory.

Another approach was based on the work in [14] where the authors solved the problem of path following for wheeled land robots using Lyapunov based nonlinear techniques and taking into account only the kinematics equations. This work was extended in [15] and [16] to deal with marine crafts, where a nonlinear controller was developed based only on the kinematic level, and backstepping techniques were used to extend the kinematic controller to include the dynamics of the system. The work in [14], [15], and [16] assumes that the position of the virtual vehicle to be tracked on the desired path is at the closest point present on the desired track to the vehicle. However, this assumption creates a shortcoming in the path following control strategy, that is the initial error of the position of the vehicle must be smaller than the smallest radius of curvature in the path. This shortcoming was solved for wheeled robots in [17], and this work was extended for the control of marine vehicles in [18], where the controller took into account only the kinematics. Later, the work in [18] was extended in [19] to include the dynamics in the controller. See also [20].

Trajectory tracking control for a car-trailer system was addressed in [21], in which the authors proposed a scheme consisting of three steps: generate a path off line, then use it to construct a trajectory by setting the velocity profile to the maximum, after that linearize the kinematic model of the car about the generated trajectory, and finally apply a time varying linear quadratic regulator to track the trajectory.

In [22] the authors linearized the dynamic model of an underwater glider about two sets of operating points, that correspond to the case where the vehicle is diving down and the case where the vehicle is floating up. Then a linear quadratic regulator is derived to control the depth of the vehicle, and to command it to move in a saw-tooth path.

In this work, the control design for the trajectory tacking problem is simplified, where the 6DOF dynamics model of the AUV is linearized about a given optimal 3D trajectory, and a LQR controller is designed based on the linearized model. Also, in this work the problem of the restriction of the initial position error of the vehicle with respect to the trajectory is avoided, because the optimal trajectory is generated given the initial and final position and orientation of the AUV using the work in [23] and [24]. The control law is designed to be robust enough to autonomously switch modes between propulsive and gliding dynamics to ensure

3

minimal tracking error with respect to the desired trajectory. The robustness of the designed controller is investigated in the presence of underwater currents

The organization of this document will be as follows. In chapter 2 the 6DOF dynamic model of the AUV is derived. In chapter 3, a LTV state space model is obtained by linearizing the 6DOF model about a given desired trajectory, and a LQR is derived based on the LTV model and is applied to the nonlinear model. In chapter 4, an open loop simulation of the nonlinear model is presented. And the LTV model is then simulated and its response is compared with the response of the nonlinear model. The performance of the LQR when applied to the nonlinear model is analyzed in simulation, and its robustness is investigated in the presence of unknown disturbance also in chapter 4. In chapter 5, a disturbance observer is designed based on the LTV model and is applied along with the controller to the nonlinear model, and its performance is investigated in simulation. Finally, the document is concluded in chapter 6 and future research is discussed.

Chapter 2

AUV Model

In this chapter a model for the AUV is developed from the six degrees of freedom equations of motion, and the inertial frames are defined.

2.1 Kinematics

2.1.1 Inertial frames

Two frames of reference are defined: the earth-fixed frame of reference {U} and the body-fixed frame of reference {B}. The earth-fixed frame of reference (O_U, x, y, z) has a fixed origin at an arbitrary point at the surface of the ocean with the z-axis pointing downwards. This frame of reference is used to describe the orientation of the vehicle and the position of its center of mass The body-fixed frame (O_B, X_B, Y_B, Z_B) is attached to the vehicle's geometric center (which is the same as the center of buoyancy) with the x-axis pointing towards the nose of the vehicle. This reference frame is used to describe the vehicles's linear and angular velocities. The SNAME (1950) notation is used to describe the general motion of the vehicle in the six degrees of freedom as follows:

$$\eta = [\eta_1^T, \eta_2^T]^T \qquad \eta_1 = [x, y, z]^T \qquad \eta_2 = [\phi, \theta, \psi]^T$$
$$\tag{2.1}$$
$$\nu = [\nu_1^T, \nu_2^T]^T \qquad \nu_1 = [u, v, w]^T \qquad \nu_2 = [p, q, r]^T$$

where η denotes the position of the center of mass of the vehicle and its orientation vector with respect to the earth-fixed coordinate reference, ν denotes the linear and angular velocity vector of the vehicle with respect to the body-fixed coordinate reference. The frames of reference are shown in Fig. 2.1
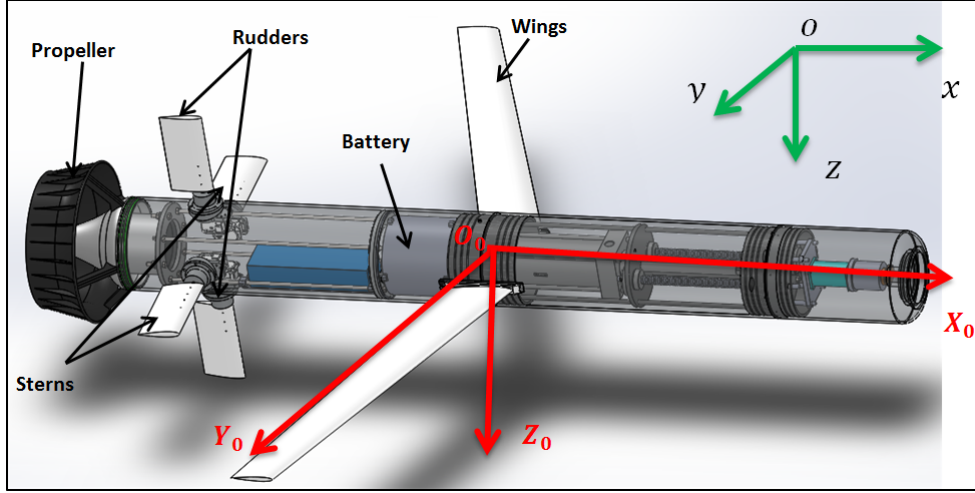
Figure 2.1: AUV with local and global frames of reference

2.1.2   Transformation Between the Two Frames of Reference

The transformation of the velocities between the body-fixed frame and the earth-fixed frame is performed by the given velocity transformation:

$$\dot{\eta} = J(\eta_2)\nu \tag{2.2}$$

where J(η) is the transformation matrix that is a function of the Euler angles: roll(ϕ), pitch(θ), and yaw(ψ).

The inverse transformation velocity can be written as follows:

$$\nu = J^{-1}(\eta_2)\dot{\eta} \tag{2.3}$$

The transformation matrix J can be written as follows:

$$J = \begin{bmatrix} J_1 & 0_{3x3} \\ 0_{3x3} & J_2 \end{bmatrix} \tag{2.4}$$

where J_1 is the linear velocity transformation matrix, and J_2 is the angular velocity transformation matrix.

Linear Velocity Transformation:

$$\dot{\eta}_1 = J_1(\eta_2)\nu_1 \tag{2.5}$$

The linear velocity transformation matrix as a function of the Euler angle (ϕ,θ,ψ) is as follows:

6

$$J_1 = \begin{bmatrix} c\psi c\theta & -s\psi c\phi + c\psi s\theta s\phi & s\psi s\phi + c\psi c\phi s\theta \\ s\psi c\theta & c\psi c\phi + s\phi s\theta s\psi & -c\psi s\phi + s\theta s\psi c\phi \\ -s\theta & c\theta s\phi & c\theta c\phi \end{bmatrix} \qquad (2.6)$$

where s, c, and t denote sin, cos, and tan respectively.

Angular Velocity Transformation:

$$\dot{\eta}_2 = J_2(\eta_2)\nu_2 \qquad (2.7)$$

The angular velocity transformation matrix as a function of the Euler angle (ϕ,θ,ψ) is as follows:

$$J_2 = \begin{bmatrix} 1 & s\phi t\theta & c\phi t\theta \\ 0 & c\phi & -s\phi \\ 0 & s\phi/c\theta & c\phi/c\theta \end{bmatrix} \qquad (2.8)$$

2.2   Vehicle Parameters and Specifications

The vehicle is equipped with a propeller, two wings, and four identical control fins placed at the rear.

2.2.1   Propeller and hull

The propeller, which is a high torque brushed DC motor, is attached at the rear of the vehicle with a maximum thrust of about 272 N. The hull of the vehicle is a cylinder made of aluminum 6061-T6 with a diameter of 8 inches (203.2 mm) and 2 meters long. The hull parameters are shown in table 2.1.

2.2.2   Wings

The two wings are fixed at the middle of the vehicle with a zero degrees angle of attack, and a span of 0.821 meters for each wing. The parameters of the wings are shown in table 2.2.

Table 2.1: Hull Parameters

Parameter	Value	Unit	Description
ρ	1025	Kg/m^3	Sea water density
r	0.1	m	outer radius of the hull cylinder
L	2	m	Length of the hull cylinder
A_f	0.061	m^2	Hull frontal area
A_p	0.4	m^2	Hull projected area (xz plane)
∇	0.0707	m^3	Estimated hull volume

Table 2.2: Wing Parameters

Parameter	Value	Unit	Description
b_{wing}	0.821	m	Span
a_{wing}	0.921	m	Max wing height above centerline
$x_{wing,rear}$	-0.075	m	x- position of the rear end of the wing with respect to the body-fixed frame
$x_{wing,front}$	0.075	m	x- position of the rear end of the wing with respect to the body-fixed frame
S_{wing}	0.1275	m^2	wing planform area

2.2.3 Fins

The four control fins are mounted in a cruciform pattern at the rear of the vehicle, two vertical fins, the rudders are used to control the yaw angle of the vehicle, and two horizontal fins, the sterns are used to control the pitch angle of the vehicle. Each fin has a span of 0.257 m and NACA 0015 cross-section. The parameters of the fins are shown in table 2.3.

Table 2.3: Fin Parameters

Parameter	Value	Unit	Description
b_{fin}	0.257	m	Span
a_{fin}	0.357	m	Max fin height above centerline
$x_{fin,rear}$	-0.76	m	x- position of the rear end of the fin with respect to the body-fixed frame
$x_{fin,front}$	-0.66	m	x- position of the front end of the fin with respect to the body-fixed frame
S_{fin}	0.0257	m^2	fin planform area

Table 2.4: Center of mass with respect to the body-fixed frame

Parameter	Value	Unit
x_G	-0.02$<x_G<$0.02	m
y_G	0	m
z_G	0.05	m

2.2.4   Vehicle Weight and Buoyancy

The dry mass of the vehicle is 71.5 Kg when it is empty of water, and 73.5 Kg when it is full. The vehicle is positively buoyant when empty, negatively buoyant when full, and neutrally buoyant when half full.

The y and z components of the center of mass of the vehicle remains fixed with respect to the body-fixed frame reference, however the x component changes as the vehicle pumps water in or out. The x-component of the center of mass is zero when the vehicle is neutrally buoyant, negative (towards the rear of the vehicle) when the vehicle is positively buoyant, and positive (towards the front of the vehicle) when the vehicle is negatively buoyant. Table 4.7b shows the position of the center of mass with respect to the origin of the body-fixed frame.

2.3   Rigid Body Dynamics

In this section, Newton's second law is applied to generate the equations of motion.

Center of gravity: The location of the center of gravity with respect to the origin of the body fixed coordinate system is as follows:

$$r_G = \begin{bmatrix} x_G \\ y_G \\ z_G \end{bmatrix} \tag{2.9}$$

The location of the center of buoyancy is at the origin of the body-fixed coordinate system.

Following the SNAME (1952) nomenclature [25], the 6DOF equations of motion,

9

as derived in [26] can be written as follows:

$$m[\dot{u} - vr + wq - x_G(q^2 + r^2) + y_G(pq - \dot{r}) + z_G(pr + \dot{q})] = \quad X$$
$$m[\dot{v} - wp + ur - y_G(r^2 + p^2) + z_G(qr - \dot{p}) + x_G(qp + \dot{r})] = \quad Y$$
$$m[\dot{w} - uq + vp - z_G(p^2 + q^2) + x_G(rp - \dot{q}) + y_G(rq + \dot{p})] = \quad Z$$
$$I_x\dot{p} + (I_z - I_y)qr - (\dot{r} + pq)I_{xz} + (r^2 - q^2)I_{yz} + (pr - \dot{q})I_{xy}$$
$$+ m[y_G(\dot{w} - uq + vp) - z_G(\dot{v} - wp + ur)] = \quad K \quad (2.10)$$
$$I_y\dot{q} + (I_x - I_z)rp - (\dot{p} + qr)I_{xy} + (p^2 - r^2)I_{zx} + (qp - \dot{r})I_{yz}$$
$$+ m[z_G(\dot{u} - vr + wq) - x_G(\dot{w} - uq + vp)] = \quad M$$
$$I_z\dot{r} + (I_y - I_x)pq - (\dot{q} + rp)I_{yz} + (q^2 - p^2)I_{xy} + (rq - \dot{p})I_{zx}$$
$$+ m[x_G(\dot{v} - wp + ur) - y_G(\dot{u} - vr + wq)] = \quad N$$

where X, Y and Z are the external forces acting on the vehicle; and K, M and N are the external moments acting on the vehicle; these forces and moments are described with respect to the body-fixed frame; m is the dry mass of the vehicle; I_x, I_y & I_z are the vehicle's moments of inertia about the X_0, Y_0 and Z_0-axes and $I_{xy}=I_{yx}$, $I_{xz}=I_{zx}$, and $I_{yz}=I_{zy}$ are products of inertia defined as:

$$I_x = \int_V (y^2 + z^2)\rho dV; \qquad I_{xy} = \int_V xy\rho dV = \int_V yx\rho dV = I_{yx}$$
$$I_y = \int_V (x^2 + z^2)\rho dV; \qquad I_{xz} = \int_V xz\rho dV = \int_V zx\rho dV = I_{zx} \quad (2.11)$$
$$I_z = \int_V (x^2 + y^2)\rho dV; \qquad I_{yz} = \int_V yz\rho dV = \int_V zy\rho dV = I_{zy}$$

The first three equations in (2.10) describe the translational motion of the vehicle, and the second three equations describe the rotational motion of the vehicle. Note that the terms corresponding to the position of the center of buoyancy with respect to the body-fixed frame are neglected and are set to zero, because it coincides with the origin of the body-fixed frame.

The vehicle's inertia tensor, I_0, with respect to the body-fixed frame can be written as follows:

$$I_0 = \begin{bmatrix} I_x & -I_{xy} & -I_{xz} \\ -I_{yx} & I_y & -I_{yz} \\ -I_{zx} & -I_{zy} & I_z \end{bmatrix} \quad (2.12)$$

Because the origin of the body-fixed frame is placed at the center of buoyancy of the vehicle, and since the vehicle is symmetric with respect to the xy and the xz

Table 2.5: Vehicle's moment of inertia about X_0, Y_0 and Z_0-axes

Parameter	Value	Unit
I_x	1.08	$Kg.m^2$
I_y	20.75	$Kg.m^2$
I_z	21.32	$Kg.m^2$

planes of the body fixed coordinate system, the values of the products of inertia are very small compared to values of I_x, I_y, and I_z, and thus can be neglected. So, the vehicle's inertia's tensor, I_0, with respect to the body-fixed reference can be reduced as follows:

$$I_0 = \begin{bmatrix} I_x & 0 & 0 \\ 0 & I_y & 0 \\ 0 & 0 & I_z \end{bmatrix} \tag{2.13}$$

The values of the moments of inertia about the axes of the body-fixed frame are shown in table 2.5.

This simplifies the equations of motion in (2.10):

$$
\begin{aligned}
m[\dot{u} - vr + wq - x_G(q^2 + r^2) + y_G(pq - \dot{r}) + z_G(pr + \dot{q})] &= & X \\
m[\dot{v} - wp + ur - y_G(r^2 + p^2) + z_G(qr - \dot{p}) + x_G(qp + \dot{r})] &= & Y \\
m[\dot{w} - uq + vp - z_G(p^2 + q^2) + x_G(rp - \dot{q}) + y_G(rq + \dot{p})] &= & Z \\
I_x\dot{p} + (I_z - I_y)qr + m[y_G(\dot{w} - uq + vp) - z_G(\dot{v} - wp + ur)] &= & K \\
I_y\dot{q} + (I_x - I_z)rp + m[z_G(\dot{u} - vr + wq) - x_G(\dot{w} - uq + vp)] &= & M \\
I_z\dot{r} + (I_y - I_x)pq + m[x_G(\dot{v} - wp + ur) - y_G(\dot{u} - vr + wq)] &= & N
\end{aligned}
\tag{2.14}
$$

Vectorial Representation: Equation (2.14) can be expressed in a vectorial form, which is more compact, as:

$$M_{RB}\dot{\nu} + C_{RB}(\nu)\nu = \tau_{RB} + \delta d \tag{2.15}$$

where $\nu = [u, v, w, p, q, r]^T$ is the linear and angular velocity vector in the body fixed frame as defined in (2.1), and $\tau_{RB} = [X, Y, Z, K, M, N]^T$ is a vector containing the external forces and moments in the X_0, Y_0 and Z_0 directions of the body-fixed frame. M_{RB} is the rigid-body inertia matrix, and C_{RB} is the matrix containing the Coriolis vector term and the centripetal vector term. And $\delta d = [\delta d_x, \delta d_x, \delta d_y, \delta d_z, \delta d_k, \delta d_m, \delta d_n]^T$ is a vector of length 6 which contains unknown disturbance forces and moments expressed with respect to the body fixed frame.

The rigid-body inertia matrix can be written as follows:

$$
M_{RB} = \begin{bmatrix}
m & 0 & 0 & 0 & mz_G & -my_G \\
0 & m & 0 & -mz_G & 0 & mx_G \\
0 & 0 & m & my_G & -mx_G & 0 \\
0 & -mz_G & my_G & I_x & 0 & 0 \\
mz_G & 0 & -mx_G & 0 & I_y & 0 \\
-my_G & mx_G & 0 & 0 & 0 & I_z
\end{bmatrix}
\tag{2.16}
$$

The matrix containing the Coriolis and the centripetal terms can be written as follows:

$$
C_{RB} = \begin{bmatrix}
0 & 0 & 0 & m(y_Gq + z_Gr) & -m(x_Gq - w) & -m(x_Gr + v) \\
0 & 0 & 0 & -m(y_Gp + w) & m(z_Gr + x_Gp) & -m(y_Gr - u) \\
0 & 0 & 0 & -m(z_Gp - v) & -m(z_Gq + u) & m(x_Gp + y_Gq) \\
-m(y_Gq + z_Gr) & m(y_Gp + w) & m(z_Gp - v) & 0 & I_zr & -I_yq \\
m(x_Gq - w) & -m(z_Gr + x_Gp) & m(z_Gq + u) & -I_zr & 0 & I_xp \\
m(x_Gr + v) & m(y_Gr - u) & -m(x_Gp + y_Gq) & I_yq & -I_xp & 0
\end{bmatrix}
\tag{2.17}
$$

2.4 External Forces and Moments

In this section, the external forces and moments acting on the vehicle, which are the components on the RHS of the equations of motion in (2.14), with respect to the body-fixed frame are introduced. The total external forces and moments acting on the vehicle have the following components:

$$
\tau_{ext} = \tau_{hydrostatic} + \tau_{addedmass} + \tau_{drag} + \tau_{lift} + \tau_{propeller}
\tag{2.18}
$$

where $\tau_{hydrostatic}$ is the hydrostatic forces and moments, $\tau_{addedmass}$ is the term corresponding to the forces and moments generated by the added mass, τ_{drag} are the drag forces and moments due to skin friction, τ_{lift} are the lift forces and moments, and $\tau_{propeller}$ are the thrust force and moment generated by the propeller.

2.4.1 Hydrostatic Forces and Moments

The hydrostatic forces and moments are the combined effects of the vehicle's weight and buoyancy forces. Let m be the mass of the vehicle, ∇ be the volume of the vehicle, ρ be the density of the sea water, and g be the gravitational acceleration, then the weight of the vehicle can be expressed as $W = m.g$, and the buoyancy force is expressed as $B = \rho\nabla g$. It is desired to express these forces with respect to the body-fixed frame. This can be done using the linear matrix

transformation J_1 from (2.6) as follows:

$$f_W(\eta_2) = J_1^{-1} \begin{bmatrix} 0 \\ 0 \\ W \end{bmatrix} \qquad f_B(\eta_2) = J_1^{-1} \begin{bmatrix} 0 \\ 0 \\ B \end{bmatrix} \tag{2.19}$$

So the hydrostatic forces and moments acting on the vehicle can be expressed with respect to the body-fixed frame as follows:

$$\begin{aligned} F_{hydrostatic} &= f_W - f_B \\ M_{hyrostatics} &= r_G \times f_W - r_B \times f_B \end{aligned} \tag{2.20}$$

where r_G and r_B are the position vectors of the center of mass and the center of buoyancy of the vehicle, respectively, with respect to the body fixed frame. Equation (2.20) can be expanded to yield the following equations in the X_0, Y_0, and Z_0 directions of the body-fixed frame:

$$\begin{aligned} X_{hydrostatic} &= -(W - B)sin\theta \\ Y_{hydrostatic} &= (W - B)cos\theta sin\phi \\ Z_{hydrostatic} &= (W - B)cos\theta cos\phi \\ K_{hydrostatic} &= (y_G W - y_B B)cos\theta cos\phi - (Z_G W - z_B B)cos\theta sin\phi \\ M_{hydrostatic} &= -(x_G W - x_B B)cos\theta cos\phi - (z_G W - z_B B)sin\theta \\ N_{hydrostatic} &= (x_G W - x_B B)sin\phi cos\theta + (y_G W - y_B B)sin\theta \end{aligned} \tag{2.21}$$

Since the origin of the body fixed frame is chosen to be at the center of buoyancy of the vehicle, $r_B = [0, 0, 0]^T$. So the hydrostatic forces and moments in (2.21) can be simplified as follows:

$$\begin{aligned} X_{hydrostatic} &= -(W - B)sin\theta \\ Y_{hydrostatic} &= (W - B)cos\theta sin\phi \\ Z_{hydrostatic} &= (W - B)cos\theta cos\phi \\ K_{hydrostatic} &= y_G W cos\theta cos\phi - Z_G W cos\theta sin\phi \\ M_{hydrostatic} &= -x_G W cos\theta cos\phi - z_G W sin\theta \\ N_{hydrostatic} &= x_G W cos\phi + y_G W sin\theta \end{aligned} \tag{2.22}$$

2.4.2 Added Mass

Added mass, as defined in [26], is a force generated due to inertia added to a body as it moves through a certain fluid. As a submerged body accelerates or decelerates through a certain fluid, it moves some of the surrounding fluids. For simplicity, it can be modeled as a mass of the fluid move with the body.

13

The added mass forces and moments are separated to an added inertia matrix, M_A, and a matrix of hydrodynamic Coriolis and centripetal terms denoted C_A.

$$\tau_{addedmass} = -M_A\dot{\nu} - C_A(\nu)\nu \tag{2.23}$$

To derive the two matrices, the concept of fluid kinetic energy along with Kirchoff's equation, which relates the fluid kinetic energy to the forces and moments acting on the vehicle, are used as explained in [26]. The fluid kinetic energy can be expressed in the following matrix form as a quadratic form of the vehicle axis velocity vector components:

$$T_A = \frac{1}{2}\nu^T M_A \nu \tag{2.24}$$

where M_A is a 6x6 added inertia matrix defined as:

$$M_A = \begin{bmatrix} X_{\dot{u}} & X_{\dot{v}} & X_{\dot{w}} & X_{\dot{p}} & X_{\dot{q}} & X_{\dot{r}} \\ Y_{\dot{u}} & Y_{\dot{v}} & Y_{\dot{w}} & Y_{\dot{p}} & Y_{\dot{q}} & Y_{\dot{r}} \\ Z_{\dot{u}} & Z_{\dot{v}} & Z_{\dot{w}} & Z_{\dot{p}} & Z_{\dot{q}} & Z_{\dot{r}} \\ K_{\dot{u}} & K_{\dot{v}} & K_{\dot{w}} & K_{\dot{p}} & K_{\dot{q}} & K_{\dot{r}} \\ M_{\dot{u}} & M_{\dot{v}} & M_{\dot{w}} & M_{\dot{p}} & M_{\dot{q}} & M_{\dot{r}} \\ N_{\dot{u}} & N_{\dot{v}} & N_{\dot{w}} & N_{\dot{p}} & N_{\dot{q}} & N_{\dot{r}} \end{bmatrix} \tag{2.25}$$

The SNAME (1952) notation [25] is used to describe the added mass forces and moments. For example, the hydrodynamic added mass force in the Y_B direction of the body fixed frame {B} due to the acceleration $\dot{u}$ in the X_B direction of the body fixed frame {B} is expressed as follows:

$$Y_{addedmass} = Y_{\dot{u}}\dot{u} \qquad \textbf{where} \qquad Y_{\dot{u}} = \frac{\delta Y}{\delta \dot{u}} \tag{2.26}$$

Since most of the time the vehicle will be completely submerged under water, it is assumed that the mass coefficients are constant. Also, from the fluid energy equation in (2.24), it is seen that the matrix added inertia matrix M_A is positive definite. In addition, experience has shown that assuming M_A to be a symmetric matrix is a good approximation, see [26]. Hence:

$$M_A = M_A^T > 0 \tag{2.27}$$

M_A can be further simplified because the vehicle is symmetric with respect to the $X_B Y_B$ and the $X_B Z_B$ planes. Hence the simplified added mass inertia can be written as follows:

$$M_A = \begin{bmatrix} X_{\dot{u}} & 0 & 0 & 0 & 0 & 0 \\ 0 & Y_{\dot{v}} & 0 & 0 & 0 & Y_{\dot{r}} \\ 0 & 0 & Z_{\dot{w}} & 0 & Z_{\dot{q}} & 0 \\ 0 & 0 & 0 & K_{\dot{p}} & 0 & 0 \\ 0 & 0 & Z_{\dot{q}} & 0 & M_{\dot{q}} & 0 \\ 0 & Y_{\dot{r}} & 0 & 0 & 0 & N_{\dot{r}} \end{bmatrix} \tag{2.28}$$

Consider the Kirchhoff's equations in vector form for translational and rotational motion:

$$\frac{d}{dt}(\frac{\delta T}{\delta \nu_1}) + \nu_2 \times \frac{\delta T}{\delta \nu_1} = \tau_1$$
$$\frac{d}{dt}(\frac{\delta T}{\delta \nu_2}) + \nu_2 \times \frac{\delta T}{\delta \nu_2} + \nu_1 \times \frac{\delta T}{\delta \nu_1} = \tau_2 \tag{2.29}$$

where T is the kinetic energy, the equations in (2.29) are applied on the fluid kinetic energy equation in (2.24) to get the added mass forces and moments. For more details on the derivation of the added mass forces and moments, review [26].

$$X_{added\ mass} = X_{\dot{u}}\dot{u} + Z_{\dot{w}}wq + Z_{\dot{q}}q^2 - Y_{\dot{v}}vr - Y_{\dot{r}}r^2$$
$$Y_{added\ mass} = Y_{\dot{v}}\dot{v} + Y_{\dot{r}}\dot{r} + X_{\dot{u}}ur - Z_{\dot{w}}wp - Z_{\dot{q}}pq$$
$$Z_{added\ mass} = Z_{\dot{w}}\dot{w} + Z_{\dot{q}}\dot{q} - X_{\dot{u}}uq + Y_{\dot{v}}vp + Y_{\dot{r}}rp$$
$$K_{added\ mass} = K_{\dot{p}}\dot{p} - (Y_{\dot{v}} - Z_{\dot{w}})vw - (Y_{\dot{r}} + Z_{\dot{q}})wr + (Y_{\dot{r}} + Z_{\dot{q}})vq - (M_{\dot{q}} - N_{\dot{r}})qr$$
$$M_{added\ mass} = M_{\dot{q}}\dot{q} + Z_{\dot{q}}\dot{w} - (Z_{\dot{w}} - X_{\dot{u}})wu - Y_{\dot{r}}vp + (K_{\dot{p}} - N_{\dot{r}})rp$$
$$N_{added\ mass} = N_{\dot{r}}\dot{r} + Y_{\dot{r}}\dot{v} - (X_{\dot{u}} - Y_{\dot{v}})uv + Y_{\dot{r}}ur + Z_{\dot{q}}wp - (K_{\dot{p}} - M_{\dot{q}})pq \tag{2.30}$$

The hydrodynamic matrix containing the Coriolis and centripital terms can be written as follows. For more details about the derivation of the matrix, review [26].

$$C_A = \begin{bmatrix} 0 & 0 & 0 & 0 & -a_3 & a_2 \\ 0 & 0 & 0 & a_3 & 0 & -a_1 \\ 0 & 0 & 0 & -a_2 & a_1 & 0 \\ 0 & -a_3 & a_2 & 0 & -b_3 & b_2 \\ a_3 & 0 & -a_1 & b_3 & 0 & -b_1 \\ -a_2 & a_1 & 0 & -b_2 & b_1 & 0 \end{bmatrix} \tag{2.31}$$

where:

$$a_1 = X_{\dot{u}}u$$
$$a_2 = Y_{\dot{v}}v + Y_{\dot{r}}r$$
$$a_3 = Z_{\dot{w}}w + Z_{\dot{q}}q$$
$$b_1 = K_{\dot{p}}p$$
$$b_2 = M_{\dot{q}}q$$
$$b_3 = Y_{\dot{r}}v + N_{\dot{r}}r \tag{2.32}$$

2.4.3 Drag Forces and Moments

The drag forces are mainly due skin friction between the fluid and the vehicle as it moves through. The drag forces and moments can be written in a vectorial

form as follows:

$$\tau_{drag} = D(\nu)\nu \tag{2.33}$$

where $D(\nu)$ is a 6×6 matrix containing the drag coefficients and it can be written as follows:

$$D(\nu) = \begin{bmatrix} X_{u|u|} & X_{v|v|} & X_{w|w|} & X_{p|p|} & X_{q|q|} & X_{r|r|} \\ Y_{u|u|} & Y_{v|v|} & Y_{w|w|} & Y_{p|p|} & Y_{q|q|} & Y_{r|r|} \\ Z_{u|u|} & Z_{v|v|} & Z_{w|w|} & Z_{p|p|} & Z_{q|q|} & Z_{r|r|} \\ K_{u|u|} & K_{v|v|} & K_{w|w|} & K_{p|p|} & K_{q|q|} & K_{r|r|} \\ M_{u|u|} & M_{v|v|} & M_{w|w|} & M_{p|p|} & M_{q|q|} & M_{r|r|} \\ N_{u|u|} & N_{v|v|} & N_{w|w|} & N_{p|p|} & N_{q|q|} & N_{r|r|} \end{bmatrix} \tag{2.34}$$

Since the vehicle is symmetric with respect to the X_0Y_0 and the X_0Z_0 planes of the body-fixed frames, the damping matrix can be simplified as follows:

$$D(\nu) = \begin{bmatrix} X_{u|u|}|u| & 0 & 0 & 0 & 0 & 0 \\ 0 & Y_{v|v|}|v| & 0 & 0 & 0 & Y_{r|r|}|r| \\ 0 & 0 & Z_{w|w|}|w| & 0 & Z_{q|q|}|q| & 0 \\ 0 & 0 & 0 & K_{p|p|}|p| & 0 & 0 \\ 0 & 0 & M_{w|w|}|w| & 0 & M_{q|q|}|q| & 0 \\ 0 & N_{v|v|}|v| & 0 & 0 & 0 & N_{r|r|}|r| \end{bmatrix} \tag{2.35}$$

Note that the damping matrix is not symmetric as the added mass inertia matrix. The drag forces and moments acting on the vehicle in the X_0, Y_0, and Z_0 directions are expressed as follows:

$$\begin{aligned} X_{drag} &= X_{u|u|}u|u| \\ Y_{drag} &= Y_{v|v|}v|v| + Y_{r|r|}r|r| \\ Z_{drag} &= Z_{w|w|}w|w| + Z_{q|q|}q|q| \\ K_{drag} &= K_{p|p|}p|p| \\ M_{drag} &= M_{q|q|}q|q| + M_{w|w|}w|w| \\ N_{drag} &= N_{r|r|}r|r| + N_{v|v|}v|v| \end{aligned} \tag{2.36}$$

2.4.4   Lift Forces and Moments

The lift forces and moments acting on the vehicle are the sum of the body lift forces and moments and the fins and wings forces and moments.

$$\tau_{lift} = \tau_{lift,\ body} + \tau_{lift,\ fins\ \&\ wings} \tag{2.37}$$

16

Body lift forces and moments

The body lift forces and moments are the result of the vehicle moving at a certain angle of attack through the fluid, which will cause a flow separation and hence a pressure difference between the upper part and the lower part of the vehicle. This pressure difference creates a lift force that act on the center of mass and lift moments.

Body lift Forces

The body lift forces are calculated using the following empirical formula provided in [27]:

$$L_{body} = -\frac{1}{2}\rho A_p c_{yd} u^2 \tag{2.38}$$

where ρ is the water density, A_p is the hull's projected area on the $X_B Y_B$ and the $X_B Z_B$ planes of the body fixed frame, and c_{yd} is the body lift coefficient, which Hoerner [27] expresses as follows:

$$c_{yd} = \frac{dc_{yd}}{d\beta}\beta \tag{2.39}$$

where β is the hull's angle of attack in radians expressed as follows:

$$tan\beta = \frac{w}{u} \implies \beta \approx \frac{w}{u} \tag{2.40}$$

The derivative term $\frac{dc_{yd}}{d\beta}$ in (2.39) can be calculated using the following relation ship provided by Hoerner [27]:

$$\frac{dc_{yd}^o}{d\beta^o} = c_{yd\beta}^o = (\frac{l}{d})c_{y\beta}^o \tag{2.41}$$

where l is the vehicle's length, and d is its outer diameter. Also, Hoerner stated in [27] that:

$$for \quad 6.7 \leq \frac{l}{d} \leq 10, \quad c_{y\beta}^o = 0.003 \tag{2.42}$$

The body lift slope $\frac{dc_{yd}^o}{d\beta^o}$ calculated in (2.41) is in degrees and is converted to radians as follows:

$$c_{yd\beta} = c_{yd\beta}^o(\frac{180}{\pi}) \tag{2.43}$$

17

After substituting $c_{yd\beta}$ from (2.43) and β from (2.40) into (2.38) the following body lift forces are obtained:

$$Y_{lift,body} = -\frac{1}{2}\rho A_p c_{yd\beta} uv$$
$$Z_{lift,body} = -\frac{1}{2}\rho A_p c_{yd\beta} uw \qquad (2.44)$$

The equations in (2.44) can be written as follows:

$$Y_{lift,body} = Y_{uvl} uv$$
$$Z_{lift,body} = Z_{uwl} uw \qquad (2.45)$$

where Y_{uvl} and Z_{uwl} are the body lift coefficients:

$$Y_{uvl} = Z_{uwl} = -\frac{1}{2}\rho A_p c_{yd\beta} \qquad (2.46)$$

Body lift Moments

According to Hoerner [27], the body lift force acts on a point between 0.7 and 0.6 of the length of the body measured from its nose, so the moment arm can be calcultaed as follows:

$$x_{cp} = -0.65l - x_{zero} \qquad (2.47)$$

where x_{zero} is the position of the origin of the body-fixed frame with respect to the nose of the vehicle. Hence, the body lift moments can be written as follows:

$$M_{lift,body} = -\frac{1}{2}\rho A_p c_{yd\beta} x_{cp} uw$$
$$N_{lift,body} = \frac{1}{2}\rho A_p c_{yd\beta} x_{cp} uv \qquad (2.48)$$

The equations in (2.48) can be written as follows:

$$M_{lift,body} = M_{uwl} uw$$
$$N_{lift,body} = N_{uvl} uv \qquad (2.49)$$

where M_{uwl} and N_{uvl} are the body lift moments coefficients:

$$M_{uwl} = -N_{uvl} = -\frac{1}{2}\rho A_p c_{yd\beta} x_{cp} \qquad (2.50)$$

Fins and wings lift forces and moments

The vehicle's yaw and pitch can be controlled by changing the angle of vertical and the horizontal fins respectively. The wings are fixed and have zero angle of attack. During the gliding mode when the vehicle's density is less or greater than that of water, the wings allow the vehicle to glide forward while it is ascending or descending. In gliding mode, without the wings, the vehicle would move upward or downward in a vertical direction only and it will not glide forward.

Fins lift forces and moments

The empirical formula of the fin lift forces and moments as suggested in [28] can be written as follows:

$$L_{fin} = \frac{1}{2}\rho c_L S_{fin}\delta_e v_e^2$$
$$M_{fin} = x_{fin}L_{fin}$$

(2.51)

where c_L is the fin lift coefficient, δ_e is the fin effective angle in radians, v_e is the effective fin velocity, and x_{fin} is the axial position of the fin post with respect to the body-fixed frame.

The fin lift forces and moments as derived in [28] can be written as follows:

$$Y_{lift,fins} = \rho c_{L\alpha}S_{fin}[u^2\delta r - uv - x_{fin}(ur)]$$
$$Z_{lift,fins} = -\rho c_{L\alpha}S_{fin}[u^2\delta s + uw - x_{fin}(uq)]$$
$$M_{lift,fins} = \rho c_{L\alpha}S_{fin}x_{fin}[u^2\delta s + uw - x_{fin}(uq)]$$
$$N_{lift,fins} = \rho c_{L\alpha}S_{fin}x_{fin}[u^2\delta r - uv - x_{fin}(ur)]$$

(2.52)

where δr and δs are the rudder and stern angles of the fins, and $c_{L\alpha}$ is the fin lift coefficient. An empirical formula that expresses the fin lift coefficient as a function of the angle of attack α is given by:

$$c_{L\alpha} = \frac{dc_L}{d_\alpha} = [\frac{1}{2\bar{\alpha}\pi} + \frac{1}{\pi(AR_e)}]^{-1}$$

(2.53)

where $\bar{\alpha}$ is estimated by Hoerner [27] to be 0.9, and AR_e is the effective fin aspect ratio and that can be calculated as follows:

$$AR_e = 2(AR) = 2(\frac{b_f in^2}{S_f in})$$

(2.54)

where $b_f in$ is the span of the fin.

19

2.4.5   Propeller Forces and Moments

The thrust force generated by the propeller is assumed to be constant in the positive X_B direction of the body fixed frame. Also, the propeller is assumed to generate a constant moment in the roll (X_B) direction of the body-fixed frame.

2.4.6   Disturbance Forces and Moments

The robustness of the linear controller to be designed in the later chapter is investigated under the presence of an unknown disturbance, which is mainly caused by underwater current. In order to investigate the effect of disturbance on the performance of the controller, the unknown underwater current is modeled as an unknown force field that acts on the center of mass of the vehicle. This force field is expressed with respect to the global frame as follows:

$$\delta D = \begin{bmatrix} \delta D_x \\ \delta D_y \\ \delta D_z \end{bmatrix}, \tag{2.55}$$

where δD_x, δD_y, and δD_z are disturbance forces along the x, y, and z axes of the global frame, respectively. To include these forces in the 6DOF nonlinear model in (2.15), they should be expressed with respect to the body-fixed frame. This can be done using the linear matrix transformation $J1$ from (2.6) as follows:

$$f_{\delta D}(\eta_2) = J_1^{-1}.\delta D = J_1^{-1}. \begin{bmatrix} \delta D_x \\ \delta D_y \\ \delta D_z \end{bmatrix}, \tag{2.56}$$

The disturbance forces and moments acting on the vehicle's center of mass can be expressed as follows:

$$F_{\delta D} = f_{\delta D} = \begin{bmatrix} \delta d_x \\ \delta d_y \\ \delta d_z \end{bmatrix},$$

$$M_{\delta D} = r_G \times f_{\delta D} = \begin{bmatrix} \delta d_k \\ \delta d_m \\ \delta d_n \end{bmatrix}, \tag{2.57}$$

where r_G is the position vector of the center of mass of the vehicle with respect to the body fixed frame. δd_x, δd_y, and δd_z are the disturbance forces along the X_0, Y_0, and Z_0 axes of the body fixed frame, respectively. δd_k, δd_m, and δd_n are the disturbance moments about the X_0, Y_0, and Z_0 axes of the body fixed frame,

respectively. Denote by:

$$\delta d = \begin{bmatrix} \delta d_x \\ \delta d_y \\ \delta d_z \\ \delta d_k \\ \delta d_m \\ \delta d_n \end{bmatrix}, \tag{2.58}$$

to be the vector that contains the disturbance forces and moments that acts on the vehicle's center of mass expressed with respect to the body fixed frame.

2.4.7 Full 6-DOF Equations of Motion with the Combined External Forces and Moments

The full 6-DOF equations of motion with the combined external forces and moments are expressed as follows:

$$
\begin{aligned}
m[\dot{u} - vr + wq - x_G(q^2 + r^2) + y_G(pq - \dot{r}) + z_G(pr + \dot{q})] = & - (W - B)sin\theta \\
& + X_{\dot{u}}\dot{u} + Z_{\dot{w}}wq + Z_{\dot{q}}q^2 - Y_{\dot{v}}vr - Y_{\dot{r}}r^2 \\
& + X_{u|u|}u|u| \\
& + X_{Thrust} \\
& + \delta d_x
\end{aligned}
\tag{2.59}
$$

$$
\begin{aligned}
m[\dot{v} - wp + ur - y_G(r^2 + p^2) + z_G(qr - \dot{p}) + x_G(qp + \dot{r})] = & (W - B)cos\theta sin\phi \\
& + Y_{\dot{v}}\dot{v} + Y_{\dot{r}}\dot{r} + X_{\dot{u}}ur - Z_{\dot{w}}wp - Z_{\dot{q}}pq \\
& + Y_{v|v|}v|v| + Y_{r|r|}r|r| \\
& + Y_{uvl}uv \\
& + \rho c_{L\alpha,fin}S_{fin}[u^2\delta r - uv - x_{fin}(ur)] \\
& + \delta d_y
\end{aligned}
\tag{2.60}
$$

$$m[\dot{w} - uq + vp - z_G(p^2 + q^2) + x_G(rp - \dot{q}) + y_G(rq + \dot{p})] = (W - B)cos\theta cos\phi$$
$$+ Z_{\dot{w}}\dot{w} + Z_{\dot{q}}\dot{q} - X_{\dot{u}}uq + Y_{\dot{v}}vp + Y_{\dot{r}}rp$$
$$+ Z_{w|w|}w|w| + Z_{q|q|}q|q|$$
$$+ Z_{uwl}uw$$
$$- \frac{1}{2}\rho c_{L\alpha,fin}S_{fin}[u^2\delta s_{right} + uw - x_{fin}(uq)]$$
$$- \frac{1}{2}\rho c_{L\alpha,fin}S_{fin}[u^2\delta s_{left} + uw - x_{fin}(uq)]$$
$$- \rho c_{L\alpha,wing}S_{wing}[uw - x_{wing}(uq)]$$
$$+ \delta d_z$$

$$(2.61)$$

$$I_x\dot{p} + (I_z - I_y)qr + m[y_G(\dot{w} - uq + vp) - z_G(\dot{v} - wp + ur)] = y_G W cos\theta cos\phi - Z_G W cos\theta sin\phi$$
$$+ K_{\dot{p}}\dot{p} - (Y_{\dot{v}} - Z_{\dot{w}})vw - (Y_{\dot{r}} + Z_{\dot{q}})wr$$
$$+ (Y_{\dot{r}} + Z_{\dot{q}})vq - (M_{\dot{q}} - N_{\dot{r}})qr$$
$$+ K_{p|p|}p|p|$$
$$+ K_{propeller}$$
$$- \frac{1}{2}\rho c_{L\alpha,fin}S_{fin}y_{fin,right}[u^2\delta s_{right} + uw - x_{fin}(uq)]$$
$$- \frac{1}{2}\rho c_{L\alpha,fin}S_{fin}y_{fin,left}[u^2\delta s_{left} + uw - x_{fin}(uq)]$$
$$+ \delta d_k$$

$$(2.62)$$

$$I_y\dot{q} + (I_x - I_z)rp + m[z_G(\dot{u} - vr + wq) - x_G(\dot{w} - uq + vp)] = -x_G W cos\theta cos\phi - z_G W sin\theta$$
$$+ M_{\dot{q}}\dot{q} + Z_{\dot{q}}\dot{w} - (Z_{\dot{w}} - X_{\dot{u}})wu - Y_{\dot{r}}vp + (K_{\dot{p}} - N_{\dot{r}})rp - Z_{\dot{q}}qu$$
$$+ M_{q|q|}q|q| + M_{w|w|}w|w|$$
$$+ M_{uwl}uw$$
$$+ \frac{1}{2}\rho c_{L\alpha,fin}S_{fin}x_{fin}[u^2\delta s_{right} + uw - x_{fin}(uq)]$$
$$+ \frac{1}{2}\rho c_{L\alpha,fin}S_{fin}x_{fin}[u^2\delta s_{left} + uw - x_{fin}(uq)]$$
$$+ \rho c_{L\alpha,wing}S_{wing}x_{wing}[uw - x_{wing}(uq)]$$
$$+ \delta d_m$$

$$(2.63)$$

$$I_z\dot{r} + (I_y - I_x)pq + m[x_G(\dot{v} - wp + ur) - y_G(\dot{u} - vr + wq)] = x_G W cos\phi + y_G W sin\theta$$
$$+ N_{\dot{r}}\dot{r} + Y_{\dot{r}}\dot{v} - (X_{\dot{u}} - Y_{\dot{v}})uv$$
$$+ Y_{\dot{r}}ur + Z_{\dot{q}}wp - (K_{\dot{p}} - M_{\dot{q}})pq$$
$$+ N_{r|r|}r|r| + N_{v|v|}v|v|$$
$$+ N_{uvl}uv$$
$$+ \rho c_{L\alpha,fin}S_{fin}x_{fin}[u^2\delta r - uv - x_{fin}(ur)]$$
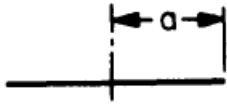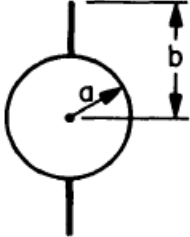$$+ \delta d_n$$

$$(2.64)$$
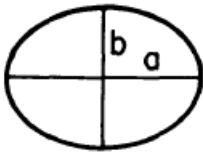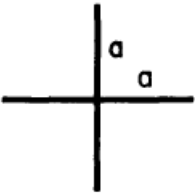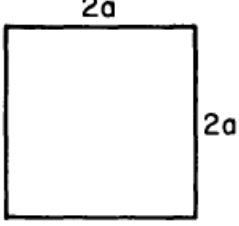
2.5 Hydrodynamic Coefficients

In this section, the added mass and the drag coefficients for the forces and moments acting on the vehicle are calculated.

2.5.1 Added Mass coefficients

The added mass derivatives in the added mass inertia matrix in (2.28) are calculated analytically. Calculating the added mass coefficients in three dimensions is difficult, especially for geometries that have complex features. In this work, the added mass coefficients are calculated using the strip theory, in which the outer geometry of the vehicle is divided into a number of strips. Then, 2-dimensional hydrodynamic coefficients for added mass are computed for each strip and integrated over the length of the body to yield the 3-dimensional coefficients. The

Table 2.6: Added Mass Coefficients for Various Two-Dimentional Bodies, [1]

Added-Mass Coefficients for Various Two-Dimensional Bodies.

m_{11}: $\pi\rho a^2$	$\pi\rho b^2$	0
m_{22}: $\pi\rho a^2$	$\pi\rho a^2$	$\pi\rho a^2$
m_{66}: 0	$\frac{1}{8}\pi\rho(a^2 - b^2)^2$	$\frac{1}{8}\pi\rho a^4$
m_{11}: $\pi\rho[a^2 + (b^2 - a^2)^2/b^2]$	$\pi\rho a^2$	$4.754\,\rho a^2$
m_{22}: $\pi\rho a^2$	$\pi\rho a^2$	$4.754\,\rho a^2$
m_{66}: $*$	$\frac{2}{\pi}\rho a^4$	$0.725\,\rho a^4$

*For the finned circle the added moment of inertia is given by the formula

$$m_{66} = \rho a^4 (\pi^{-1} \csc^4\alpha\, [2\alpha^2 - \alpha \sin 4\alpha + \tfrac{1}{2} \sin^2 2\alpha] - \pi/2)$$

2-dimensional added mass coefficients for various 2-dimensional bodies are shown

23
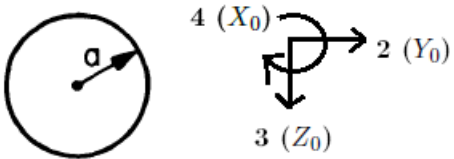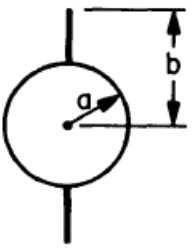
in table 2.6, where $sin\alpha$ is expressed as follows:

$$sin\alpha = \frac{2ab}{(a^2+b^2)} \quad and \quad \frac{\pi}{2} < \alpha < \pi \tag{2.65}$$

In this work, the circle and the finned circle are used from table 2.6, where a is the radius of the cylinder, and b is the projected distance on the $Y_B Z_B$ plane measured from the centerline of the cylinder to the tip of the fin or the wing. The value of b changes whether integrating over the fins or over the wings.

Table 2.7 is similar to table 2.6, with the only difference is the numbering of

Table 2.7: Added Mass Coefficients for circle and finned circle

$m22: \quad \pi\rho a^2$

$m33: \quad \pi\rho a^2$

$m44: \quad 0$

$m22: \quad \pi\rho[a^2 + \frac{(b^2-a^2)^2}{b^2}]$

$m33: \quad \pi\rho a^2$

$m44: \quad \rho a^4(\pi^{-1}csc^4\alpha[2\alpha^2 - \alpha sin4\alpha + \frac{1}{2}sin^2 2\alpha] - \pi/2)$

the axes which are chosen to be convenient with the body-fixed frame axes. The direction of translation in the direction of the X_B, Y_B and Z_B is numbered 1, 2, and 3 respectively, and the direction of rotation about the X_B, Y_B, and Z_B are numbered 4, 5, and 6 respectively.

The 3-dimensional added mass coefficients can be calculated by integrating the

24

2-dimensional added mass coefficients over the length of the vehicle, and the diagonal coefficients of the added mass matrix can be calculated using the following equations:

$$X_{\dot{u}} = -\int_{-L/2}^{L/2} m_{11}^{(2D)}(y,z)dx \tag{2.66}$$

$$Y_{\dot{v}} = -\int_{-L/2}^{L/2} m_{22}^{(2D)}(y,z)dx \tag{2.67}$$

$$Z_{\dot{w}} = -\int_{-L/2}^{L/2} m_{33}^{(2D)}(y,z)dx \tag{2.68}$$

$$K_{\dot{p}} = -\int_{-L/2}^{L/2} m_{44}^{(2D)}(y,z)dx \tag{2.69}$$

$$M_{\dot{q}} = -\int_{-L/2}^{L/2} m_{55}^{(2D)}(y,z)dx \tag{2.70}$$

$$N_{\dot{r}} = -\int_{-L/2}^{L/2} m_{66}^{(2D)}(y,z)dx \tag{2.71}$$

Note that the coefficients in (2.66), (2.70), and (2.71) can not be calculated using table (2.7), and calculating the coefficient in (2.69) is involving.

Diagonal added mass coefficients

Axial added mass

Since it is difficult to calculate the added mass coefficient in (2.66). Blevins [2] provided an empirical formula for calculating it:

$$X_{\dot{u}} = -\frac{4\alpha\rho\pi}{3}(\frac{l}{2})(\frac{d}{2})^2 \tag{2.72}$$

$$X_{\dot{u}} = -\frac{4\beta\rho\pi}{3}(\frac{d}{2})^3 \tag{2.73}$$

where α and β are empirical parameters measured by Blevins [2] and they depend on the vehicle's length to diameter ratio. Table 2.8 shows the axial added mass parameters for various length to diameter ratios:

Table 2.8: Axial Added Mass Parameters, Blevins [2]

l/d	α	β
0.01	–	0.6348
0.1	6.148	0.6148
0.2	3.008	0.6016
0.4	1.428	0.5712
0.6	0.9078	0.5447
0.8	0.6514	0.5211
1.0	0.5000	0.5000
1.5	0.3038	0.4557
2.0	0.2100	0.4200
2.5	0.1563	0.3908
3.0	0.1220	0.3660
5.0	0.05912	0.2956
7.0	0.03585	0.2510
10.0	0.02071	0.2071

Cross Flow Added Mass

The cross flow added mass coefficients can be calculated using strip theory explained in combination with table (2.7) is used.

let:

$$
\begin{aligned}
ma &= \pi\rho a^2 & for\ the\ hull \\
ma_f &= \pi\rho[a_{fin}^2 + \frac{(b_{fin}^2 - a_{fin}^2)^2}{b_{fin}^2}] & for\ the\ fins \\
ma_w &= \pi\rho[a_{wing}^2 + \frac{(b_{wing}^2 - a_{wing}^2)^2}{b_{wing}^2}] & for\ the\ wings
\end{aligned}
\tag{2.74}
$$

Using (2.67) and (2.68), the coefficients $Y_{\dot{v}}$ and $Z_{\dot{w}}$ can be computed as follows:

$$
Y_{\dot{v}} = -\int_{-l/2}^{x_{fin,rear}} ma\ dx - \int_{x_{fin,rear}}^{x_{fin,front}} ma_f\ dx - \int_{x_{fin,front}}^{l/2} ma\ dx
\tag{2.75}
$$

$$
\begin{aligned}
Z_{\dot{w}} = &-\int_{-l/2}^{x_{fin,rear}} ma\ dx - \int_{x_{fin,rear}}^{x_{fin,front}} ma_f\ dx - \int_{x_{fin,front}}^{x_{wing,rear}} ma\ dx \\
&-\int_{x_{wing,rear}}^{x_{wing,front}} ma_w\ dx - \int_{x_{wing,front}}^{l/2} ma\ dx
\end{aligned}
\tag{2.76}
$$

According to table 2.7, the coefficients $M_{\dot{q}}$ and $N_{\dot{r}}$ can be computed as suggested in [28] as follows:

$$
\begin{aligned}
M_{\dot{q}} &= -\int_{-l/2}^{l/2} x^2 m_{33} \; dx \\
&= -\int_{-l/2}^{x_{fin,rear}} x^2 ma \; dx - \int_{x_{fin,rear}}^{x_{fin,front}} x^2 ma_f \; dx - \int_{x_{fin,front}}^{x_{wing,rear}} x^2 ma \; dx \quad (2.77) \\
&\quad - \int_{x_{wing,rear}}^{x_{wing,front}} x^2 ma_w \; dx - \int_{x_{wing,front}}^{l/2} x^2 ma \; dx
\end{aligned}
$$

$$
\begin{aligned}
N_{\dot{r}} &= -\int_{-l/2}^{l/2} x^2 m_{22} \; dx \\
&= -\int_{-l/2}^{x_{fin,rear}} x^2 ma \; dx - \int_{x_{fin,rear}}^{x_{fin,front}} x^2 ma_f \; dx - \int_{x_{fin,front}}^{x_{l/2}} x^2 ma \; dx
\end{aligned}
\quad (2.78)
$$

Rolling Added Mass

During roll movement it is assumed that the vehicle's hull is smooth and does not generate any added mass effect. The added mass effect during roll movement is mainly due to the wings and fins. The rolling added mass $K_{\dot{p}}$ is calculated using the empirical formula provided by Blevins [2]:

$$
K_{\dot{p}} = -\int_{x_{fin,rear}}^{x_{fin,front}} \frac{2}{\pi} \rho b_{fin}^4 dx - \int_{x_{wing,rear}}^{x_{wing,front}} \frac{2}{\pi} \rho b_{wing}^4 dx \quad (2.79)
$$

where b_{fin} and b_{wing} are is the fin and wing heights above the vehicle centerline.

Cross terms added mass coefficients (off-diagonal coefficients)

According to table 2.7, the coefficients $Z_{\dot{q}}$ and $Y_{\dot{r}}$ can be computed as suggested in [28] as follows:

$$
\begin{aligned}
Z_{\dot{q}} &= -\int_{-l/2}^{l/2} x m_{33} dx \\
&= -\int_{-l/2}^{x_{fin,rear}} x ma \; dx - \int_{x_{fin,rear}}^{x_{fin,front}} x ma_f \; dx - \int_{x_{fin,front}}^{x_{wing,rear}} x ma \; dx \quad (2.80) \\
&\quad - \int_{x_{wing,rear}}^{x_{wing,front}} x ma_w \; dx - \int_{x_{wing,front}}^{l/2} x ma \; dx
\end{aligned}
$$

$$
\begin{aligned}
Y_{\dot{r}} &= -\int_{-l/2}^{l/2} x m_{22} \, dx \\
&= -\int_{-l/2}^{x_{fin,rear}} x m a \, dx - \int_{x_{fin,rear}}^{x_{fin,front}} x m a_f \, dx - \int_{x_{fin,front}}^{x_{l/2}} x m a \, dx
\end{aligned}
\tag{2.81}
$$

Table 2.9 shows the values of the added mass coefficients:

Table 2.9: Added mass coefficients

Coefficient	Value	Unit	Description
$X_{\dot{u}}$	-1.14	Kg	Axial added mass
$Y_{\dot{v}}$	-99.253	Kg	Cross-flow added mass
$Z_{\dot{w}}$	-499.687	Kg	Cross-flow added mass
$K_{\dot{p}}$	-72.6019	Kg.m/rad^2	Rolling added mass
$M_{\dot{q}}$	-39.815	Kg.m/rad^2	Cross-flow added mass
$N_{\dot{r}}$	-39.065	Kg.m/rad^2	Cross-flow added mass
$Y_{\dot{r}}$	-24.746	Kg.m/rad	Cross term added mass
$Z_{\dot{q}}$	24.747	Kg.m/rad	Cross term added mass

2.5.2 Drag coefficients

The drag coefficients in (2.35) are calculated analytically.

Axial drag coefficient

The axial drag coefficient can be calculated using the empirical formula presented in [28]:

$$
X_{u|u|} = -\frac{1}{2}\rho c_d A_f
\tag{2.82}
$$

where A_f is the frontal area of the vehicle (see table 2.1), and c_d is the axial drag coefficient of the vehicle. Triantafyllou [29] provided an empirical formula to calculate c_d:

$$
c_d = \frac{c_{ss}\pi A_p}{A_f}\left[1 + 60\left(\frac{d}{l}\right)^3 + 0.0025\left(\frac{l}{d}\right)\right]
\tag{2.83}
$$

where c_{ss} is the Schoenherr's value for skin friction of a flat plate estimated to be 3.397×10^{-3} in [30], and $A_p = ld$ is the vehicle's planform area.

Cross flow drag coefficients

The method used to calculate the cross flow drag coefficients is similar to the strip theory used to calculate the added mass coefficients. The cross flow drag coefficients of the vehicle is the sum of the drag coefficients over the cylinder plus the drag coefficients over the fins and the wings.

Let:

$$\gamma = \frac{1}{2}\rho C_{dc}$$
$$\nu_f = \frac{1}{2}\rho S_{fin}C_{df} \tag{2.84}$$
$$\nu_w = \frac{1}{2}\rho S_{wing}C_{dw}$$

where C_{dc} is the drag coefficient of a cylinder, which Hoerner [27] estimates it to be 1.1, S_{fin} and S_{wing} are the planform areas of the fin and the wing (see table 2.1), C_{df} and C_{dw} are the cross flow drag coefficients of fins and wings, that are derived using the formula developed by Whicker and Fehlner [31]:

$$C_{df} = 0.1 + 0.7t_{fin}$$
$$C_{dw} = 0.1 + 0.7t_{wing} \tag{2.85}$$

where t_{fin} and t_{wing} are the ratios of the width of the top and the bottom of the fins and the wings, respectively

The drag coefficients $Y_{v|v|}$, $Z_{w|w|}$, $M_{q|q|}$ and $N_{r|r|}$ are calculated as follows:

$$Y_{v|v|} = -\gamma \int_{-l/2}^{l/2} 2r \ dx - 2\nu_f$$
$$Z_{w|w|} = -\gamma \int_{-l/2}^{l/2} 2r \ dx - 2\nu_f - 2\nu_w$$
$$M_{q|q|} = -\gamma \int_{-l/2}^{l/2} 2x^3 r \ dx - 2x_{fin}^3\nu_f - 2x_{wing}^3\nu_w \tag{2.86}$$
$$N_{r|r|} = -\gamma \int_{-l/2}^{l/2} 2x^3 r \ dx - 2x_{fin}^3\nu_f$$

Rolling Drag

Prestero [28] approximated the rolling drag of the vehicle to be generated because of the fins and wings component of the cross flow drag coeffecient ($Y_{v|v|}$). The roll drag force can be calculated according to [28] as follows:

$$F = (Y_{vv,fin}r_{mean,fin})r_{mean,fin}^2 p|p| + (Y_{vv,wing}r_{mean,wing})r_{mean,wing}^2 p|p| \tag{2.87}$$

29

Table 2.10: Drag coefficients

Coefficient	Value	Unit	Description
$X_{u|u|}$	-4.593	Kg/m	Axial drag
$Y_{v|v|}$	-246.574	Kg/m	Cross-flow drag
$Z_{w|w|}$	-351.124	Kg/m	Cross-flow drag
$K_{p|p|}$	-10.33	$Kg.m^2/rad^2$	Rolling drag
$M_{q|q|}$	-9.295	$Kg.m^2/rad^2$	Cross-flow drag
$N_{r|r|}$	-9.25	$Kg.m^2/rad^2$	Cross-flow drag
$Y_{r|r|}$	12.172	$Kg.m/rad^2$	Cross term drag
$Z_{q|q|}$	-12.76	$Kg.m/rad^2$	Cross term drag
$M_{w|w|}$	23.857	Kg	Cross term drag
$N_{v|v|}$	-16.016	Kg	Cross term drag

where $Y_{vv,fin}$ and $Y_{vv,wing}$ are the fins and wings components of the vehicle cross-flow drag coefficient, respectively, $r_{mean,fin}$ and $r_{mean,wing}$ are the mean fin and wing height above the centerline of the vehicle, respectively. The rolling drag coefficient is expressed as follows:

$$K_{p|p|} = (Y_{vv,fin}r_{mean,fin})r_{mean,fin}^2 + (Y_{vv,wing}r_{mean,wing})r_{mean,wing}^2 \qquad (2.88)$$

Cross terms drag coefficients

According to [28] the coefficients $Z_{q|q|}$, $Y_{r|r|}$, $M_{w|w|}$ & $N_{v|v|}$ can be computed as follows:

$$
\begin{aligned}
Y_r|r| &= -\gamma \int_{-l/2}^{l/2} 2x|x|r \; dx - 2x_{fin}|x_{fin}|.\nu_f \\
Z_q|q| &= \gamma \int_{-l/2}^{l/2} 2x|x|r \; dx + 2x_{fin}|x_{fin}|.\nu_f + 2x_{wing}|x_{wing}|.\nu_w \\
M_w|w| &= \gamma \int_{-l/2}^{l/2} 2xr \; dx - 2x_{fin}.\nu_f - 2x_{wing}.\nu_w \\
N_v|v| &= -\gamma \int_{-l/2}^{l/2} 2xr \; dx + 2x_{fin}.\nu_f
\end{aligned}
\qquad (2.89)
$$

Table 2.10 shows the values of the drag coefficients that are used in the model:

Chapter 3

Linear Model, Linearization, and Control Design

In this chapter the nonlinear model in (2.15) and (2.2) is linearized about a given three-dimensional trajectory parameterized with respect to time, to get a linear time variant (LTV) state space model. A linear quadratic regulator is designed based on the linearized model, and the derived control law is applied to the nonlinear model. Also in this chapter, the robustness of the controller is investigated in the presence of disturbance.

3.1 Linear Model and Linearization about a Dessired Trajectory

In this section, the nonlinear model in (2.15) and (2.2) is linearized about a given 3D trajectory parametrized with respect to time: $\gamma(t) = \{x_{eq}(t), y_{eq}(t), z_{eq}(t)\}$. This trajectory represents the desired position of the vehicle with respect to {U} at each instant of time. By setting the mass to be constant for the thrust mode, and variable between m_{min} and m_{max} for the gliding mode, the model in (2.15) is used to represent both modes of operation. Based on the given trajectory it is decided which mode of operation is used, and whether to use constant or variable mass in the nonlinear model before linearizing it about the given trajectory.

3.1.1   Nonlinear State Space Form

The nonlinear model in (2.15) and (2.2) can be written in the state space form as:

$$\dot{\chi} = F(\chi, U, m) + \Delta d ,$$

$$\textbf{where} \qquad \Delta d = \begin{bmatrix} M_{inertia}^{-1} \cdot \delta d \\ 0_{6 \times 1} \end{bmatrix} , \qquad (3.1)$$

which includes the 6 dynamic equations of motion of the vehicle in (2.15), and the 6 kinematic equations from the transformation between {U} and {B} in (2.2). $\chi = [\nu,\ \eta]^T$ is the state vector of length 12, $U = [X_{thrust}\ ,\ \delta_r\ ,\ \delta_{s,right}\ ,\ \delta_{s,left}]^T$ is the vector containing the inputs of length 4, and m is the mass of the vehicle. $M_{inertia}$ is the inertia matrix of the vehicle that include the added mass inertia matrix (M_A) calculated in (2.28). δd is the vector containing the unknown disturbance forces and moments. The vector of zeros corresponds to the six kinematic equations that are included in the nonlinear state space form.

Since Δd is unknown, it is not considered in the linearization and control design. The nonlinear state space model which is used for linearization and control design can be written as follows:

$$\dot{\chi} = F(\chi, U, m), \qquad (3.2)$$

In thrust mode the mass of the vehicle is set to a constant value, which makes the vehicle neutrally buoyant, so the nonlinear state space form for the thrust mode is written as:

$$\dot{\chi} = F(\chi, U, m_{neutral}) , \qquad (3.3)$$

where $m_{neutral}$ is the mass of the vehicle when it is half full of sea water (neutrally buoyant). In the gliding mode the mass of the vehicle is considered to be variable between two values m_{min} and m_{max}, where m_{min} is the mass of the vehicle when it is empty of sea water (the vehicle is positively buoyant), and m_{max} is the mass of the vehicle when it is full of sea water (the vehicle is negatively buoyant). However, keeping the mass variable in (3.2) makes the linearization very difficult and challenging. Therefore, to simplify the linearization process in gliding mode, the mass of the vehicle is set to be constant to m_{min} when it is floating up, and to m_{max} when it is diving down. So, the nonlinear state space form for the gliding mode is written as:

$$\dot{\chi} = F(\chi, U, m_{min}) \quad \textit{when the vehicle is floating up,}$$
$$\dot{\chi} = F(\chi, U, m_{max}) \quad \textit{when the vehicle is diving down.} \qquad (3.4)$$

Thus, before linearizing the nonlinear model about the given 3D trajectory, the desired mass of the vehicle should be determined in order simplify the linearization process. The mass of the vehicle is determined based on the given trajectory, which will be explained in more detail in the following sections.

3.1.2 Calculating the Equilibrium States and Deciding which Mode of Operation to Use Based on the Equilibrium Trajectory

In order to linearize the model in (3.2) about the equilibrium trajectory, the desired mode of operation should be determined first, so that the corresponding value of the vehicle's mass is identified and substituted in (3.2). The desired mode of operation is determined based on the velocity profile of the given trajectory. Also, in the gliding mode, the desired mass used for the vehicle is determined based on the equilibrium pitch angle of the trajectory, so if the equilibrium pitch angle is positive, the vehicle should float up to follow the desired trajectory, and therefore the desired mass is equal to m_{min}. Whereas, if the equilibrium pitch angle is negative, the vehicle should dive down to track the desired trajectory, and therefore the desired mass should be equal to m_{max}.

The equilibrium states $\left(\chi_{eq}(t)\right)$ and inputs $\left(U_{eq}(t)\right)$ that satisfy the desired trajectory $\left(\gamma(t)\right)$ must be known, which will be varying with respect to time. Of the equilibrium states, only the position of the vehicle with respect to {U} is given as a function of time $\eta_{1,eq} = [x_{eq}(t),\ y_{eq}(t),\ z_{eq}(t)]^T$. The rest of the equilibrium states need to be calculated.

In order to calculate the desired orientation of vehicle along the trajectory $\eta_{2,eq}(t) = [\phi_{eq}(t),\ \theta_{eq}(t),\ \psi_{eq}(t)]^T$, consider the Frenet-Seret {FS} frame associated with each point on the path at each instant of time with its unit vectors: T (tangent to the path), N (normal to the path and pointing towards the center of curvature of the path), and $B = T \times N$, as shown in Fig. 3.1. The position of the origin of the Frenet-Seret frame, O_{FS}, with respect to {U} is the desired position of the vehicle $\left(\eta_{1,eq} = [x_{eq}(t),\ y_{eq}(t),\ z_{eq}(t)]^T\right)$. The desired orientation (Euler angles) parametrizes the rotation matrix from the {FS} frame to the {U} frame, as shown in (3.5):

$$R_{\{FS\}}^{\{U\}} = \begin{bmatrix} T(t)^{\{U\}} & N(t)^{\{U\}} & B(t)^{\{U\}} \end{bmatrix} = \begin{bmatrix} c\psi_{eq}c\theta_{eq} & -s\psi_{eq}c\phi_{eq} + c\psi_{eq}s\theta_{eq}s\phi_{eq} & s\psi_{eq}s\phi_{eq} + c\psi_{eq}c\phi_{eq}s\theta_{eq} \\ s\psi_{eq}c\theta_{eq} & c\psi_{eq}c\phi_{eq} + s\phi_{eq}s\theta_{eq}s\psi_{eq} & -c\psi_{eq}s\phi_{eq} + s\theta_{eq}s\psi_{eq}c\phi_{eq} \\ -s\theta_{eq} & c\theta_{eq}s\phi_{eq} & c\theta_{eq}c\phi_{eq} \end{bmatrix}$$

$$(3.5)$$

where the vectors $T^{\{U\}}$, $N^{\{U\}}$, $B^{\{U\}}$ are the unit vectors of the {FS} expressed with respect to {U}. This notation is consistent with the notation introduced in [32]. To calculate the coordinates of the unit vectors of {FS} with respect to
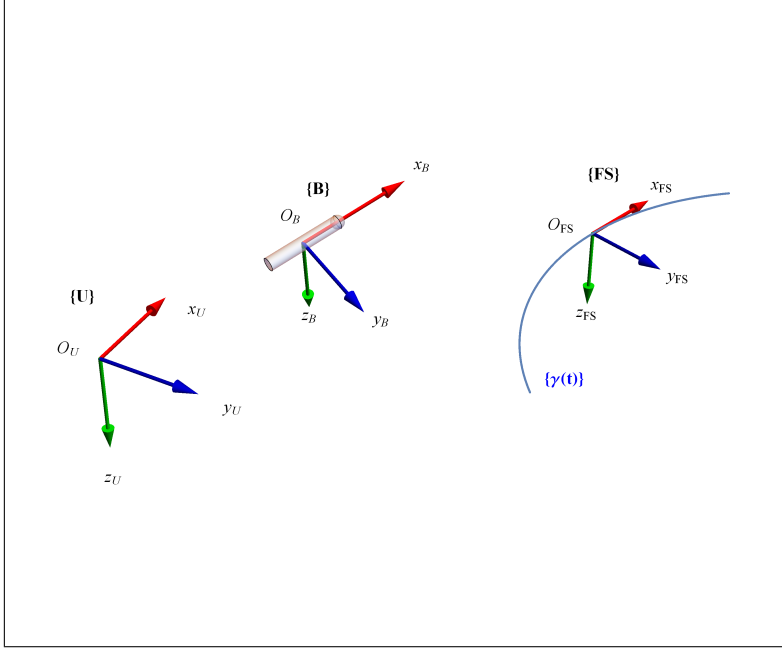
Figure 3.1: AUV Tracking a 3D trajectory

{U}, the given 3D trajectory $\gamma(t)$ is reparametrized with respect to the arc length to get $\alpha(s) = \{x_{eq}(s), y_{eq}(s), z_{eq}(s)\}$. The arc-length is defined as:

$$s = \int_{\gamma} |\dot{\gamma}(t)| dt , \tag{3.6}$$

where $\dot{\gamma}(t)$ is the first time derivative of $\gamma(t)$, and $|\dot{\gamma}(t)|$ is the absolute velocity of the curve with respect to {U}. The coordinates of the unit vectors $T(s)$ and $N(s)$ with respect to {U} are calculated by differentiating $\alpha(s)$ with respect to s once and twice, respectively, and $B(s) = T(s) \times N(s)$. The vectors are then reparametrized with respect to time. For more details about Frenet frames, see [33]. Equation (3.5) is solved to get the desired equilibrium Euler angles ($\eta_{2,eq}(t)$). Using similar approach as in [32], the equilibrium pitch angle (θ_{eq}) is first calculated using the first element of the third row of the transformation matrix in (3.5) as follows:

$$\theta_{eq} = -sin^{-1}\Big(T_z(t)^{\{U\}}\Big), \tag{3.7}$$

where $T_z(t)^{\{U\}}$ is the z-coordinate of the vector $T(t)^{\{U\}}$ with respect to {U}. Since the pitch angle is desired to be zero degrees, the first solution from (3.7) is chosen. Then the equilibrium roll angle (ϕ_{eq}) is calculated using the second element of the third row of the transformation matrix in (3.5) as follows:

$$\phi_{eq} = sin^{-1}\Big(sec(\theta_{eq}).N_z(t)^{\{U\}}\Big), \tag{3.8}$$

34

where $N_z(t)^{\{U\}}$ is the z component of the vector $N(t)^{\{U\}}$ with respect to $\{U\}$. Similarly as the pitch angle, the first solution is chosen for the equilibrium roll angle. The yaw angle is calculated using the first and second elements of the first column of the transformation matrix in (3.5) as follows:

$$\psi_{eq} = Tan^{-1}\left(\frac{T_y(t)^{\{U\}}}{T_x(t)^{\{U\}}}\right) + K\pi \qquad K \in \mathbb{N} \tag{3.9}$$

where $T_x(t)^{\{U\}}$ and $T_y(t)^{\{U\}}$ are the x and the y components of the vector $T(t)^{\{U\}}$ with respect to $\{U\}$, respectively. The equilibrium yaw angle is not bounded between $[-\pi,\ \pi]$.

The rest of the equilibrium states $\nu_{eq}(t)$, which represent the equilibrium linear and angular velocities with respect to $\{U\}$ expressed in $\{FS\}$, are the equilibrium velocities that satisfy the given equilibrium trajectory $\gamma(t)$ and are calculated as follows:

$$\nu_{eq}(t) = \left(R_{\{FS\}}^{\{U\}}\right)^{-1}.\dot{\eta}_{eq}(t), \tag{3.10}$$

where $\left(R_{\{FS\}}^{\{U\}}\right)^{-1}$ is the inverse of the transformation matrix $R_{\{FS\}}^{\{U\}}$ from (3.5), and it is parametrized with respect to the equilibrium Euler angles (ϕ_{eq}, θ_{eq} & ψ_{eq}), and $\dot{\eta}_{eq}(t)$ is the time derivative of $\eta_{eq}(t)$.

The desired mode of operation can be determined based on the equilibrium forward velocity (u_{eq}); if u_{eq} is around 1.5 m/sec, then the vehicle switches to thrust mode and the mass of the vehicle is equal to $m_{neutral}$. However, if u_{eq} is around 0.2 m/sec, then the vehicle switches to the gliding mode and the mass of the vehicle is equal to m_{min} or m_{max}. In gliding mode, the value of the mass is determined based on the equilibrium pitch angle according to the following equation:

$$m = tanh\left(\frac{-\theta_{eq}(t)}{\epsilon}\right) + m_{neutral}, \tag{3.11}$$

where the function $tanh$ is used to avoid the discontinuity between m_{min} and m_{max}, when the equilibrium pitch angle changes from positive to negative. The constant ϵ is used to control the rate of the transition between m_{min} and m_{max}. The x-position of the vehicle's center of gravity with respect to the body fixed frame $\{B\}$ (x_G) is coupled with the mass of the vehicle, so when the mass of the vehicle changes between m_{min} and m_{max}, x_G changes between -0.02m and 0.02m respectively according to the following relation:

$$x_G = 0.02 \times (m - m_{neutral}), \tag{3.12}$$

where m is calculated from(3.11). In thrust mode, m is constant and equal to $m_{neutral}$, so x_G is zero.

In gliding mode, the vehicle is driven by the hydro-static forces (buoyancy and weight) which act around the center of the vehicle; in this case, when floating up or diving down, the x-axis of the body fixed frame will not be tangent to the desired 3D trajectory while tracking it, as in thrust mode. So, the forward and the vertical velocities ($u(t)$ and $w(t)$) will be different than the equilibrium values calculated from (3.10), similarly, the vehicle's pitch angle will not be equal to the equilibrium pitch angle (θ_{eq}) calculated from (3.7). To track these equilibrium values, the vehicle will have to exert more effort and consume more energy, which will defeat the purpose of the gliding mode, that is to conserve energy. And since in gliding mode the desired trajectory to be tracked is a saw-tooth path, the nonlinear model is linearized about constant operating points for the pitch angle θ, the forward velocity u, and the vertical velocity w, and the rest of the variable equilibrium states that are calculated from (3.5) and (3.10). The gliding mode is divided into two phases, diving phase and floating phase. In each phase, the equilibrium values for the pitch angle and the vertical velocity are considered constant and different from the other phase. The equilibrium forward velocity is assumed to be constant and fixed for both phases. The constant equilibrium states are calculated as follows:

$$
\begin{aligned}
u_{eq}^* &= 0.2 m/s, \\
w_{eq}^*(t) &= 0.0402 \times tanh\left(\frac{-\theta_{eq}(t)}{\epsilon}\right) \ m/sec, \\
\theta_{eq}^*(t) &= 0.2796 \times tanh\left(\frac{\theta_{eq}(t)}{\epsilon}\right) \ rad,
\end{aligned}
\tag{3.13}
$$

where the function $tanh$ is used to avoid the discrete transition between the two values of the equilibrium pitch (θ_{eq}^*) and the equilibrium vertical velocity (w_{eq}^*), which occurs when the vehicle switches between the two phases $\Big($when $\theta_{eq}(t)$ calculated in (3.7) changes sign$\Big)$. Similarly as in (3.11), the constant ϵ is used to control the rate of the transition between the values of θ_{eq}^* and w_{eq}^* that correspond to each phase. The $*$ is used to distinguish between the constant equilibrium forward velocity, vertical velocity, and pitch angle used for gliding mode instead of the variable equilibrium forward velocity, vertical velocity, and pitch angle that are calculated in (3.10) and (3.7). The values 0.2, 0.0402, and 0.2796 in (3.13) are determined from the open loop simulation for the case of moving forward in a saw-tooth path. Table (3.1) summarizes the equilibrium states that are used to linearize the nonlinear model after determining the mode of operation.

36

Table 3.1: Equilibrium states and desired mass

Equilibrium states and desired mass	Thrust mode	Gliding mode (Diving)	Gliding mode (Floating)
x_{eq}	given from $\gamma(t)$	given from $\gamma(t)$	given from $\gamma(t)$
y_{eq}	given from $\gamma(t)$	given from $\gamma(t)$	given from $\gamma(t)$
z_{eq}	given from $\gamma(t)$	given from $\gamma(t)$	given from $\gamma(t)$
ϕ_{eq}	calculated from (3.8)	calculated from (3.8)	calculated from (3.8)
θ_{eq}	calculated from (3.7)	$-0.2796\ rad$	$0.2796\ rad$
ψ_{eq}	calculated from (3.9)	calculated from (3.9)	calculated from (3.9)
u_{eq}	calculated from (3.10)	$0.2\ m/sec$	$0.2\ m/sec$
v_{eq}	calculated from (3.10)	calculated from (3.10)	calculated from (3.10)
w_{eq}	calculated from (3.10)	$0.0402\ m/sec$	$-0.0402\ m/sec$
p_{eq}	calculated from (3.10)	calculated from (3.10)	calculated from (3.10)
q_{eq}	calculated from (3.10)	calculated from (3.10)	calculated from (3.10)
r_{eq}	calculated from (3.10)	calculated from (3.10)	calculated from (3.10)
Desired mass	$m_{neutral} = 72.5\ Kg$	$m_{max} = 73.5\ Kg$	$m_{min} = 71.5\ Kg$

3.1.3 Calculating the Equilibrium Inputs that Satisfy the Equilibrium Trajectory

The equilibrium inputs (U_{eq}) that satisfy the equilibrium trajectory $\big(\gamma(t)\big)$ need to be calculated to linearize the system about them. The equilibrium inputs can be calculated from (3.2) evaluated at the equilibrium trajectory:

$$\dot{\chi}_{eq} = F(\chi_{eq}, U_{eq}, m_{desired}). \tag{3.14}$$

However, the inputs do not appear in the kinematic equations, which are included in (3.2) and (3.14); therefore, only the six dynamic equations from (3.14) are needed to calculate the equilibrium inputs. The six dynamic equations from (2.15), evaluated at the equilibrium states, can be written in the following form:

$$\dot{\nu}_{eq} = f_1(\nu_{eq}, \phi_{eq}, \theta_{eq}, U_{eq}, m_{desired}). \tag{3.15}$$

$\dot{\nu}_{eq}, \nu_{eq},\ \phi_{eq},\ \theta_{eq}$, and $m_{desired}$ in (3.15) are known, and only the equilibrium inputs vector U_{eq} is unknown and need to be solved for. The value of $m_{desired}$ in (3.14) and (3.15) is constant. Equation (3.15) can be simplified into the following linear form with respect to the unknown equilibrium inputs vector:

$$N.U_{eq} = b, \tag{3.16}$$

37

where N is a 6×4 matrix and b is a vector of length 6, and both are known. The system of equations in (3.16) is overdetermined, since there are only four unknowns, equilibrium inputs (X_{thrust}, δ_r, $\delta_{s,right}$ and $\delta_{s,left}$), and six equations. Therefore, a solution for U_{eq} that satisfies the six equations does not exist. The solution for U_{eq} is one that minimizes error $e = N.U_{eq} - b$ in the least mean square sense, and it can be found to be:

$$U_{eq} = \left(N^T N\right)^{-1} N^T b. \tag{3.17}$$

3.1.4 Linear Time Variant State Space Model

Now that the equilibrium states $\left(\chi_{eq}(t)\right)$, the equilibrium inputs $\left(U_{eq}(t)\right)$, and the desired mass of the vehicle ($m_{desired}$) are calculated using the desired trajectory $\left(\gamma(t)\right)$, equation (3.2) can be linearized and written in the following LTV state space form:

$$\dot{\tilde{\chi}}(t) = A(t)\tilde{\chi}(t) + B(t)\tilde{U}(t) \tag{3.18}$$

where $\tilde{\chi} = \chi - \chi_{eq}$ and $\tilde{U} = U - U_{eq}$. $A(t)$ is a 12×12 matrix and $B(t)$ is a 12×4 matrix, and they are calculated from equation (3.2) as follows [34]:

$$A(t) = \left.\frac{\partial F}{\partial \chi}\right|_{\substack{\chi = \tilde{\chi}_{eq}(t) \\ U = \tilde{U}_{eq}(t)}} \qquad B(t) = \left.\frac{\partial F}{\partial U}\right|_{\substack{\chi = \tilde{\chi}_{eq}(t) \\ U = \tilde{U}_{eq}(t)}} \tag{3.19}$$

The output equation of the state space model in (3.18) is written as follows:

$$y(t) = C\tilde{\chi}(t) + D\tilde{U}(t) \tag{3.20}$$

C is a 12×12 matrix and D is a 12×4 matrix. The system is assumed to be fully observable and all states are available for measuring at each instant of time, so matrices C and D are assumed to be:

$$C = I_{12 \times 12} \qquad D = 0_{12 \times 4} \tag{3.21}$$

where $I_{12 \times 12}$ is a 12×12 identity matrix. The steps for linearization about a given trajectory are summarized in Algorithm (1).

3.2 Control Design

In this section, a linear quadratic regulator is designed based on the linearized model, and the derived control law is applied to the nonlinear model.

Consider the linear time variant state space model in equation (3.18), the feedback LQR control law is written as follows:

$$U(t) = -k(t)\tilde{\chi}(t) \; , \tag{3.22}$$

where $U(t)$ is the vector of the feedback control inputs of length 4, $\tilde{\chi}(t) = \chi(t) - \chi_{eq}(t)$ is state error vector of length 12, and $k(t)$ is a 4×12 matrix containing the control gains, which vary with time. The control gains of the LQR control law are calculated such that the control law in (3.22) minimizes the following cost function:

$$H = \frac{1}{2} \int \left(\chi^T Q \chi + U^T R U \right) dt \; , \tag{3.23}$$

where Q is a 12×12 weighing matrix for the states, R is 4×4 weighing matrix for the inputs, and both matrices are positive semi-definite.

The control gains k that minimize the cost function H are calculated as follows:

$$k(t) = -R^{-1}B(t)^T P(t) \; , \tag{3.24}$$

where $P(t)$ is a 12×12 matrix and is calculated by solving the following differential algebraic Reccati equation:

$$A(t)^T P(t) + P(t)A(t) + Q - P(t)B(t)R^{-1}B(t)^T P(t) = -\dot{P}(t) \; , \tag{3.25}$$

which is solved numerically at each time step.

The weighing matrices are chosen by tuning, and they change depending on the type of trajectory. In this work three trajectories are used for simulation: Helix with constant pitch and three dimensional Dubin's trajectory for the thrust mode; and a saw-tooth trajectory for the gliding mode. The R matrix is chosen to be identity matrix of size 4×4 for all the trajectory cases:

$$R = \begin{bmatrix} 1 & 0 & 0 & 0 \\ 0 & 1 & 0 & 0 \\ 0 & 0 & 1 & 0 \\ 0 & 0 & 0 & 1 \end{bmatrix} \; . \tag{3.26}$$

The Q matrix is chosen differently for each trajectory case, and after tuning the

following values are chosen for each trajectory case:

$$
Q_{Helix} =
\begin{bmatrix}
1 & 0 & 0 & 0 & 0 & 0 & 0 & 0 & 0 & 0 & 0 & 0 \\
0 & 1 & 0 & 0 & 0 & 0 & 0 & 0 & 0 & 0 & 0 & 0 \\
0 & 0 & 1 & 0 & 0 & 0 & 0 & 0 & 0 & 0 & 0 & 0 \\
0 & 0 & 0 & 1 & 0 & 0 & 0 & 0 & 0 & 0 & 0 & 0 \\
0 & 0 & 0 & 0 & 1 & 0 & 0 & 0 & 0 & 0 & 0 & 0 \\
0 & 0 & 0 & 0 & 0 & 1 & 0 & 0 & 0 & 0 & 0 & 0 \\
0 & 0 & 0 & 0 & 0 & 0 & 10^6 & 0 & 0 & 0 & 0 & 0 \\
0 & 0 & 0 & 0 & 0 & 0 & 0 & 10^6 & 0 & 0 & 0 & 0 \\
0 & 0 & 0 & 0 & 0 & 0 & 0 & 0 & 10^6 & 0 & 0 & 0 \\
0 & 0 & 0 & 0 & 0 & 0 & 0 & 0 & 0 & 10^6 & 0 & 0 \\
0 & 0 & 0 & 0 & 0 & 0 & 0 & 0 & 0 & 0 & 10^6 & 0 \\
0 & 0 & 0 & 0 & 0 & 0 & 0 & 0 & 0 & 0 & 0 & 10^6
\end{bmatrix},
$$

$$
Q_{Dubin} =
\begin{bmatrix}
1 & 0 & 0 & 0 & 0 & 0 & 0 & 0 & 0 & 0 & 0 & 0 \\
0 & 1 & 0 & 0 & 0 & 0 & 0 & 0 & 0 & 0 & 0 & 0 \\
0 & 0 & 1 & 0 & 0 & 0 & 0 & 0 & 0 & 0 & 0 & 0 \\
0 & 0 & 0 & 1 & 0 & 0 & 0 & 0 & 0 & 0 & 0 & 0 \\
0 & 0 & 0 & 0 & 1 & 0 & 0 & 0 & 0 & 0 & 0 & 0 \\
0 & 0 & 0 & 0 & 0 & 1 & 0 & 0 & 0 & 0 & 0 & 0 \\
0 & 0 & 0 & 0 & 0 & 0 & 10^4 & 0 & 0 & 0 & 0 & 0 \\
0 & 0 & 0 & 0 & 0 & 0 & 0 & 10^4 & 0 & 0 & 0 & 0 \\
0 & 0 & 0 & 0 & 0 & 0 & 0 & 0 & 10^4 & 0 & 0 & 0 \\
0 & 0 & 0 & 0 & 0 & 0 & 0 & 0 & 0 & 10^4 & 0 & 0 \\
0 & 0 & 0 & 0 & 0 & 0 & 0 & 0 & 0 & 0 & 10^4 & 0 \\
0 & 0 & 0 & 0 & 0 & 0 & 0 & 0 & 0 & 0 & 0 & 10^4
\end{bmatrix},
\qquad (3.27)
$$

$$
Q_{Saw-tooth} =
\begin{bmatrix}
1 & 0 & 0 & 0 & 0 & 0 & 0 & 0 & 0 & 0 & 0 & 0 \\
0 & 1 & 0 & 0 & 0 & 0 & 0 & 0 & 0 & 0 & 0 & 0 \\
0 & 0 & 1 & 0 & 0 & 0 & 0 & 0 & 0 & 0 & 0 & 0 \\
0 & 0 & 0 & 1 & 0 & 0 & 0 & 0 & 0 & 0 & 0 & 0 \\
0 & 0 & 0 & 0 & 1 & 0 & 0 & 0 & 0 & 0 & 0 & 0 \\
0 & 0 & 0 & 0 & 0 & 1 & 0 & 0 & 0 & 0 & 0 & 0 \\
0 & 0 & 0 & 0 & 0 & 0 & 1 & 0 & 0 & 0 & 0 & 0 \\
0 & 0 & 0 & 0 & 0 & 0 & 0 & 1 & 0 & 0 & 0 & 0 \\
0 & 0 & 0 & 0 & 0 & 0 & 0 & 0 & 1 & 0 & 0 & 0 \\
0 & 0 & 0 & 0 & 0 & 0 & 0 & 0 & 0 & 1 & 0 & 0 \\
0 & 0 & 0 & 0 & 0 & 0 & 0 & 0 & 0 & 0 & 1 & 0 \\
0 & 0 & 0 & 0 & 0 & 0 & 0 & 0 & 0 & 0 & 0 & 1
\end{bmatrix},
$$

As observed for the helix and the 3D Dubin's trajectory cases, more weights are put on the position and orientation of the vehicle, since the main objective is for the vehicle to follow the desired trajectory with minimum error in the vehicle's position and orientation. In saw-tooth case (gliding mode), all the states are given the same weight, because if more weights are put on the position and orientation, the vehicle will have to use more effort and energy to minimize the error for its position and orientation, which will defeat the purpose of the gliding mode.

Algorithm 1 Linearization about a given trajectory

<u>Given:</u>
1: **Nonlinear Model:** $\dot{\chi} = F(\chi, U, m)$
2: **Trajectory:** $\gamma(t)^{\{U\}} = \{x_{eq}(t), y_{eq}(t), z_{eq}(t)\}$ with respect to the global frame $\{U\}$

Calculating Equilibrium States:
3: **Define:** Frenet-Sertet Frames $\{FS\}$ at each point on $\gamma(t)$.
4: **Calculate:** The coordinates of the unit vectors of $\{FS\}$ $T(t)^{\{U\}}$, $N(t)^{\{U\}}$ & $B(t)^{\{U\}}$ with respect to $\{U\}$
5: **Calculate:** The equilibrium Euler angles $\eta_{2eq}^{\{U\}}(t) = [\phi_{eq}(t),\ \theta_{eq}(t),\ \psi_{eq}(t)]^T$ using equation (3.5)
6: **Calculate:** The equilibrium velocities $\nu_{eq}(t) = [u_{eq}(t),\ v_{eq}(t),\ w_{eq}(t),\ p_{eq}(t),\ q_{eq}(t),\ r_{eq}(t)]^T$ using equation (3.10)

Setting the Mass of the Vehicle:
7: **Check:** The value of the equilibrium forward velocity (u_{eq})
8: **if** $u_{eq} = 1.5\ m/sec$ **then**
9:     **Switch:** to Thrust mode
10:     **Set:** $m_{desired}$ to be $m_{neutral}$
11: **else if** $u_{eq} = 0.2\ m/sec$ **then**
12:     **Switch:** to Gliding mode
13:     **Substitute:** θ_{eq}, u_{eq}, and w_{eq} calculated in steps 5 and 6, with θ_{eq}^*, u_{eq}^*, and w_{eq}^* that are calculated from (3.13)
14:     **if** $\theta_{eq} < 0$ **then**
15:         **Set:** $m_{desired}$ to be m_{max} **(Diving down)**
16:     **else if** $\theta_{eq} > 0$ **then**
17:         **Set:** $m_{desired}$ to be m_{min} **(Floating up)**
18:     **end if**
19: **end if**

Calculating the Equilibrium Inputs:
20: **Substitute**: $\eta_{eq}(t)$, $\nu_{eq}(t)$, and $m_{desired}$ in the nonlinear dynamic equations $\dot{\nu}_{eq}(t) = f1\Big(\nu_{eq}(t), \phi_{eq}(t), \theta_{eq}(t), U_{eq}(t), m_{desired}\Big)$
21: **Rewrite:** The overdetermined system $\dot{\nu}_{eq}(t) = f1\Big(\nu_{eq}(t), \phi_{eq}(t), \theta_{eq}(t), U_{eq}(t),$ $m_{desired}\Big)$ as a linear algebraic form with respect to $U_{eq}(t)$, $N.U_{eq} = b$
22: **Solve:** The overdetermined system $N.U_{eq} = b$ for $U_{eq}(t)$ by minimizing least mean square error $U_{eq} = \left(N^T N\right)^{-1} G^T b$
23: **Linearize:** The nonlinear model $\dot{\chi} = F(\chi, U, m)$, about $\chi_{eq}(t) = [\eta_{eq}(t), \nu_{eq}(t)]^T$ & $U_{eq}(t)$ to get the **linear time variant system** $\dot{\tilde{\chi}}(t) = A(t)\tilde{\chi}(t) + B(t)\tilde{U}(t)$

Chapter 4

Simulations

In this chapter, the derived nonlinear model is simulated when applying open loop control inputs. Also, the linear model is simulated when applying open loop inputs to it, and the results are compared to the results of the nonlinear model, when applying the same inputs that are applied to the linearized model. Simulation results for the controlled linear and nonlinear systems to track three-dimensional trajectory with and without disturbance are also presented in this chapter.

4.1   Open Loop Simulations for the Nonlinear Model

The model derived in the previous section is simulated on MATLAB Simulink. As mentioned before, there are two modes of operation, thrust mode and gliding mode. For the thrust mode there are 5 inputs: thrust force (X_{Thrust}) , two rudder fins (δ_r), which are assumed to be coupled for simplicity, and two stern fins ($\delta_{s,right}$ and $\delta_{s,left}$). For the gliding mode there are also 5 inputs: mass of the vehicle (m) , two rudder fins (δ_r), which are assumed to be coupled for simplicity, and two stern fins ($\delta_{s,right}$ and $\delta_{s,left}$).
The desired outputs are the 12 states of the system, which are the linear and angular velocities (ν) expressed with respect to the body fixed frame, and the position and orientation of the vehicle (η) with respect to the inertial frame of reference.

4.1.1   Thrust Mode

In this section, the basic motion paths (horizontal straight line, circle, diving up and diving down) for the thrust mode are simulated. The vehicle starts from the origin of the inertial frame, and its initial orientation is taken when the body fixed frame has the same orientation as the inertial frame. The vehicle accelerates from zero linear and angular velocities. The simulation time is 200 seconds.

Moving in a straight line

To move in a straight line only one input is needed, which is the thrust force (X_{thrust}). The applied thrust force at time zero is 150 N. Fig. 4.1 shows the position and the orientation of the vehicle with respect to the inertial frame, and the linear and angular velocities expressed in the body fixed frame.

At the beginning, the vehicle dives down a few centimeters then stabilizes to move in a straight line. The reason is that the line of action of the thrust force is along the axis that pass through the center of buoyancy, which is 5 cm above the center of gravity of the vehicle. Since the center of gravity is placed 5 cm below the center of buoyancy, self correcting moments are generated from the restoring forces (buoyancy and weight), so if the vehicle is pitching up or down, the self correcting moment will tend to return it to the zero pitch orientation. Therefore, the pitch angle goes to zero after a few seconds given the self correcting moments and the lift moments generated by the lift forces acting on the fins.

Moving in circles

The inputs needed for the vehicle to move in a circular motion are: thrust force (X_{Thrust}) and rudder angle (δ_r). 150 N thrust force and -5 degrees rudder angle are applied at time zero. The initial position and orientation of the vehicle with respect to the inertial frame are $\eta_0 = [0\ 0\ 0\ 0\ 0\ 0]^T$ and the initial velocity of the vehicle expressed in the body fixed frame is $\nu_0 = [0\ 0\ 0\ 0\ 0\ 0]^T$. The model is simulated for 200 seconds. Fig. 4.2 shows the position and the orientation of the vehicle with respect to the inertial frame, and the linear and angular velocities expressed in the body fixed frame.

Although in this mode (thrust mode) the vehicle is neutrally buoyant, it is observed that the vehicle dives down and traces a helix. This is due to banking effect since the center of gravity is positioned below the geometric center. The roll angle (ϕ), also called the banking angle is plotted as a function of the simulation time in Fig. 4.2d. As observed, the roll angle is about 2 degrees, which results in pitching the vehicle downwards by about 1 degree.

To avoid banking while moving in circles, input stern angles are applied to both the left and right stern fins to reduce the roll angle to zero. Angles of 1.86 degrees and -1.86 degrees are applied to the right and left stern fin, respectively, to eliminate diving due to banking. The results of the simulation are shown in Fig. 4.3. As observed from Fig. 4.3a the vehicle moves in circles without diving, and no banking occurs because the roll angle (ϕ) is reduced to zero as shown in Fig. 4.3d. It is also observed that the vehicle dives at the beginning then the pitch angle reduces to zero (Fig. 4.3d). This is because of the same reason discussed in the "moving in a straight line" case.
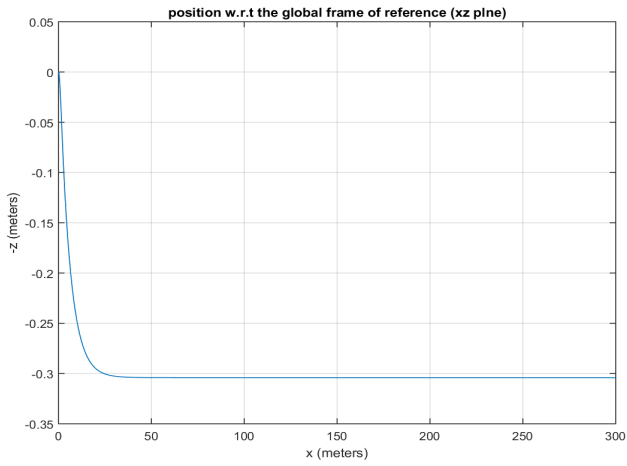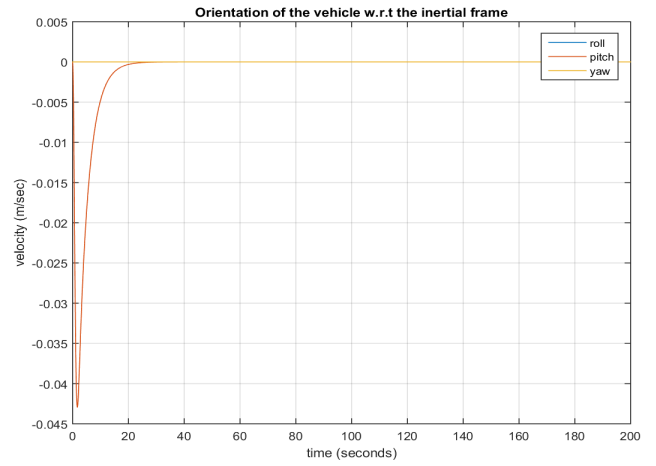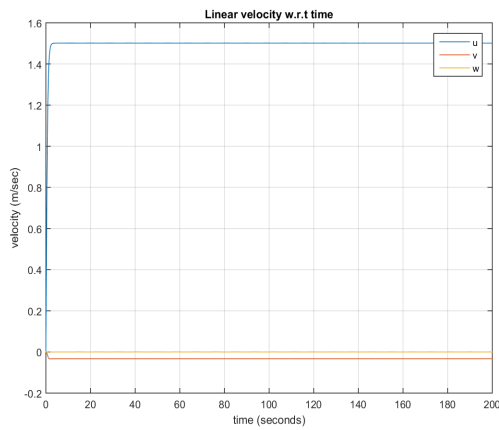
(a) Position with respect to the global frame of reference

(b) Orientation with respect to the global frame of reference
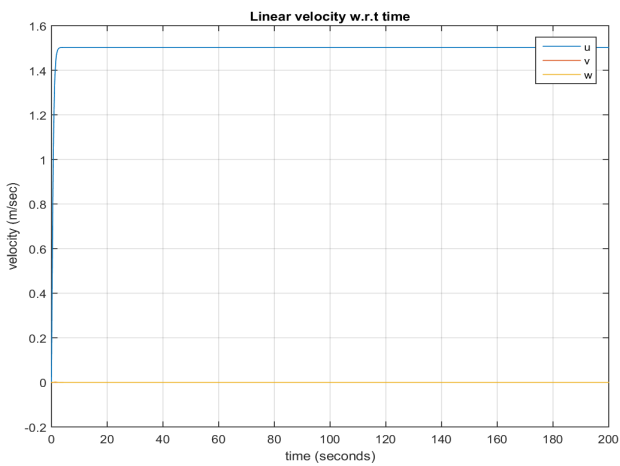
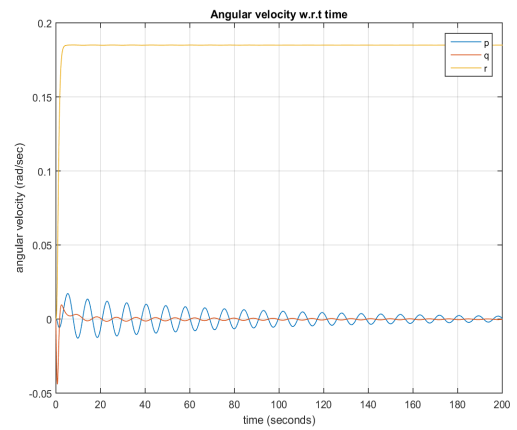(c) Linear velocity expressed in the body fixed frame
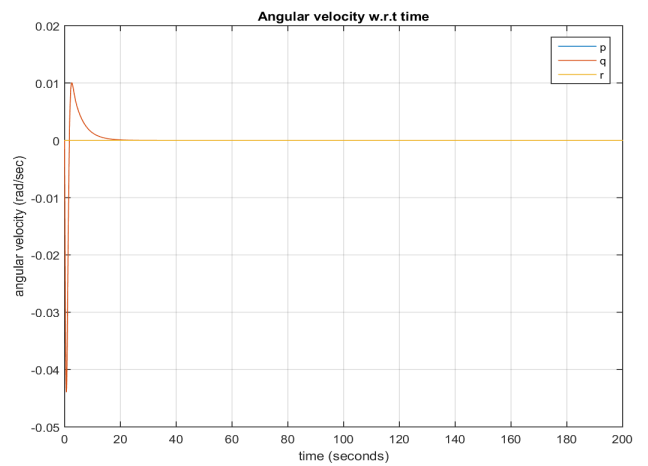
(d) Angular velocity expressed in the body fixed frame

Figure 4.1: Position and orientation with respect to the inertial frame and linear and angular velocity expressed in the body-fixed frame for the moving in straight line case
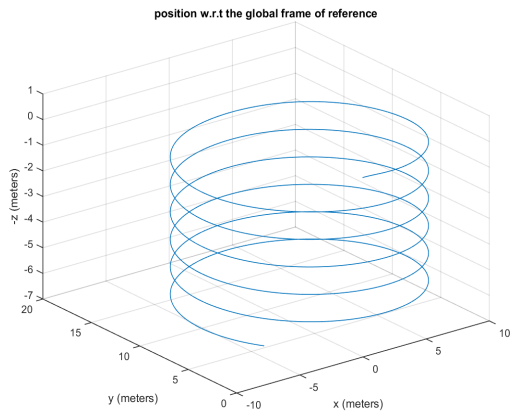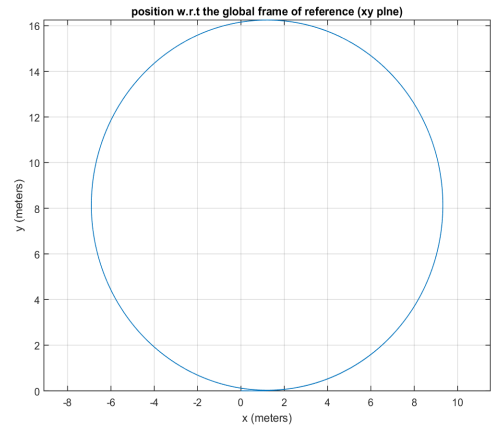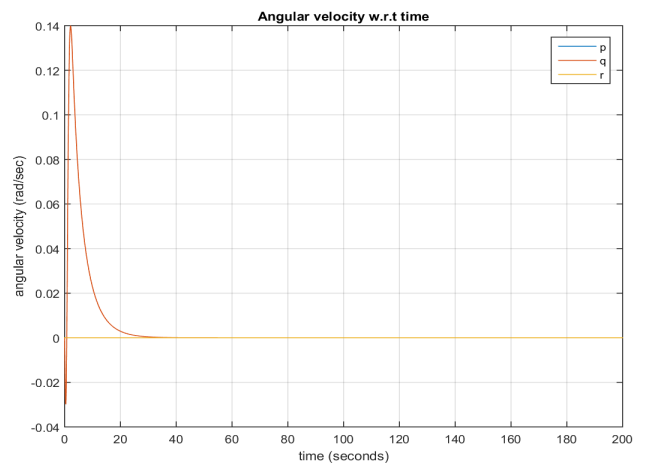
(a) Position with respect to the global frame of reference

(b) Position with respect to the global frame of reference (XY plane
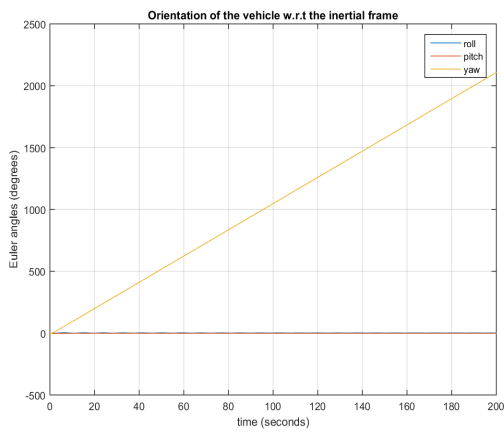
(c) Orientation with respect to the global frame of reference
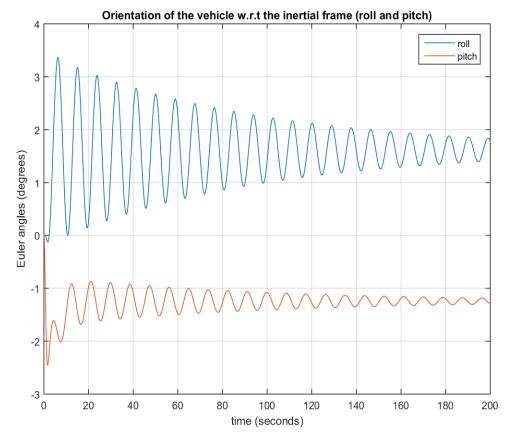
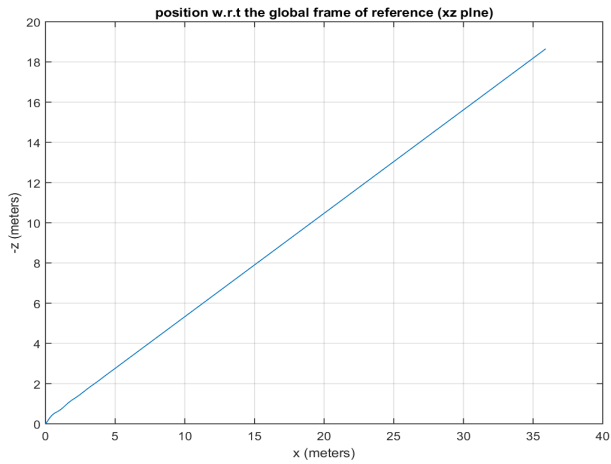(d) Roll and pitch angles with respect to the global frame of reference
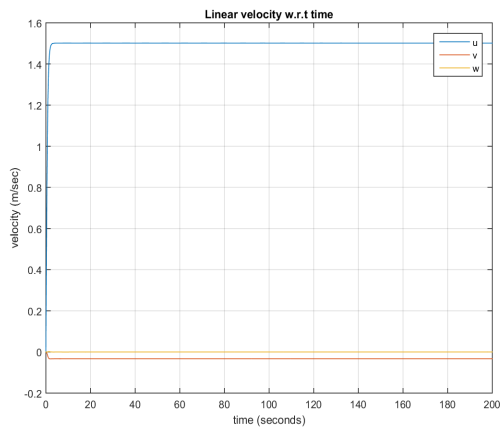
(e) Linear velocity expressed in the body fixed frame
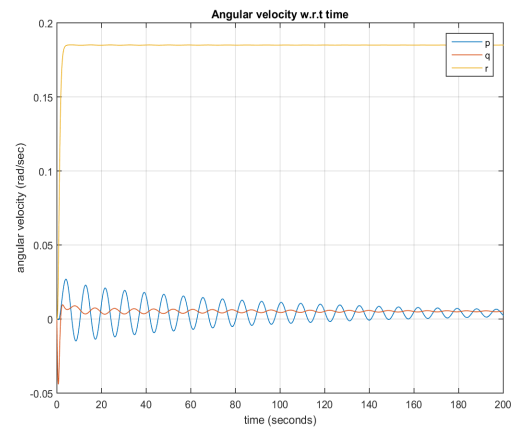
(f) Angular velocity expressed in the body fixed frame

Figure 4.2: Position and orientation with respect to the inertial frame and linear and angular velocity expressed in the body-fixed frame for moving in circles case with banking
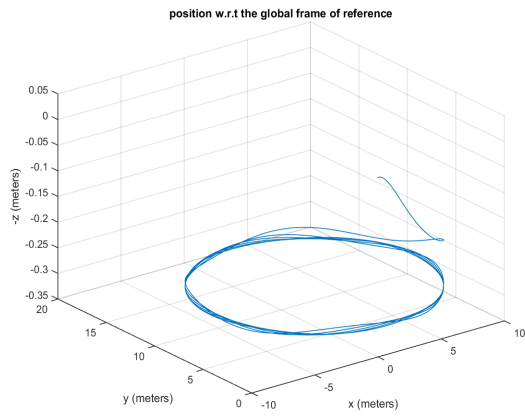
(a) Position with respect to the global frame of reference
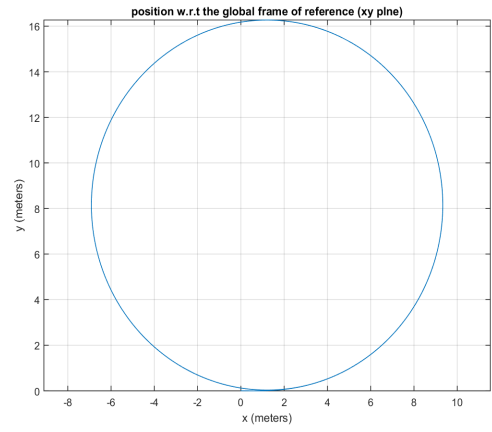
(b) Position with respect to the global frame of reference (XY plane)
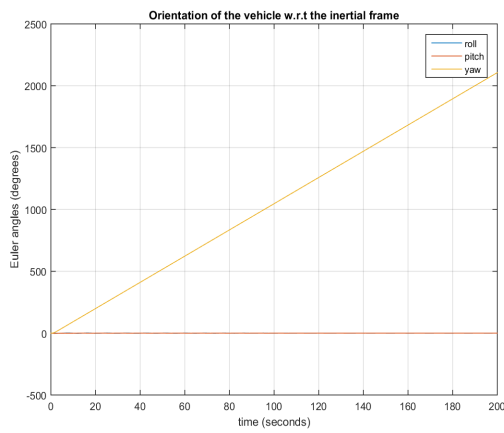
(c) Orientation with respect to the global frame of reference
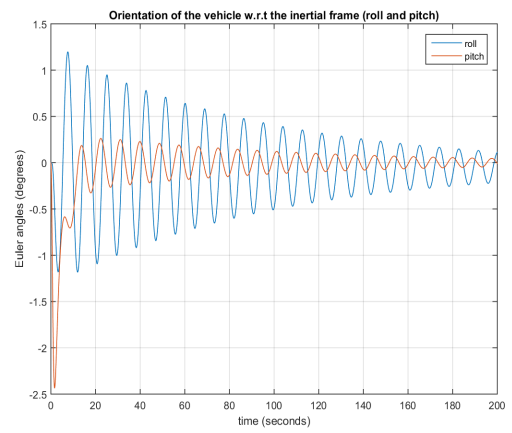
(d) Roll and pitch angles with respect to the global frame of reference

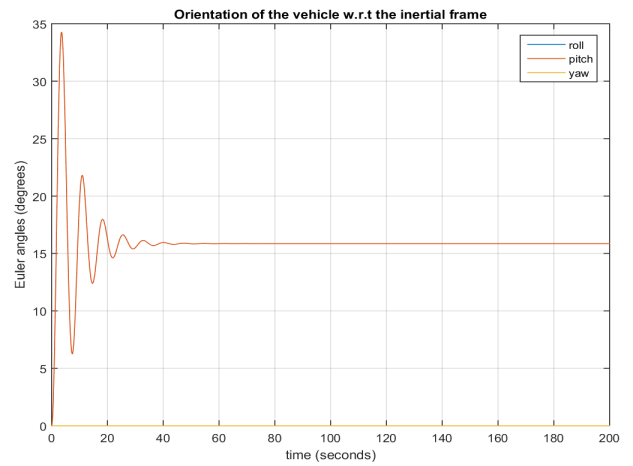(e) Linear velocity expressed in the body fixed frame

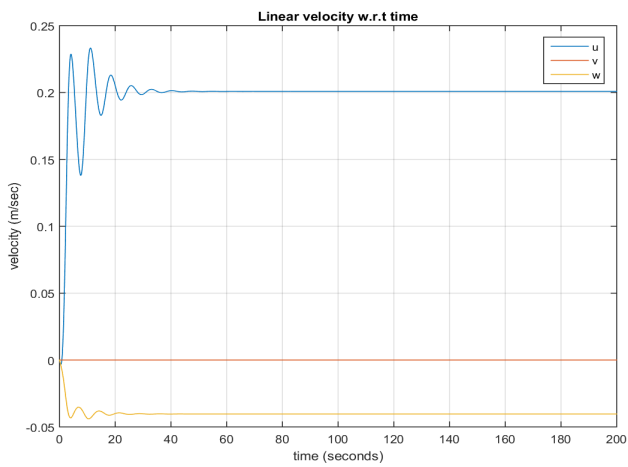(f) Angular velocity expressed in the body fixed frame

Figure 4.3: Position and orientation with respect to the inertial frame and linear and angular velocity expressed in the body-fixed frame for moving in circles case without banking

Floating up and diving down

To float up or dive down, only the thrust force (X_{Thrust}) and the stern angles of the right and left stern fins ($\delta_{s,right}$ and $\delta_{s,left}$) are needed as inputs. 150 N thrust force and -5 degrees (+5 degrees) stern angle are applied at time zero in order to float up (dive down). The initial position and orientation of the vehicle with respect to the inertial frame are $\eta_0 = [0\ 0\ 0\ 0\ 0\ 0]^T$ and the initial velocity of the vehicle expressed in the body fixed frame is $\nu = [0\ 0\ 0\ 0\ 0\ 0]^T$. The model is simulated for 200 seconds. The results for the floating up case are shown in Fig. 4.4.

4.1.2 Gliding Mode

In this mode, no thrust is applied and the propeller is turned off. The buoyancy of the vehicle is varied by pumping sea water in and out of the vehicle. The mass of the vehicle (M) becomes an input to the vehicle. Three cases are simulated: floating up (diving down) when the vehicle is positively (negatively) buoyant, floating up (diving down) with rudder angle, and moving forward in a saw-tooth shape path.

Floating up (diving down)

To float up (dive down) the mass (M) of the vehicle is set to be 71.5 Kg (73.5 Kg) at time zero, the center of mass of the vehicle is shifted to the back (front) in the x-direction, which cause the vehicle to pitch up (down). The initial position and orientation of the vehicle with respect to the inertial frame are $\eta_0 = [0\ 0\ 0\ 0\ 0\ 0]^T$ and the initial velocity of the vehicle expressed in the body fixed frame is $\nu_0 = [0\ 0\ 0\ 0\ 0\ 0]^T$. The model is simulated for 200 seconds. The results for the floating up case are shown in Fig. 4.5.

Floating up (diving down) with rudder angle

In this case, there are two inputs, the mass of the vehicle (M) and the rudder angle (δ_r). To float up (dive down) while moving in circles, the mass (M) of the vehicle is set to be 71.5 Kg (73.5 Kg) and a -5 degrees rudder angle is applied to the rudder fins at time zero. The initial position and orientation of the vehicle with respect to the inertial frame are $\eta_0 = [0\ 0\ 0\ 0\ 0\ 0]^T$ and the initial velocity of the vehicle expressed in the body fixed frame is $\nu_0 = [0\ 0\ 0\ 0\ 0\ 0]^T$. The model is simulated for 1000 seconds. The results for the floating up case are shown in Fig. 4.6. Note that the results in Fig. 4.6 are different than the results in Fig. 4.2, since in the case of Fig.4.6 the propeller is off and the vehicle's forward velocity ($0.2m/sec$) is slower than that in the case of Fig. 4.2 in which the propeller is on and the vehicle's forward velocity is $1.5m/sec$.
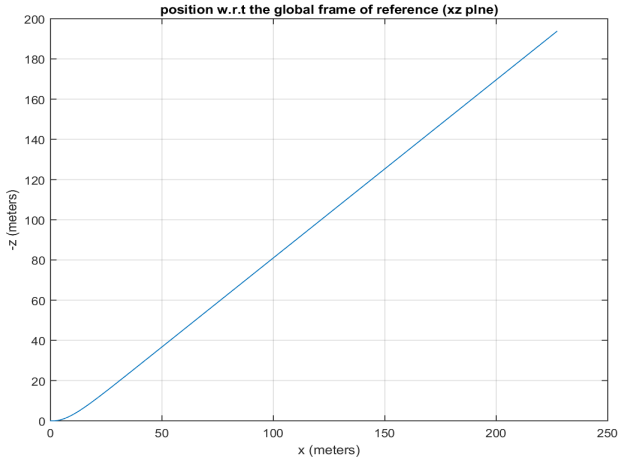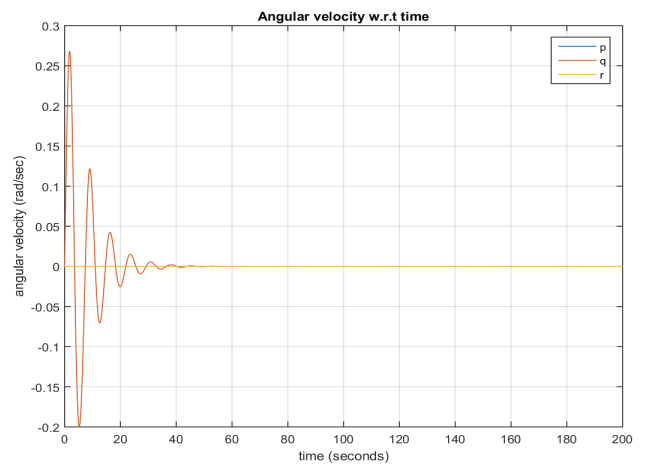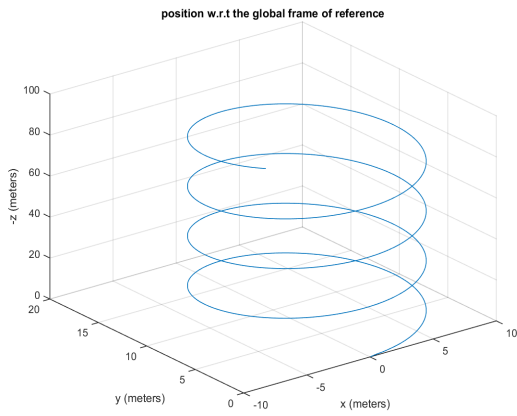
(a) Position with respect to the global frame of reference (XZ plane)
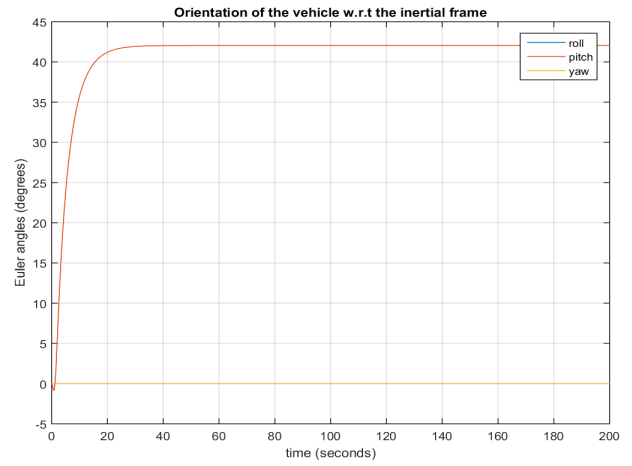
(b) Orientation with respect to the global frame of reference
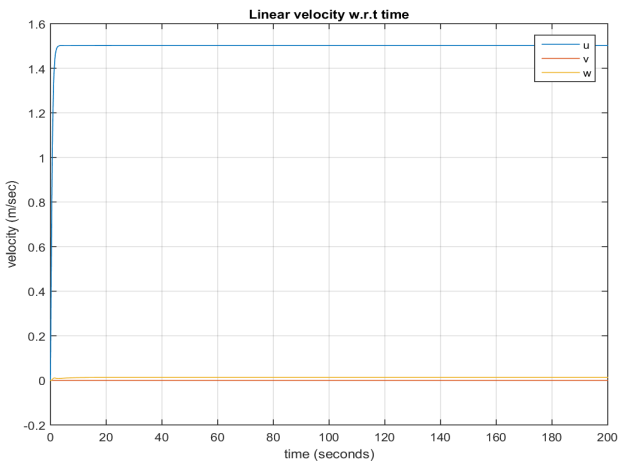
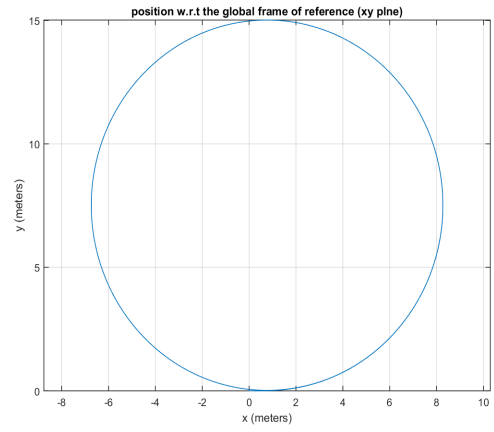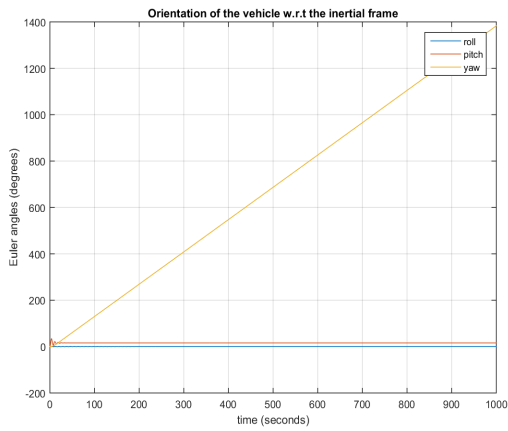(c) Linear velocity expressed in the body fixed frame

(d) Angular velocity expressed in the body fixed frame

Figure 4.4: Position and orientation with respect to the inertial frame and linear and angular velocity expressed in the body-fixed frame for the floating up case
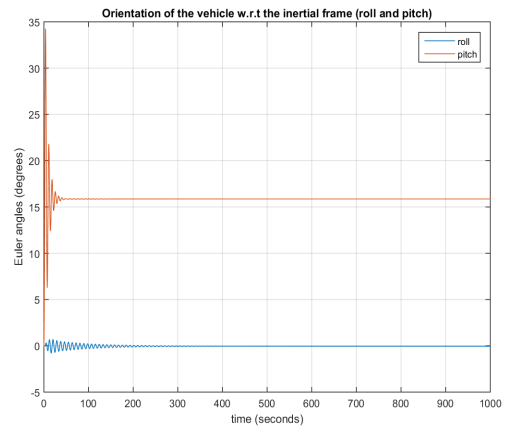
49
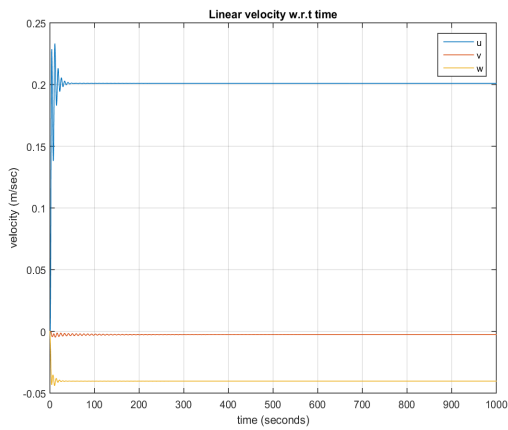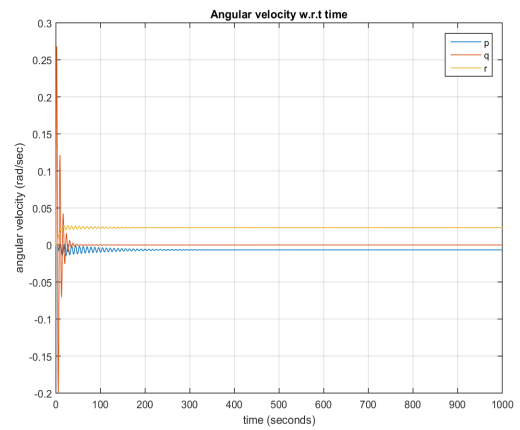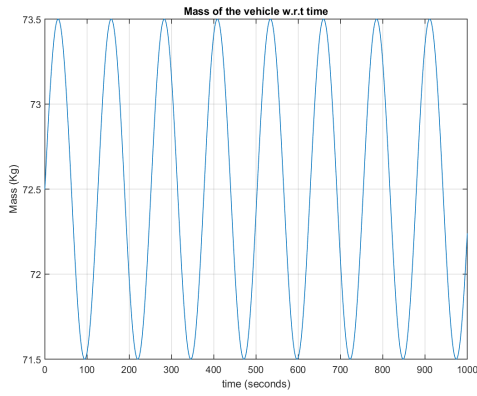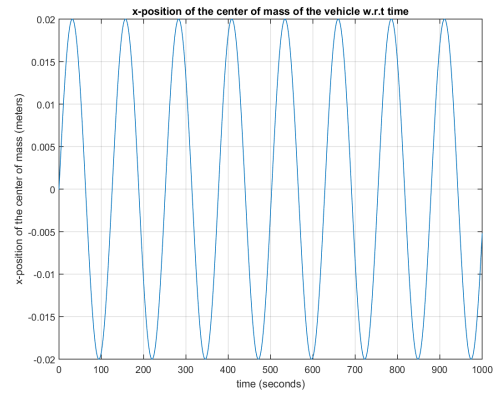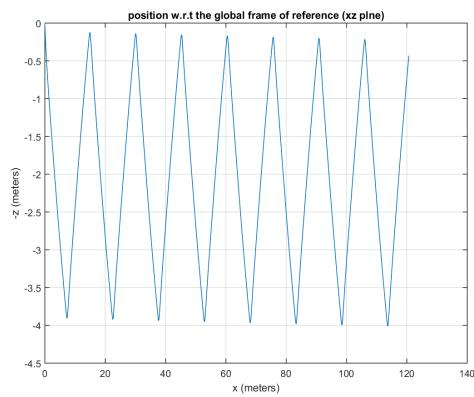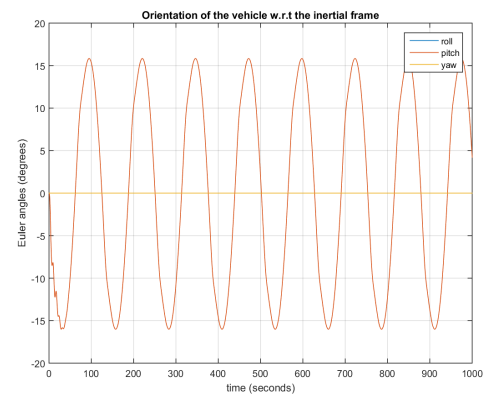
(a) Position with respect to the global frame of reference (XZ plane)

(b) Orientation with respect to the global frame of reference

(c) Linear velocity expressed in the body fixed frame

(d) Angular velocity expressed in the body fixed frame

Figure 4.5: Position and orientation with respect to the inertial frame and linear and angular velocity expressed in the body-fixed frame for the floating up case in gliding mode

(a) Position with respect to the global frame of reference

(b) Position with respect to the global frame of reference (XY plane)

(c) Orientation with respect to the global frame of reference

(d) Roll and pitch angles with respect to the global frame of reference

(e) Linear velocity expressed in the body fixed frame

(f) Angular velocity expressed in the body fixed frame

Figure 4.6: Position and orientation with respect to the inertial frame and linear and angular velocity expressed in the body-fixed frame for the floating up while moving in circles case

(a) Mass of the vehicle with respect to time

(b) x-position of the center of mass of the vehicle with respect to time

(c) Position with respect to the global frame of reference (XY plane)

(d) Orientation with respect to the global frame of reference
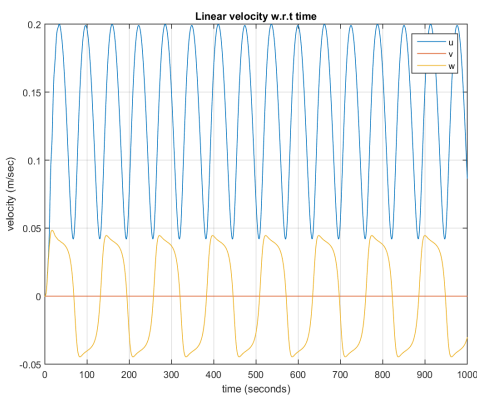
(e) Linear velocity expressed in the body fixed frame
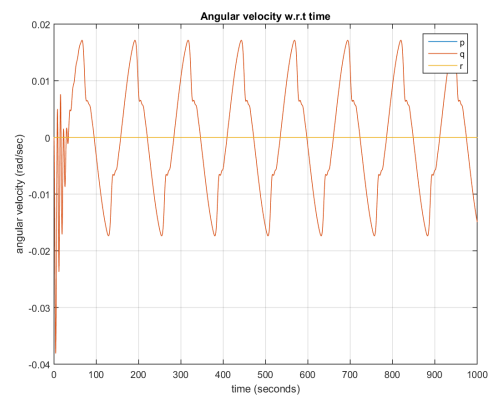
(f) Angular velocity expressed in the body fixed frame

Figure 4.7: Moving in a saw-tooth path

Moving forward in a saw-tooth path

In this case, the only one input to the system is the mass (M) of the vehicle. In order to move in a saw tooth path, the mass of the vehicle is changed in a sinusoidal wave fashion offsetted at 72.5 Kg and varies between 71.5 Kg and 73.5 Kg. The position of the center of gravity in the x-direction of the body fixed frame is related to the mass of the vehicle and it is also changed in a sinusoidal wave fashion and varies between -2 cm and 2 cm from its position at 0 cm when the vehicle is neutrally buoyant. The mass of the vehicle and the x-position of its center of mass with respect to time are shown in Fig. 4.7a and Fig. 4.7b, respectively. The simulation time is 1000 seconds, and the results are shown in Fig. 4.7.

4.2   Simulation of the Linear Model and Comparing it with the Nonlinear Model

The nonlinear model is given certain known inputs, and the resultant trajectory $(\eta_1(t) = [x(t),\ y(t),\ z(t)]^T)$ is recorded and used to linearize the model about it. Then, the same inputs that are applied to the nonlinear model, are applied to the linearized model, and the results of both models are compared. Three cases are considered: moving in a straight line, diving down, and moving in circles.
As observed in Fig. 4.8a, 4.9a, 4.10a, and 4.10b, the linear model follows the desired trajectory generated by applying known inputs to the nonlinear model, with a small error occurring at the beginning of the simulation. The error does not disappear, because the inputs are not controlled. Fig. 4.8b, 4.8c, 4.9b, and 4.9c show the pitch angle and the pitch rate of the vehicle for the moving in a straight line and the diving cases. Fig. 4.10c, and 4.10d show the pitch and the yaw angles of the vehicle for the moving in circles case.
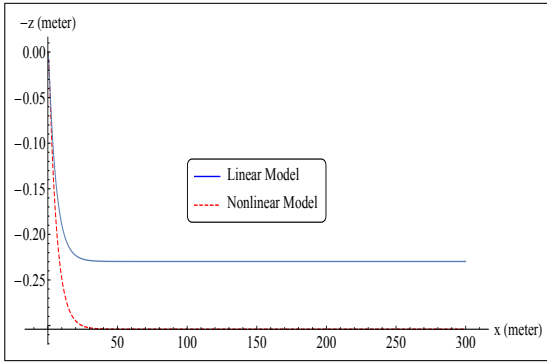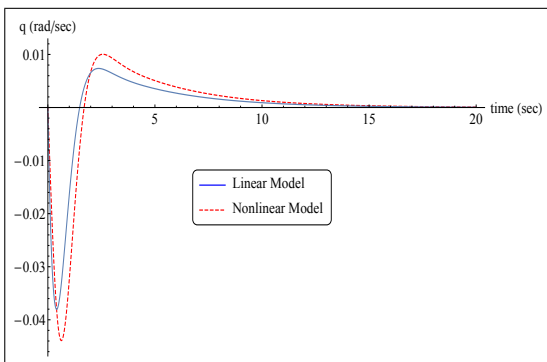
(a) Position with respect to
the inertial frame for the
moving in a straight line case
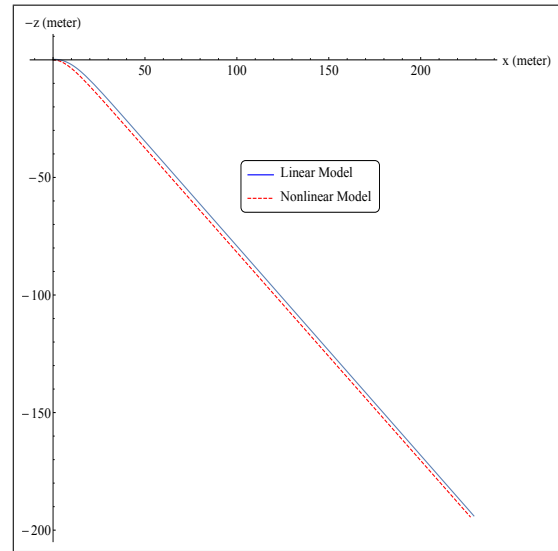(Diving Plane)
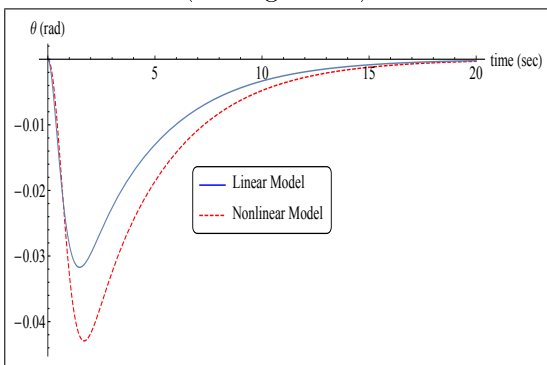
(b) Pitch angle with respect to
the inertial frame for the
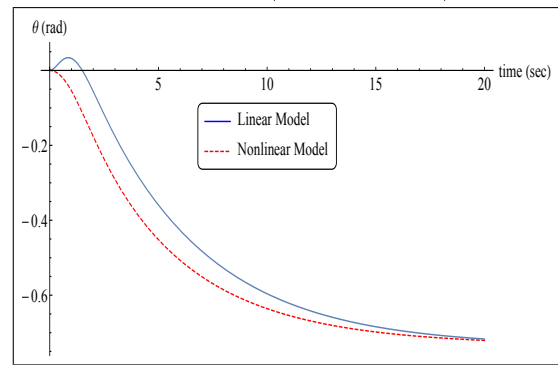moving in a straight line case

(c) Pitch rate expressed in the
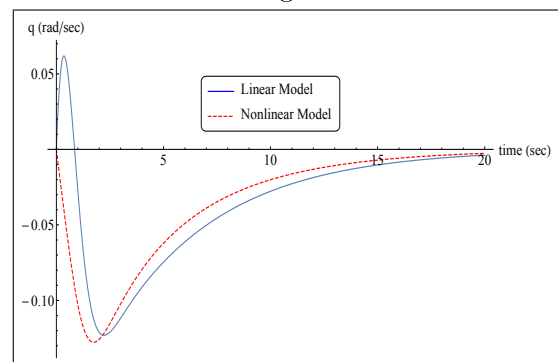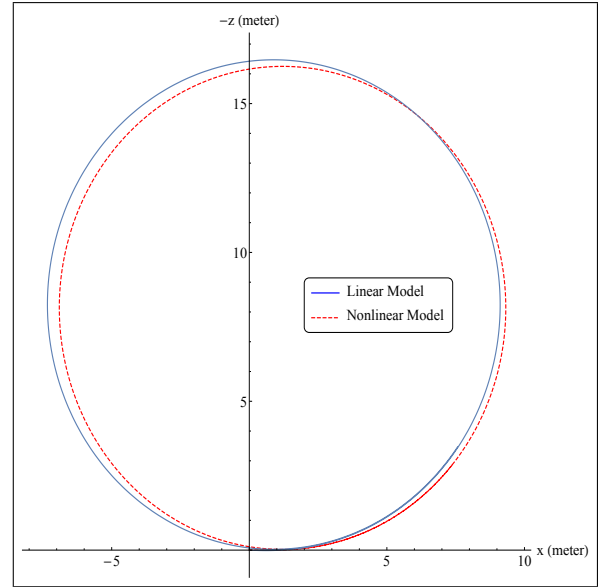body-fixed frame for the
moving in a straight line case

Figure 4.8: Comparing the open loop
simulation of the nonlinear model with
the linear model for the moving in
a straight line case.

(a) Position with respect to
the inertial frame for the
diving case (Diving Plane)

(b) Pitch angle with respect to
the inertial frame for the
diving case

(c) Pitch rate expressed in the
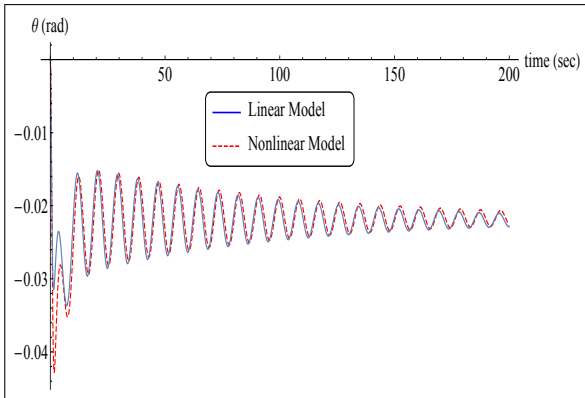body-fixed frame for the
diving case

Figure 4.9: Comparing the open loop
simulation of the nonlinear model with
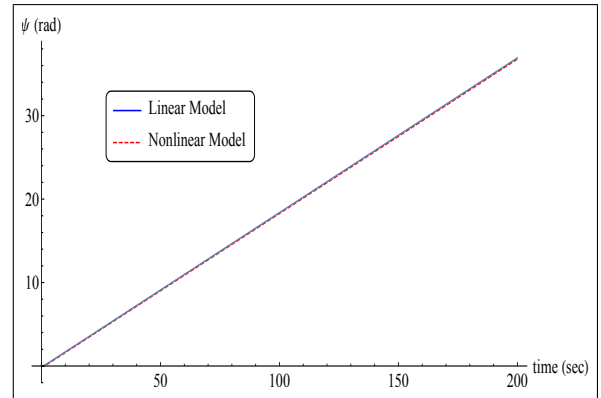the linear model for the diving case.
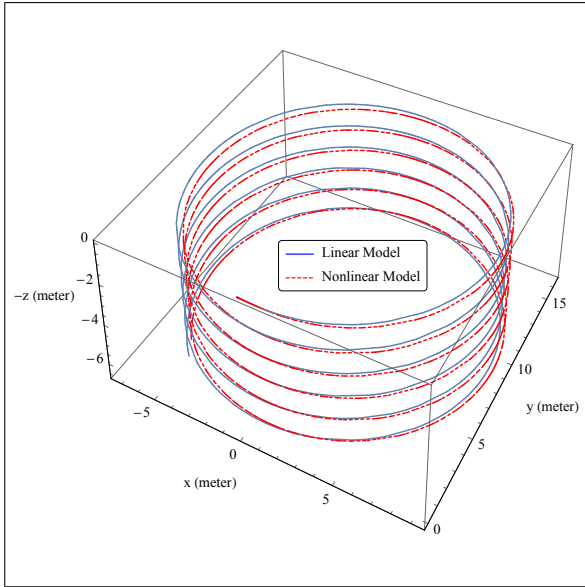
(a) Moving in circles

(b) Moving in circles (Steering Plane)

(c) Pitch angle (Moving in circles)

(d) Yaw angle (Moving in circles)

Figure 4.10: Comparing the open loop simulation of the nonlinear model with the linear model for the moving in circles case.

4.3 Closed Loop Simulation

The main target of this work is to command the AUV to track optimal 3D Dubin's trajectory generated using the method in [23] in thrust mode, which mainly consists of five parts in the following order: constant pitch helix, variable pitch helix, straight line, helix with a variable pitch, and then a helix with a constant pitch; and to track a saw-tooth trajectory with curved tips. To test the linear controller, three trajectories are used for the simulation: constant pitch helix, which resembles the first and the last portion of the 3D Dubin's trajectory; the entire 3D Dubin's trajectory, which are used to check the controller in the thrust mode; and a saw-tooth path, which corresponds to the gliding mode. In each case, the desired trajectory is considered as an input for Algorithm (1) and the nonlinear system in (3.2) is linearized about it. A LQR control law is designed based on the linearized system and is applied to the nonlinear model in (3.2) to track the desired trajectory. To validate the linear controller, a helix trajectory is recorded
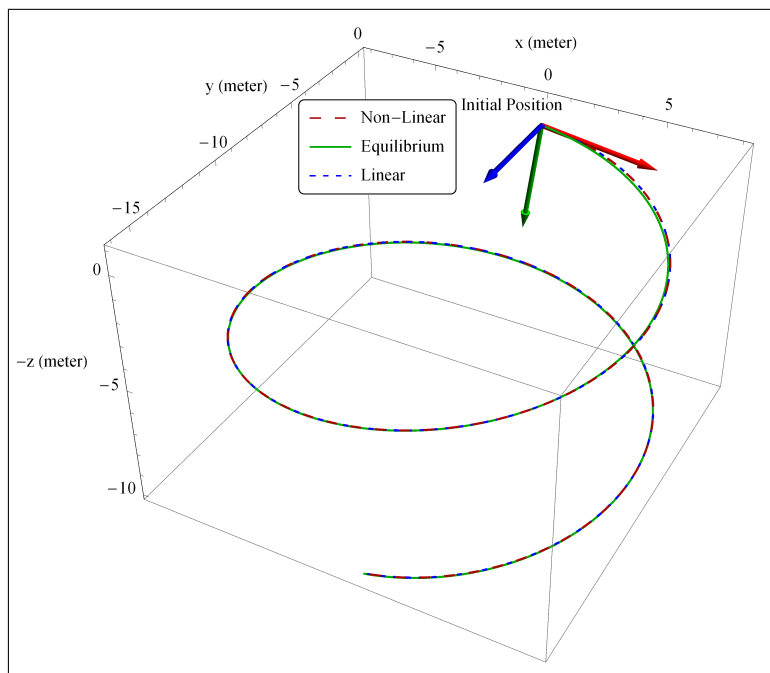

Figure 4.11: Helix Trajectory following

from open loop simulation of the nonlinear model when applying known inputs to it. This recorded trajectory of the helix is considered the desired trajectory. The open loop inputs, which are used to generate the helix trajectory from the nonlinear model, are compared to the LQR control inputs obtained from the linearized system about the helix trajectory.
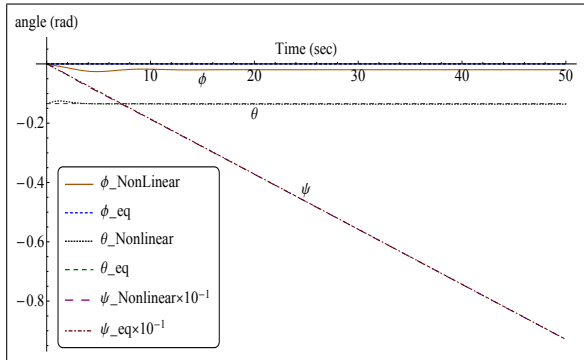
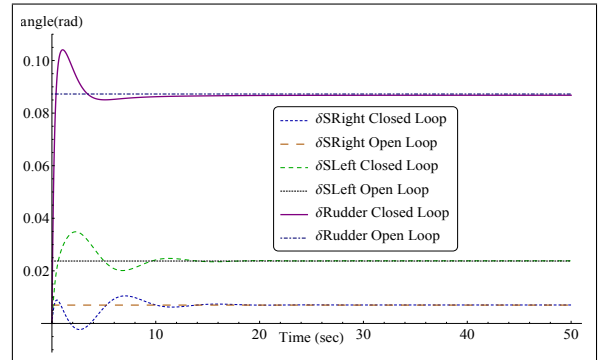Figure 4.12: Equilibrium and actual Euler angles (Helix trajectory following)

Figure 4.13: Open loop and closed loop inputs (Helix trajectory following)

The 3D Dubin's trajectory is generated using the method in [23]. The sawtooth path is chosen arbitrarily to be a curve in the diving plane that has a shape of saw teeth but with curved tips. This curve consists of straight lines, and variable pitch portions. The simulation of the linear and the nonlinear models tracking the helix, the 3D Dubin, and the saw-tooth trajectories are shown in Fig. 4.11, 4.14, and 4.17, respectively.

Since in [23] the optimal trajectory is generated given the initial and final position and orientation of the vehicle, the initial position of the vehicle is set at the starting point of the desired curve and oriented along the {FS} of the desired trajectory at time to zero in the three simulation cases.

In Fig. 4.11, the nonlinear model perfectly follows the helix trajectory (the paths of the linear and nonlinear models are on top of the desired path) with a small error at the beginning of the trajectory. This is because the actual roll angle deviates from the desired value, see Fig. 4.12, which affects the actual pitch angle (since the model is coupled) and causes a small error in the pitch angle of the vehicle in the first five seconds of the simulation. However, the pitch angle converges to the desired value, and the vehicle tracks the desired trajectory as shown in Fig. 4.11. The roll angle does not converge to its desired value because the center of mass of the vehicle is designed to be lower than the geometric center of the vehicle by 5 cm. When steering, the vehicle is forced to bank due to the centrifugal forces acting on the center of mass, which creates a roll moment about the longitudinal axis of the vehicle. However, this error does not affect the tracking of the trajectory, because the feedback control inputs, shown in Fig. 4.13, correct the pitch and yaw angles after their deviation from the desired value. Unlike the
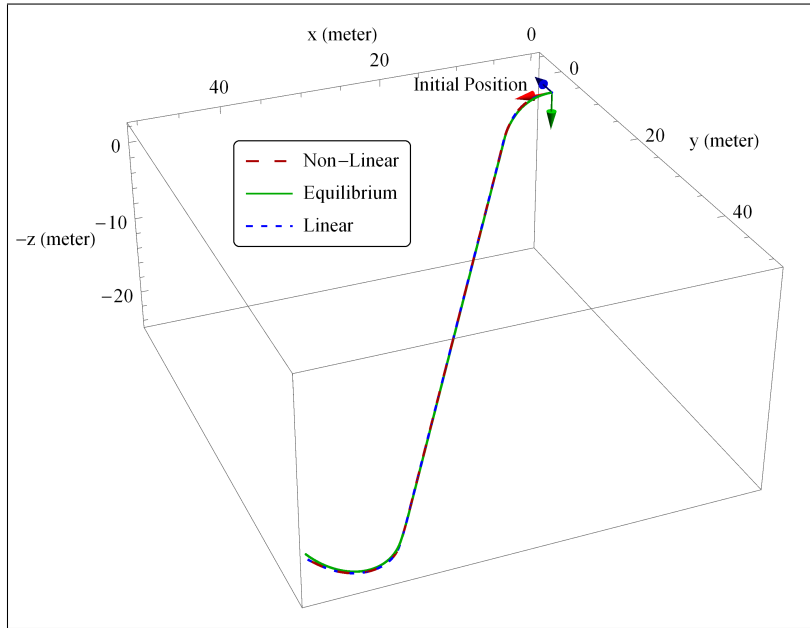
57

Figure 4.14: 3D Dubin's Trajectory tracking

results of the decoupled model in [12], the feedback controller in this work avoids conflicting control inputs, which can be observed in Fig. 4.13 where the right and the left stern angles are symmetric to each other with respect to 0.015 rad. The stern fins control the roll angle to be approximately zero (desired roll angle) while pitching the vehicle to the desired pitch angle. The input control signals applied to the nonlinear model converge to the open loop inputs used to generate the desired helix trajectory from open loop simulation. These simulation results show that the feedback control law derived from the linearized model, results in a satisfactory performance when applied to the nonlinear model.

In the case of tracking the 3D Dubin's trajectory, shown in Fig. 4.14, similar effects as in the first case occurs at the helix portion. The pitch and roll angles deviate from the desired values because of banking during steering. The actual pitch angle converges to the desired value after about 3 seconds since the beginning of the simulation, as shown in Fig. 4.15. Another deviation from the desired values for the Euler angles occurs at the transition between the helix and the straight line portions, as shown in Fig. 4.15 at time 4 seconds and 42 seconds. In Fig. 4.16, the control input angles of the fins change abruptly after each transition between the five portions of the Dubin's curve, in order to correct the deviation in the actual Euler angles from their desired values.

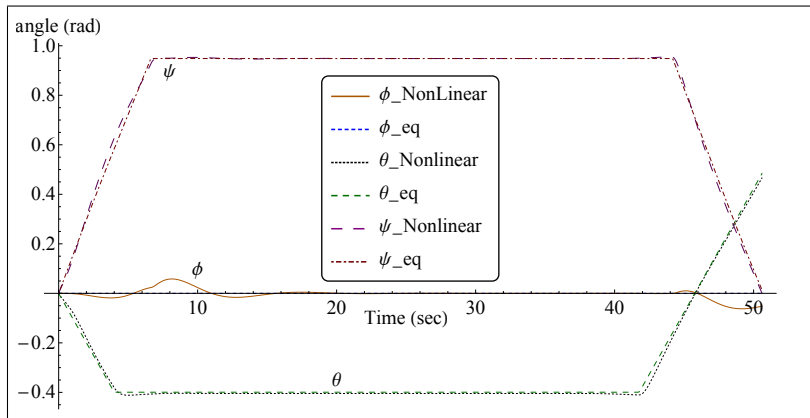In Fig. 4.17 the nonlinear model follows the first straight line portion of the

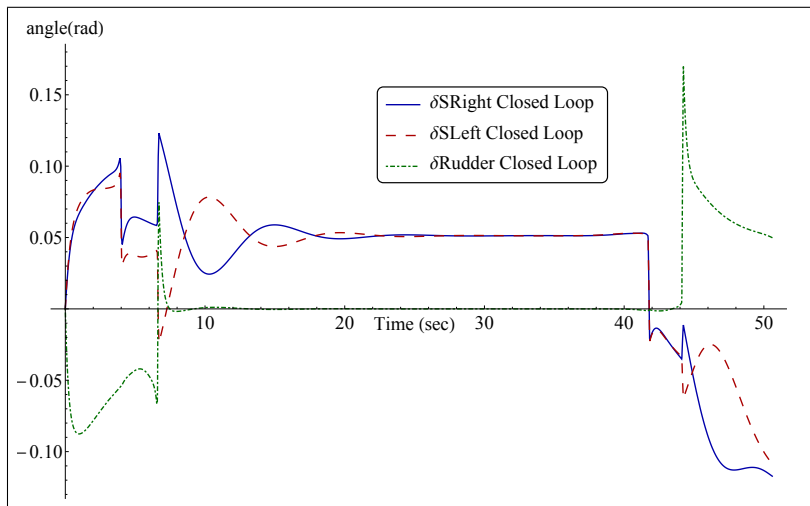Figure 4.15: Equilibrium and actual Euler angles (3D Dubin's Trajectory tracking)

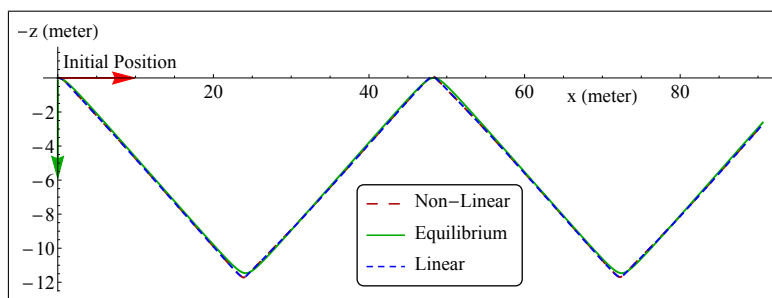Figure 4.16: Control inputs (3D Dubin's Trajectory tracking)
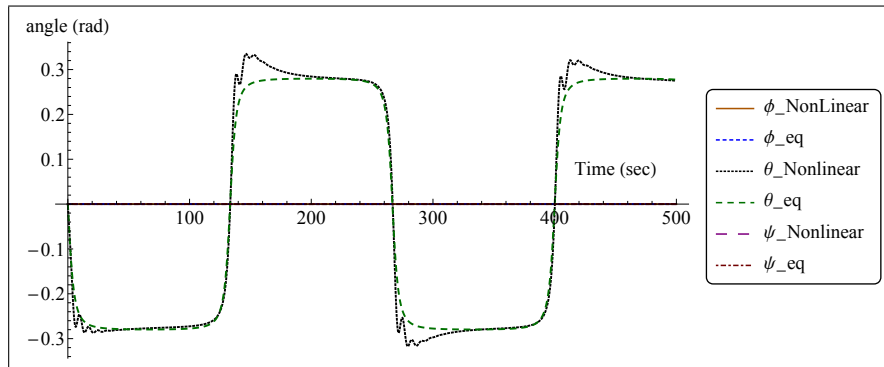

Figure 4.17: Saw-tooth Trajectory tracking

Figure 4.18: Equilibrium and actual Euler angles (Saw-tooth Trajectory tracking)
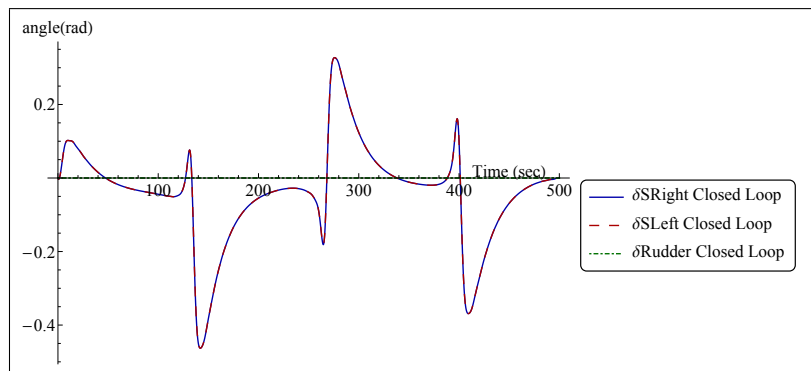

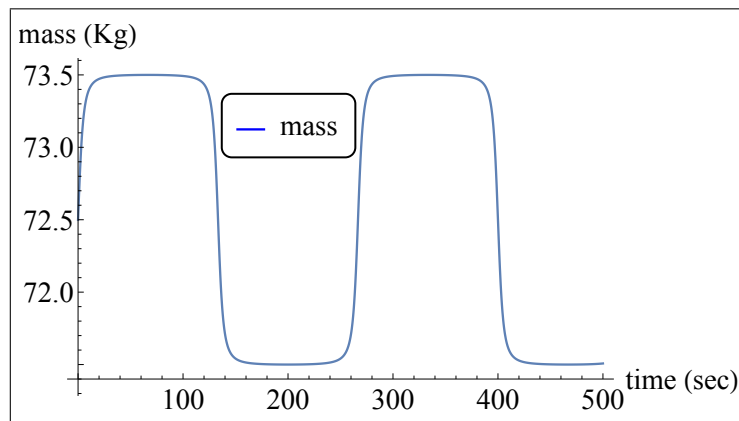Figure 4.19: Control inputs (Saw-tooth Trajectory tracking)

Figure 4.20: Mass of the vehicle

saw-tooth path, then it deviates from the desired trajectory after crossing the curved tip, where the desired pitch angle changes, as shown in Fig. 4.18. However, the actual position and pitch angle of the vehicle converge to the desired values
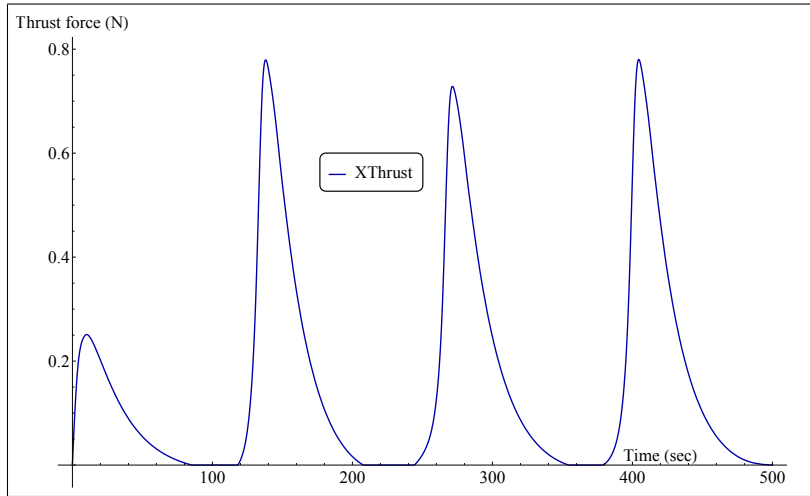
Figure 4.21: XThrust input

about 40 seconds after the deviation, which occurs when the desired trajectory changes from a straight line to a curve at each tip. The control angles of the stern fins change abruptly at each transition between a straight line and a curve, as shown in Fig. 4.19, in order to correct the pitch angle to follow the rapidly changing desired pitch. Fig. 4.20 shows the mass of the vehicle as a function of time. Fig. 4.21 shows the thrust force exerted by the propeller, as observed the force is almost zero, which validates the robustness of the controller on deciding autonomously which mode of operation to use based on the given trajectory.

4.4   Closed Loop Simulation with Disturbance

The trajectories that are used in the simulation are the same trajectories that are used in the previous simulation, which are: helix with a constant pitch and a 3D Dubin curve for thrust mode, and saw-tooth trajectory for the gliding mode. In each case, the desired trajectory is considered an input for Algorithm (1) and the nonlinear system in (3.2) is linearized about it. A LQR control law is designed based on the linearized model and is applied to the nonlinear model with disturbance in (3.1) to investigate the robustness of the controller in the presence of disturbance.

4.4.1   Tracking a Helix with constant pitch

The same helix trajectory used in the previous simulation is used again. Fig. 4.22 shows the tracking of the helix in the presence of a force field in the y-direction of the global frame {U}, where $\delta D = [0,\ 225N,\ 0]^T$. The disturbance

61

starts 15 seconds after the beginning of the simulation. Fig. 4.22 shows that when the disturbance is applied, the vehicle deviates by a small distance from the equilibrium trajectory then converges to the desired trajectory. However, it
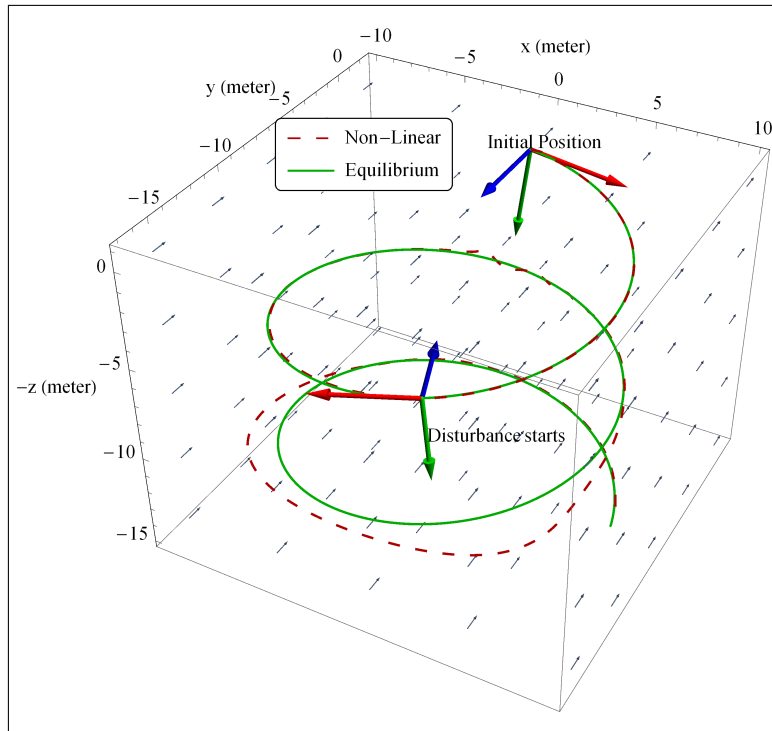

Figure 4.22: Helix Trajectory tracking in the presence of underwater current in the y direction with respect to the global frame {U}
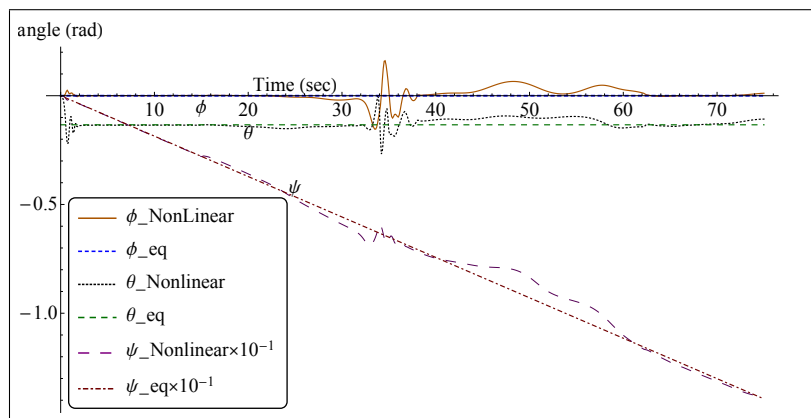

Figure 4.23: Equilibrium and actual Euler angles (Helix with disturbance in the y-direction)
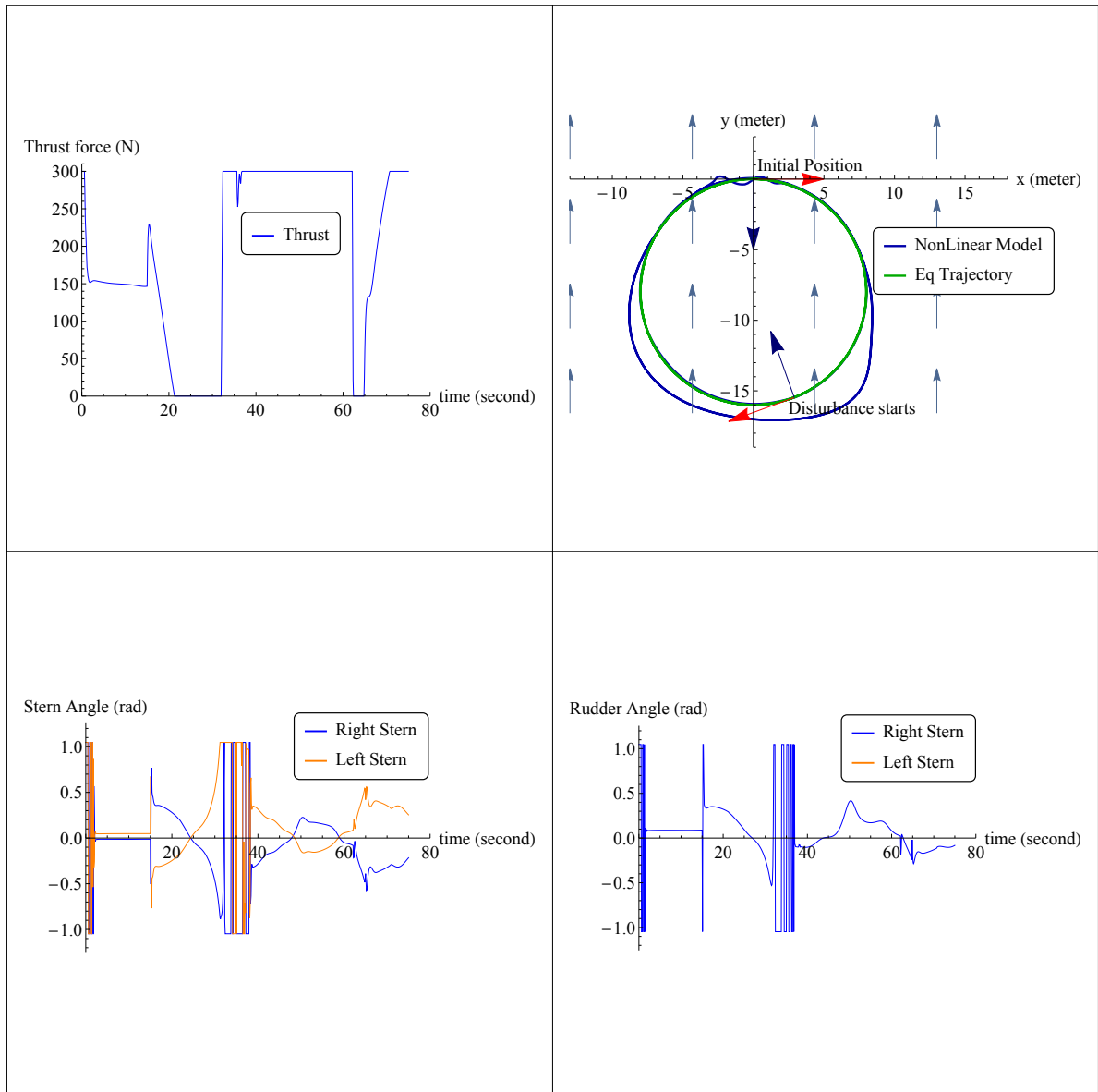
Figure 4.24: Helix Trajectory tracking (steering plane) along with the inputs (Thrust force, rudder and stern angles) as a function of time in the presence of constant underwater flow in the y-direction with respect to the global frame {U}

is observed that the vehicle is struggling when it moves upstream the current, it almost diverges from the equilibrium trajectory, but then it converges when it travels downstream the underwater current. The same can be observed for the

Euler angles in Fig.4.23. Fig. 4.24 shows the tracking of the trajectory in the steering plane, and the inputs of the vehicle (thrust force, and the rudder and the stern angles) as a function of time. As observed, the thrust force goes to maximum when the vehicle is traveling upstream the underwater current to counter it and
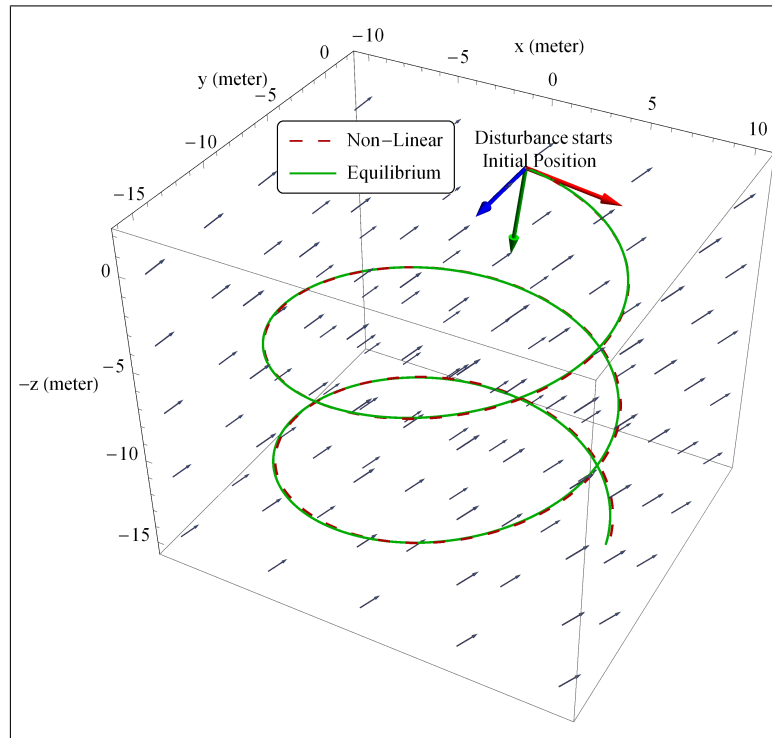

Figure 4.25: Helix Trajectory tracking in the presence of variable underwater current
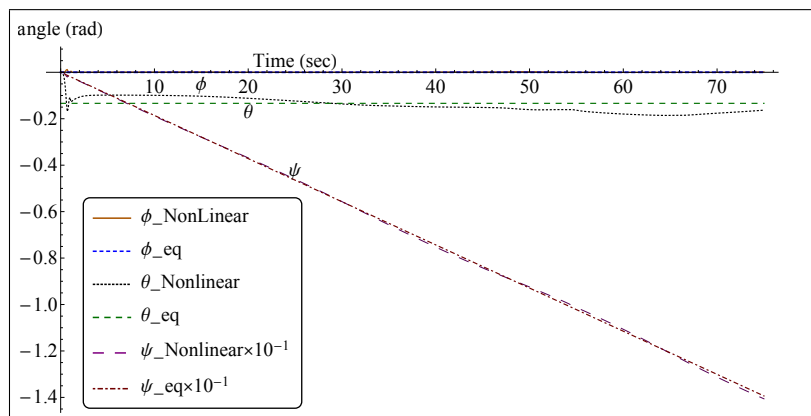

Figure 4.26: Equilibrium and actual Euler angles (Helix with variable disturbance)

64
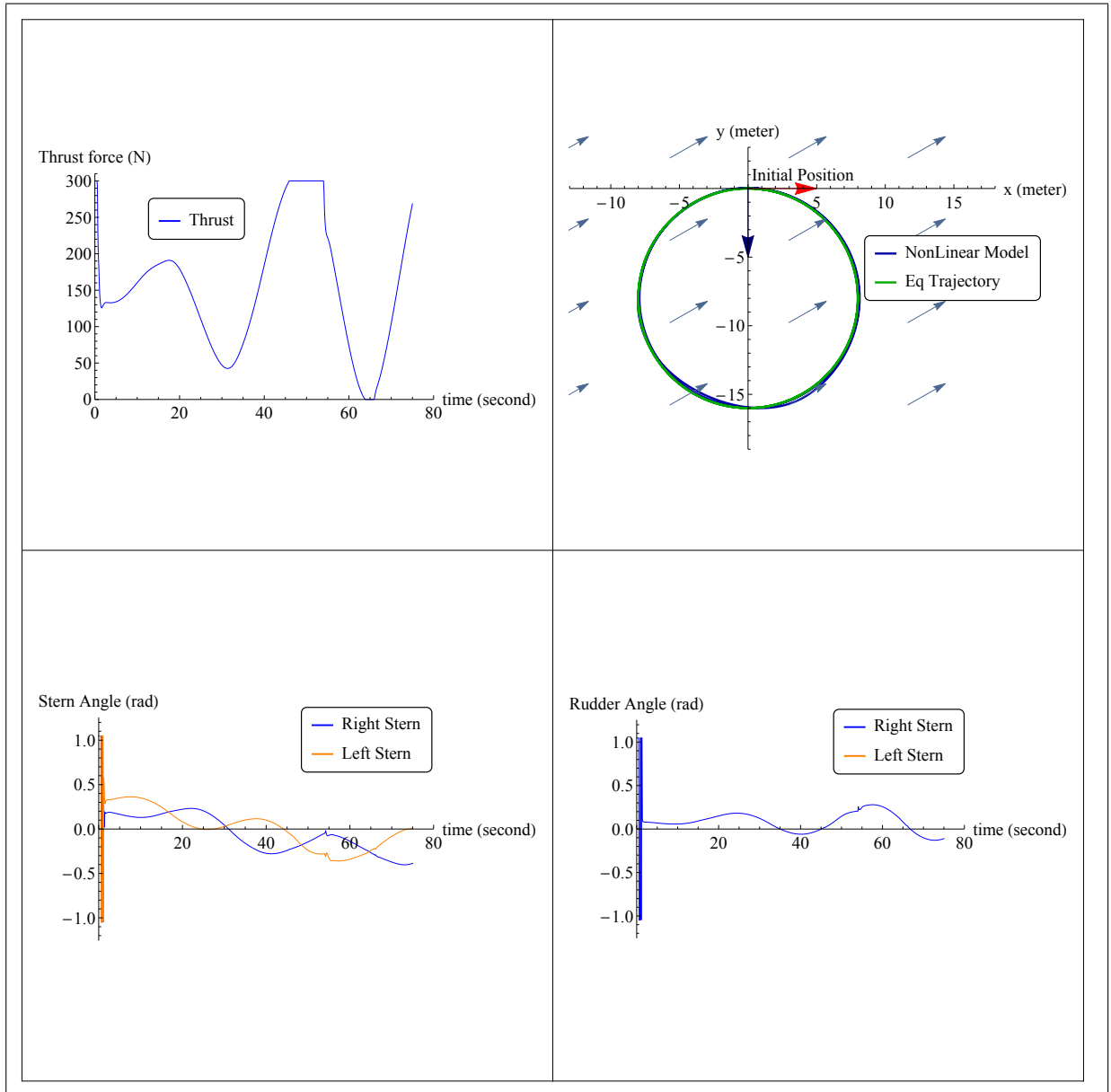
Figure 4.27: Helix Trajectory tracking (steering plane) along with the inputs (Thrust force, rudder and stern angles) as a function of time in the presence of variable underwater current

to maintain the desired velocity, and when the vehicle is traveling downstream the underwater current, it turns off the propeller to be driven by the underwater current. The rudder and the stern angles in Fig. 4.24 fluctuate rapidly when the vehicle is moving against the underwater current in order to maintain the desired

orientation and position of the vehicle.

Fig. 4.25 shows the tracking of the helix trajectory in the presence of a variable force field that varies in magnitude and direction with time, where $\delta D = [160 \times sin(0.02t), 160 \times sin(0.01t), 160 \times sin(0.05t + \frac{\pi}{2})]^T$. The disturbance starts at time zero. It is observed in Fig. 4.25 that the vehicle tracks the desired trajectory. In Fig. 4.26 it is shown that the actual Euler angles converge to the desired values. Fig. 4.27 shows the tracking of the trajectory in the steering plane along with the inputs of the vehicle as a function of time.

4.4.2 Tracking 3D Dubins Trajectory

The same Dubin curve used in the previous simulation is used again. Fig. 4.28 shows the tracking of the Dubin curve in the presence of a constant force field in the x, y, and z directions of the global frame {U}, where $\delta D = [-110N, -80N, -110N]^T$. The disturbance starts 15 seconds after the beginning of the simulation. As observed in Fig. 4.28, the vehicle converge to the desired path with small errors that occur upon the transition between the five portions of the 3D Dubin curve (constant pitch helix, variable pitch helix, straight line, variable pitch helix, and constant pitch helix). These errors can also be observed in Fig. 4.29 which
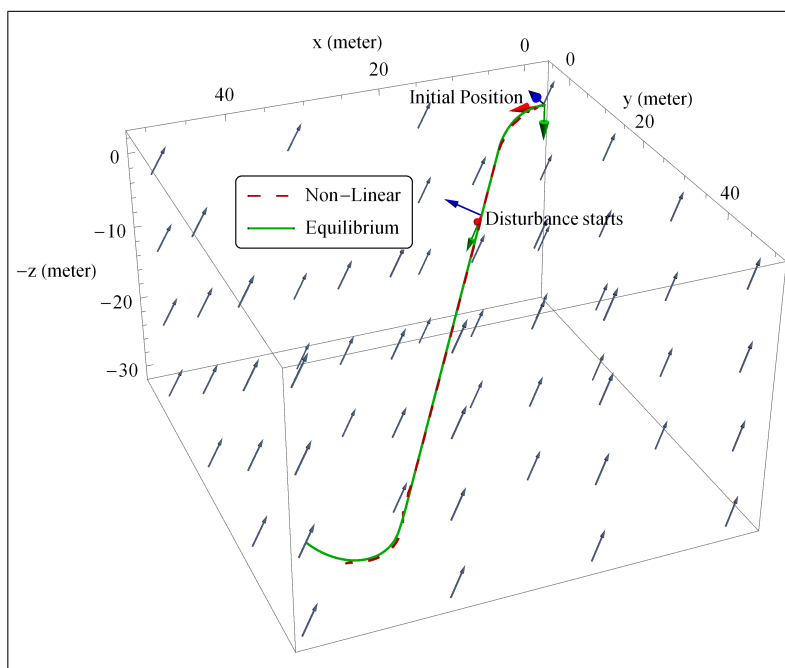

Figure 4.28: Dubin Trajectory tracking in the presence of underwater current in the x, y, and z directions with respect to the global frame {U}
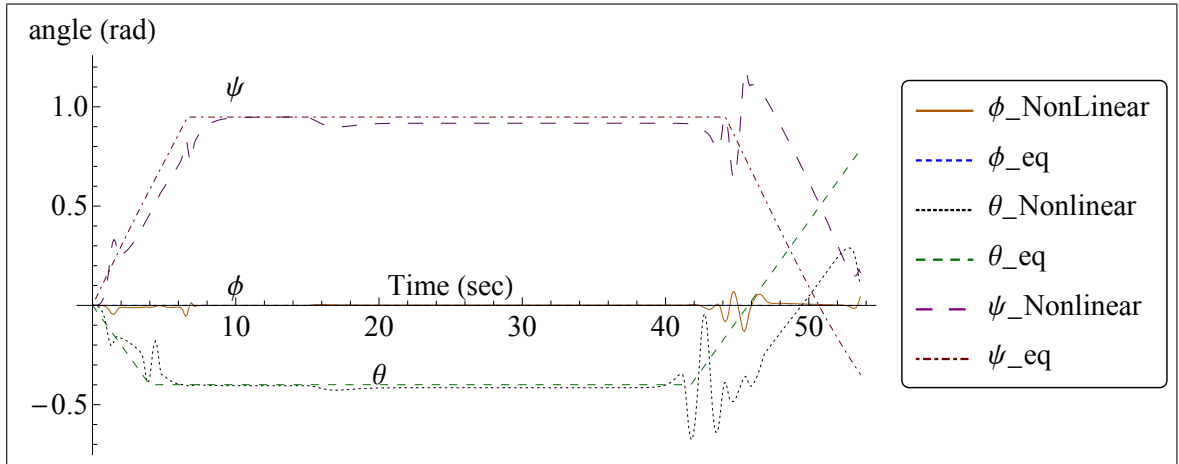
Figure 4.29: Equilibrium and actual Euler angles for Dubin trajectory tracking with constant disturbance in the x, y, and z directions with respect to the global frame {U}
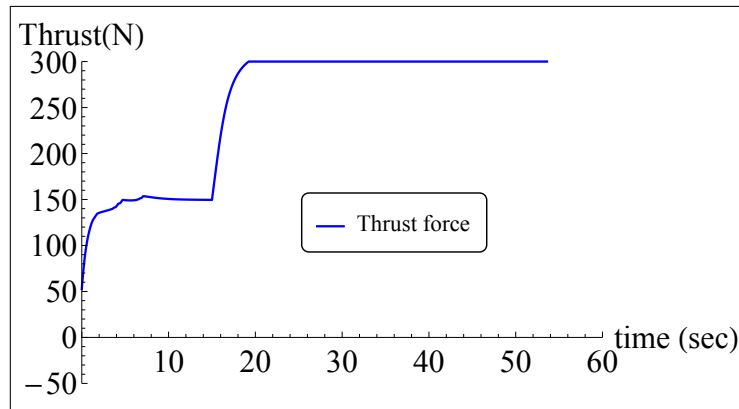

Figure 4.30: Thrust force for Dubin trajectory tracking with constant disturbance in the x, y, and z directions with respect to the global frame {U}

represents the actual and the desired Euler angles. After the vehicle deviates from the equilibrium trajectory it converges again after few seconds. This deviation occurs because the instant transition between the portions of the 3D Dubin curve requires infinite control signal for the fins, which is impossible to achieve. The control signals are presented in Fig. 4.30, 4.31, and 4.32 which correspond to the thrust force, stern angles, and the rudder angle, respectively. In order to prevent the control inputs from going to unrealistic values, saturation limits are imposed on the input signals. When the disturbance is applied the actual Euler angles deviates from the desired values, and keep a small offset from the desired values,
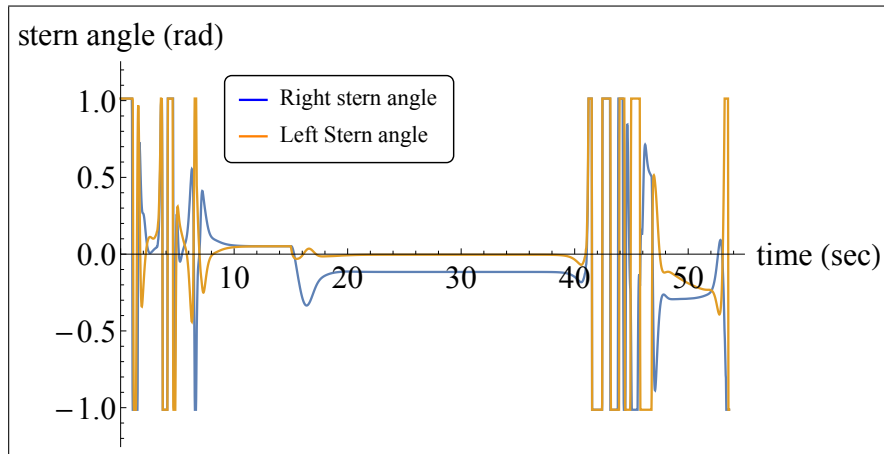
67

Figure 4.31: Stern angles for Dubin trajectory tracking with constant disturbance in the x, y, and z directions with respect to the global frame $\{U\}$
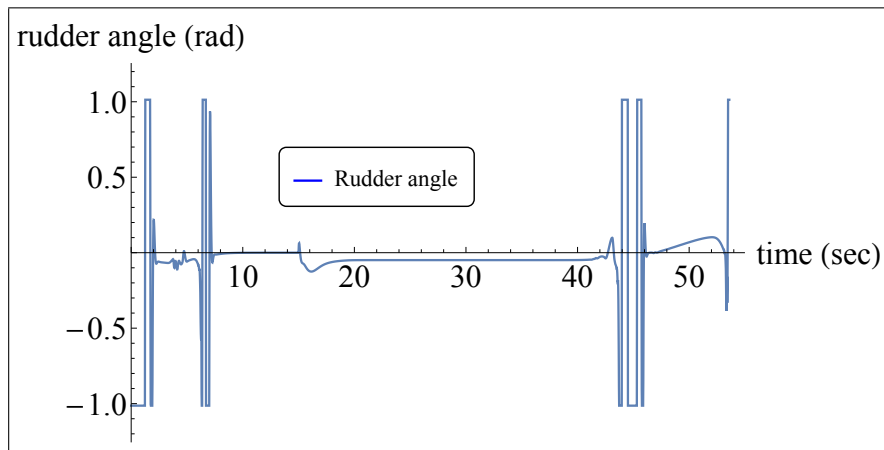
Figure 4.32: Rudder angle for Dubin trajectory tracking with constant disturbance in the x, y, and z directions with respect to the global frame $\{U\}$

also upon the transition from one portion of the Dubin curve to the other, the actual Euler angles deviates more and the desired angles and the offset increases. In Fig. 4.28 the vehicle does not reach the final destination and orientation at the end of simulation, which is because when the vehicle crosses the straight line portion to the variable pitch helix portion of the Dubin curve, it deviates from the desired path and spends some time trying to converge, which creates a delay in the tracking. This delay is depicted in Fig. 4.29, where the actual pitch and yaw angles, after 44 seconds from the beginning of the simulation, have a certain offset from their desired values, which creates a delay in the tracking performance.

68

4.4.3 Saw-tooth trajectory

The saw tooth trajectory corresponds to the gliding mode, and the same trajectory used in the previous section is used again. Fig. 4.33 shows the tracking of the saw-tooth trajectory, that corresponds to the gliding mode, in the presence of a constant force field in the y-direction of the global frame {U}, where $\delta D = [0, 25N, 0]^T$. Fig. 4.34 shows the trajectory tracking of the saw-tooth trajectory in the diving plane. As observed from both figures, when the disturbance is applied, the vehicle starts a sequence of deviating then converging to the desired trajectory, where the disturbance pushes the vehicle away from the desired trajectory, which causes the propeller to be turned on, as shown in Fig. 4.37, in order to correct the vehicle to the desired track. When the vehicle converges to the desired trajectory, the vehicle turns off the propeller and continue with the gliding mode. However after the propeller is turned off, the current pushes the vehicle away from the track, then the propeller turns on again in order to counter the disturbance.

Figure 4.33: Saw-Tooth Trajectory tracking in the presence of underwater current in the y-directions with respect to the global frame {U}

Figure 4.34: Saw-Tooth Trajectory tracking (Diving Plane) in the presence of underwater current in the y-directions with respect to the global frame {U}

69

Figure 4.35: Equilibrium and actual Euler angles for saw-tooth trajectory tracking with constant disturbance in the y-directions with respect to the global frame $\{U\}$
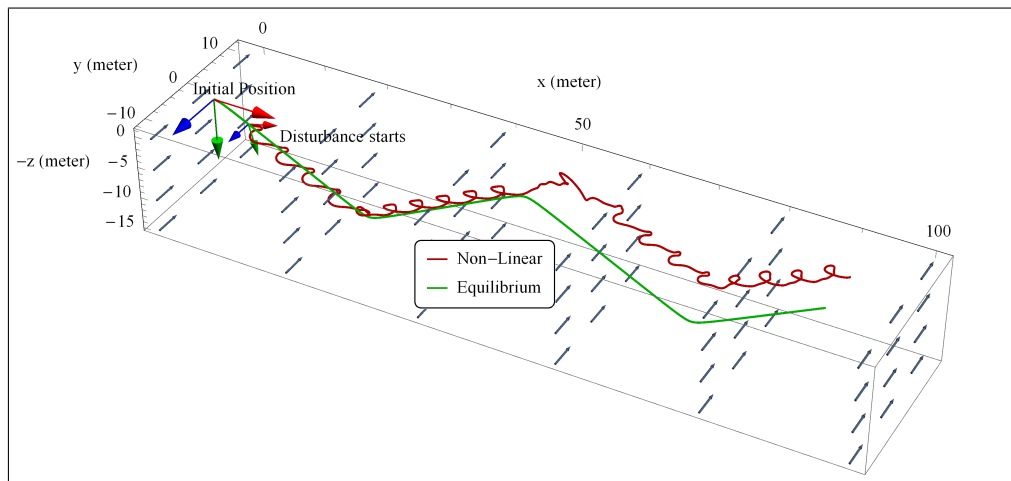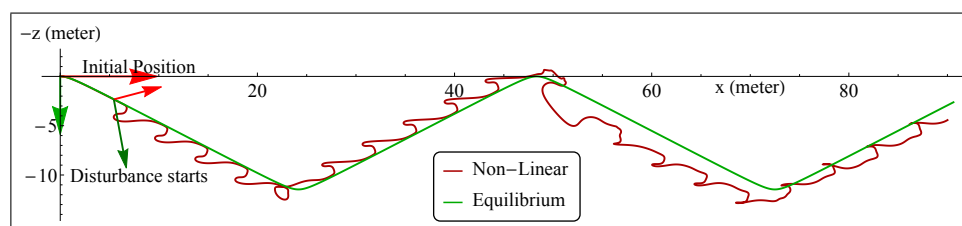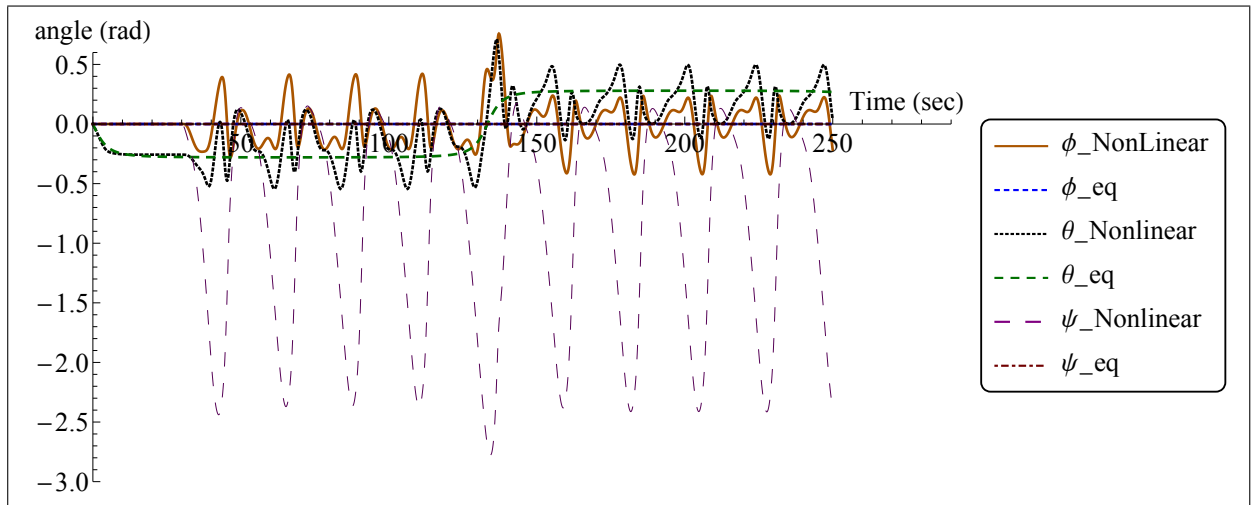

Figure 4.36: Mass of the vehicle (Saw-tooth trajectory tracking with constant disturbance in the y-direction with respect to the global frame $\{U\}$)

This sequence is continued until the vehicle crosses the first curved tip of the saw-tooth trajectory, where an offset between the vehicle and the desired trajectory is observed and the vehicle begins to converge to an offsetted trajectory. Fig. 4.35 shows the actual and the desired Euler angles, as observed in the figure, the controller gave unsatisfactory results in the presence of small disturbance ($25N$) for the gliding mode. The Euler angles shown in Fig. 4.35 are for the first 250 *sec*. Fig. 4.36 presents the mass of the vehicle as a function of time. The stern angles shown in Fig. 4.38 fluctuates in very rapidly between the saturation limits, in order to maintain the desired pitch and roll angles. The rudder angle shown in

70
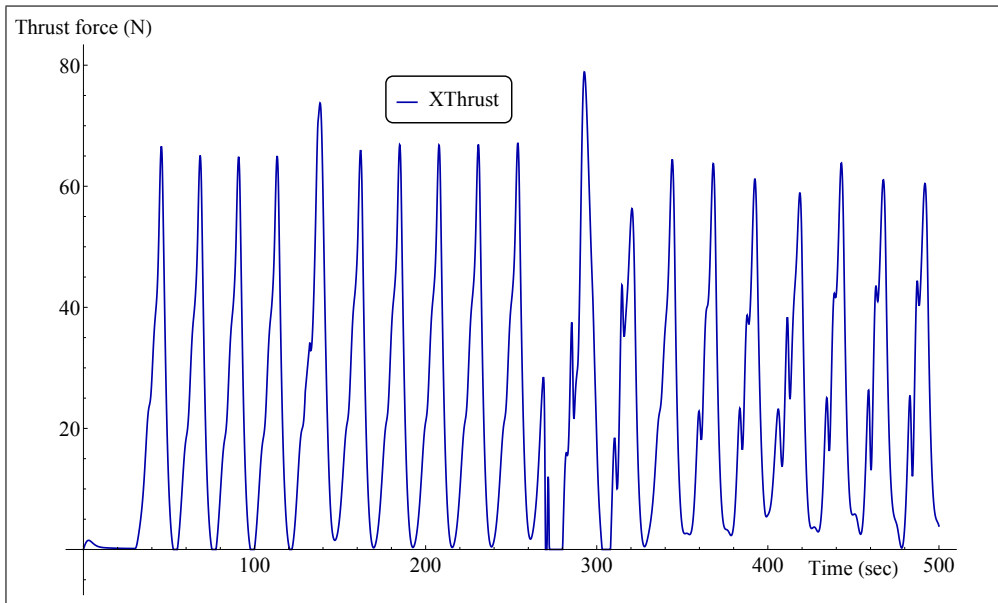
Figure 4.37: Thrust force (Saw-tooth trajectory tracking with constant disturbance in the y-direction with respect to the global frame $\{U\}$)
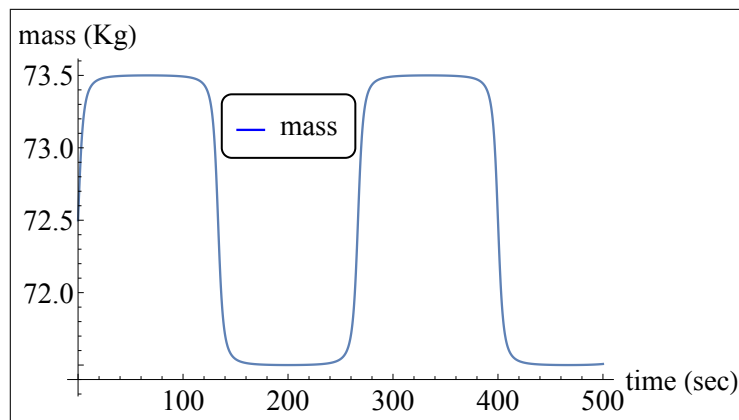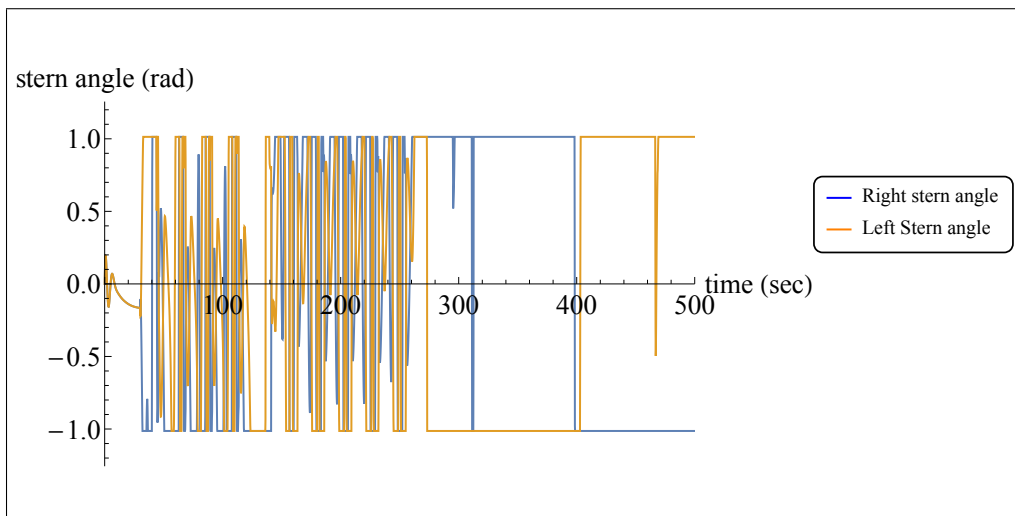

Figure 4.38: Stern angles (Saw-tooth trajectory tracking with constant disturbance in the y-direction with respect to the global frame $\{U\}$)

Fig. 4.39 saturates when the vehicle deviates from the desired trajectory and the propeller is turned on, in order to control the vehicle to converge to the desired trajectory.

71
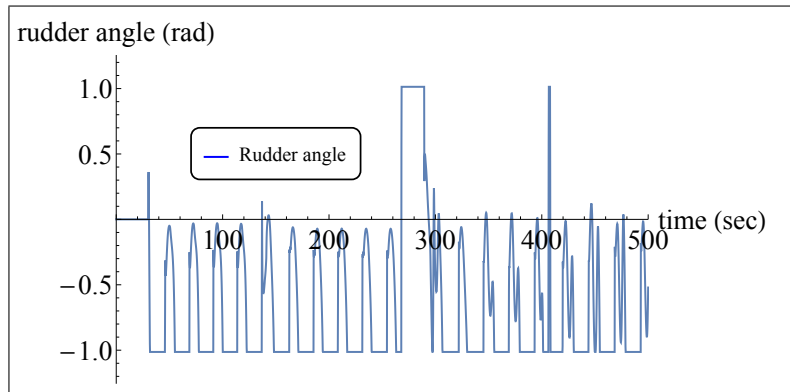
Figure 4.39: Rudder angle (Saw-tooth trajectory tracking with constant disturbance in the y-direction with respect to the global frame {U})

The above results show that designed LQR can be considered robust enough in the presence of underwater currents in the case of the thrust mode only. However, it is shown that the designed LQR has a poor performance in the presence of small disturbance ($25\ N$) when the vehicle is operating in the gliding mode.

Chapter 5

Disturbance Observer (Gliding Mode)

In this chapter, a disturbance observer is designed in order to enhance the robustness of the LQR in the presence of disturbance when the vehicle is operating in the gliding mode.

5.1 Observer Design

Consider the linear time variant state space model in (3.18) with the disturbance vector from (3.1):

$$\dot{\tilde{\chi}}(t) = A(t)\tilde{\chi}(t) + B(t)\tilde{U}(t) + \Delta d$$

$$Y = C\chi$$

$$Where \quad \Delta d = \begin{bmatrix} \Delta d_x \\ \Delta d_y \\ \Delta d_z \\ \Delta d_k \\ \Delta d_m \\ \Delta d_n \\ 0_{6\times1} \end{bmatrix} \tag{5.1}$$

The idea behind the disturbance observer, is to model the disturbance as an unknown states to be estimated. In other words, the state space model in (5.1) is augmented by including the disturbance vector Δd in the states space vector χ. The augmented states space vector and the augmented state space model become

as follows:

$$Z = [\chi, \ \Delta d_x, \ \Delta d_y, \ \Delta d_z, \ \Delta d_k, \ \Delta d_m, \ \Delta d_n]^T,$$
$$\dot{Z} - \dot{Z}_{eq} = A_Z(t)(Z - Z_{eq}) + B_Z(t)(U - U_{eq}), \tag{5.2}$$
$$Y = C_Z Z,$$

where Z is the augmented state space vector of length 18. The matrices A_Z, B_Z, and C_Z are the augmented matrices of A, B, and C in (3.18), respectively. The augmented matrices can be written as follows:

$$A_Z = \left[\begin{array}{c|c} A_{12\times12} & I_{6\times6} \\ 0_{6\times12} & 0_{12\times6} \end{array} \right], \qquad B_Z = \left[\begin{array}{c} B_{12\times4} \\ 0_{6\times4} \end{array} \right], \tag{5.3}$$

$$C_Z = \left[C_{12\times12}, \ 0_{12\times6} \right].$$

The observability matrix of the augmented state space model in (5.2) is full rank and the system is observable. So, the unknown states, which represent the disturbance, can be estimated. Before designing the controller using the method described in chapter 5, a state observer must be designed in order to estimate the states that can not be measured. The augmented state space model with states observer (Luenberger observer) can be written as follows:

$$\dot{\hat{Z}} - \dot{Z}_{eq} = A_Z(t)(\hat{Z} - Z_{eq}) + B_Z(t)(U - U_{eq}) + L(t)(CZ - C\hat{Z}) \tag{5.4}$$

where $\hat{Z}$ denote the estimated states, and L is an 18×12 matrix that contains the observer gains which is time variant. The observer gain matrix is chosen such that the error between the actual and the measured states

$$e_{est} = Z - \hat{Z} \tag{5.5}$$

is minimum, so the derivative of the error in (5.5) should be driven to zero:

$$\begin{aligned} \dot{e}_{est} &= \dot{Z} - \dot{\hat{Z}} \\ &= A_Z(t)Z + B_Z(t)U - A_Z(t)\hat{Z} - B_Z(t)U - L(t)\big(CZ - C\hat{Z}\big) \\ &= \big(A_Z(t) - LC\big)\big(Z - \hat{Z}\big) \end{aligned} \tag{5.6}$$

The observer gain can be chosen by pole placement, such that the Eigen values of the closed loop observer matrix $A_{co} = \big(A_Z(t) - LC\big)$ are at least 5 times faster than Eige values of the closed loop controller matrix $A_{cc} = \big(A_Z - B_Z K\big)$. In this work, the observer matrix L is be found in an optimal method, in a similar way

as the controller gains were calculated in chapter 5. The observer matrix can be calculated as follows:

$$L(t) = P_Z(t)C_Z^T R_Z^- 1,$$ (5.7)

where C_Z is the observer matrix in (5.3), R_Z is a 12×12 weighing matrix, and P_Z is a 12×12 matrix which can be solved for by solving the following algebraic differential equation:

$$A_Z(t)P_Z(t) + P_Z(t)A(t)^T + Q_Z - P_Z(t)C_Z^T R_Z^{-1} C_Z P_Z(t) = -\dot{P}_Z(t) ,$$ (5.8)

where Q_Z is an 18×18 weighing matrix. For more details about state observer design refer to [**?**]. Now that the state observer is designed, a LQR is designed based on the augmented state space model in(5.2) and (5.4) and the control law is written as follows:

$$U = -K_Z(t)\big(\hat{Z} - Z_{eq}\big),$$ (5.9)

where K_Z is the control gain matrix of size 4×18 that corresponds to the augmented model, it can be calculated as explained in chapter 5.

5.2   Simulation

The designed observer and the designed control law are applied to the actual 6DOF nonlinear model with the unknown disturbance in (3.1). The same saw-tooth trajectory that corresponds to the gliding mode is used again. Fig. 5.1 shows the tracking of the saw-tooth trajectory, where same disturbance as in the simulation in chapter 6 is applied ($deltaD = [0, 25N, 0]^T$). Fig. 5.2 shows the trajectory tracking of the saw-tooth trajectory in the diving plane. As observed from both figures, the tracking performance is improved versus the case where no disturbance observer is used, Fig. 4.33 and 4.34. Also, it is observed that no offset from the desired trajectory occurs after crossing the curved tips of the saw-tooth trajectory. However, the same effect as before still occurs after applying the disturbance observer, which is the continuous deviation and conversion from and to the desired trajectory, where the current pushes the vehicle away from the desired trajectory, which causes the propeller to be turned on, as shown in Fig. 5.4, in order to correct the vehicle to the desired track. When the vehicle converges to the desired trajectory, the vehicle turns off the propeller and continues with the gliding mode. However after the propeller is turned off, the current pushes the vehicle away from the track, then the propeller turns on again in order to counter the disturbance. It is noticed that when applying the disturbance observer more thrust force is used, Fig. 5.4, than without disturbance observer,
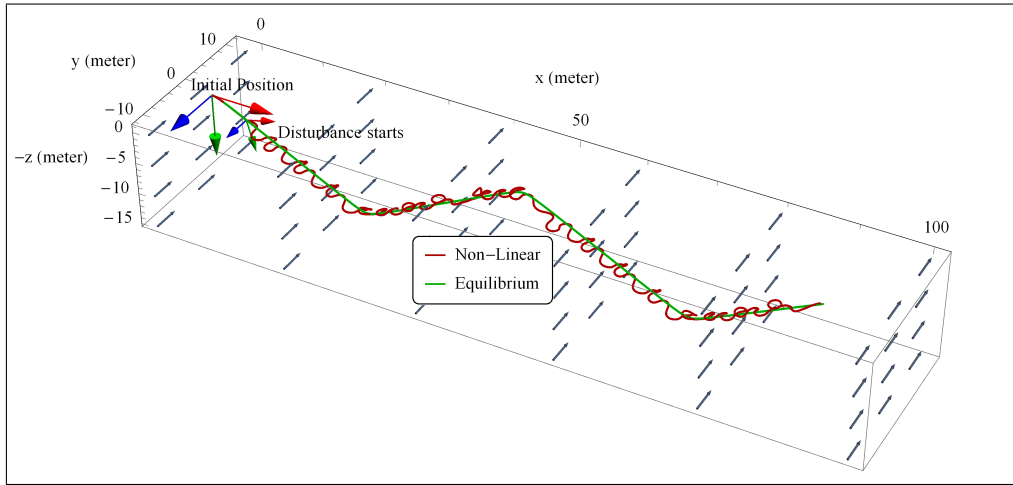
Figure 5.1: Saw-Tooth Trajectory tracking in the presence of underwater current in the y-directions with respect to the global frame {U} with disturbance observer
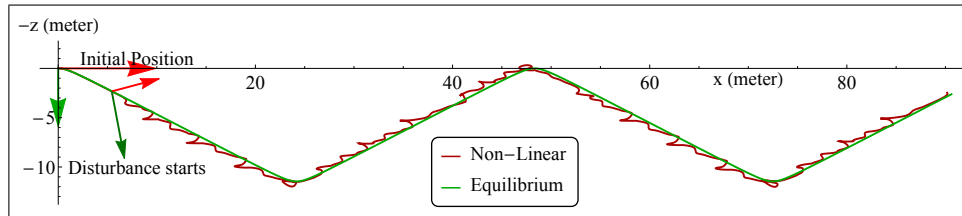

Figure 5.2: Saw-Tooth Trajectory tracking (Diving Plane) in the presence of underwater current in the y-directions with respect to the global frame {U} with disturbance observer

Fig. 4.37. Fig. 5.3 shows the actual and the desired Euler angles, in comparison with the case where observer was not applied, Fig. 4.35, it is shown that applying disturbance observer enhances the results, however the tracking performance is still unsatisfactory in the presence of small disturbance ($25N$) for the gliding mode, as the fluctuation between converging and diverging from the trajectory still exists. The stern angles shown in Fig. 5.5 fluctuates rapidly between the saturation limits, in order to maintain the desired pitch and roll angles. The rudder angle shown in Fig. 5.6 saturates when the vehicle deviates from the desired trajectory and the propeller is turned on, in order to control the vehicle to converge to the desired trajectory.
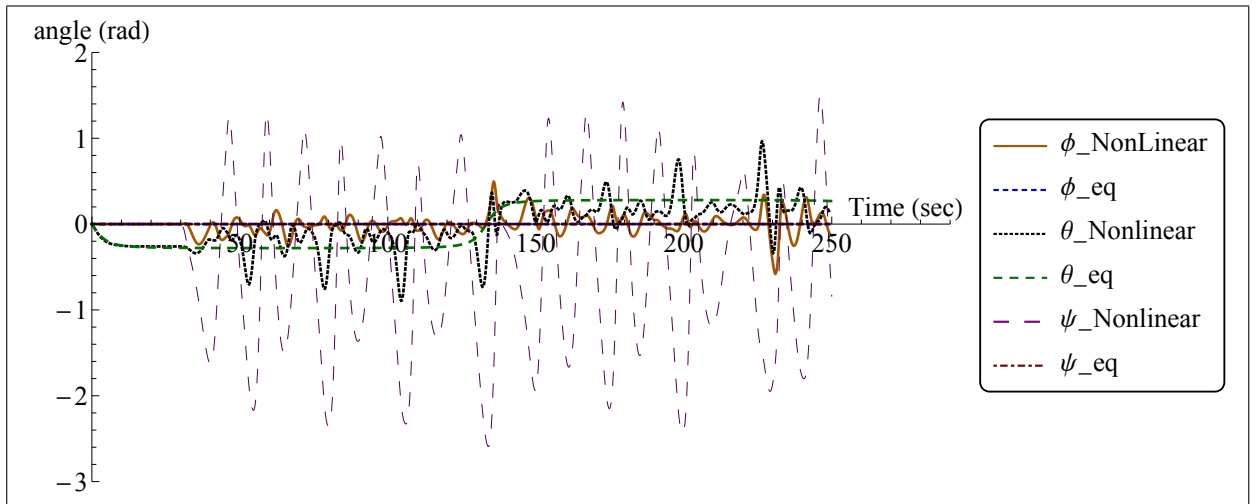
Figure 5.3: Equilibrium and actual Euler angles for saw-tooth trajectory tracking with constant disturbance in the y-directions with respect to the global frame {U} with disturbance observer

Figure 5.4: Thrust force (Saw-tooth trajectory tracking with constant disturbance in the y-direction with respect to the global frame {U} with disturbance observer

Figure 5.5: Stern angles (Saw-tooth trajectory tracking with constant disturbance in the y-direction with respect to the global frame {U} with disturbance observer

Figure 5.6: Rudder angle (Saw-tooth trajectory tracking with constant disturbance in the y-direction with respect to the global frame {U} with disturbance observer
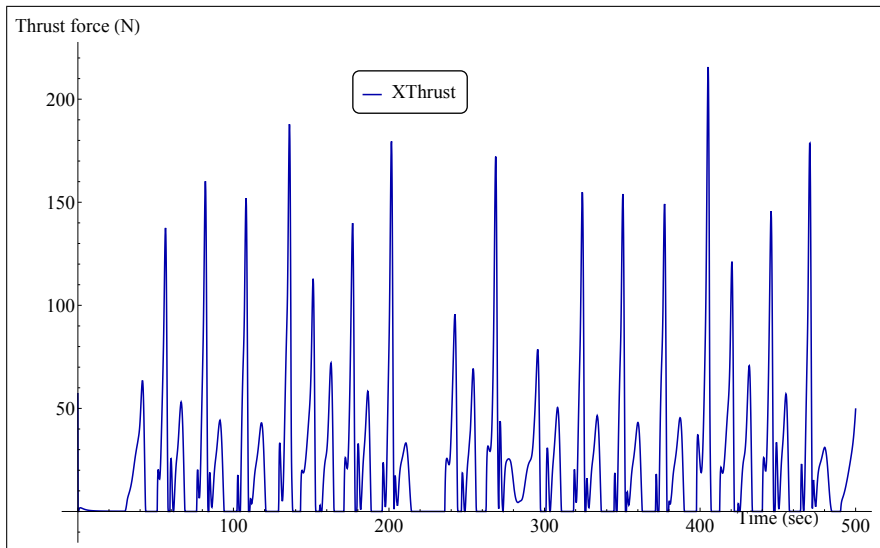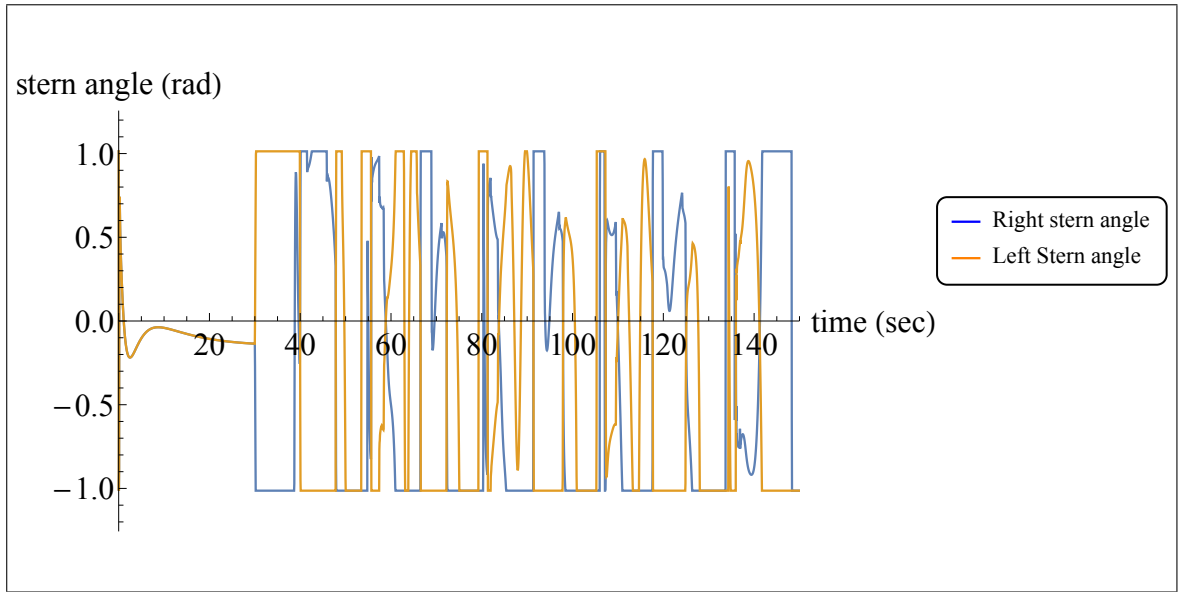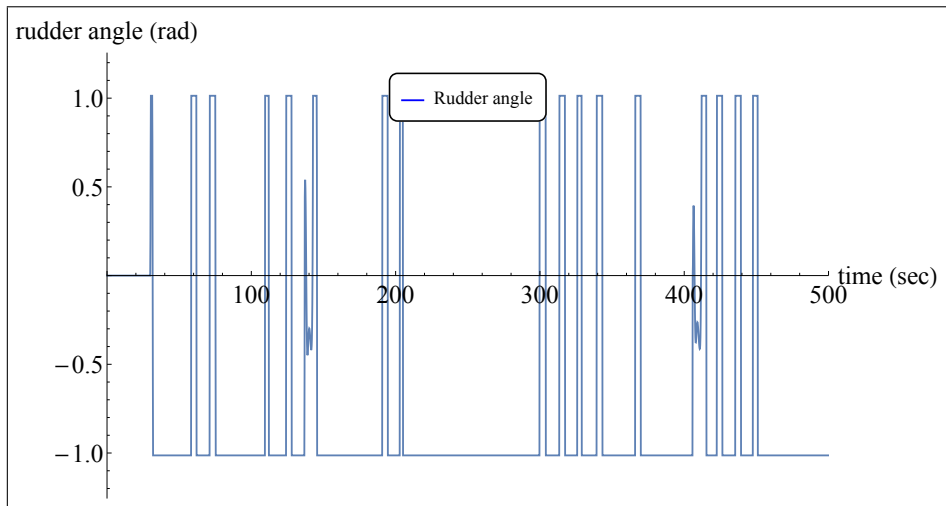
78

Chapter 6

Conclusion

In this work, a 6DOF dynamics and kinematics model of a H-AUV is derived and simulated. The control design for the trajectory tracking problem is simplified by linearizing the 6DOF dynamics and kinematics model of the H-AUV about a given optimal 3D trajectory. A feedback LQR control law, which includes multiple inputs, is designed based on the linearized model and applied to the nonlinear model. The designed controller is able to decide autonomously which mode of operation to use depending on the type of trajectory. The closed loop nonlinear system is simulated to track basic trajectory maneuvers: helix and 3D Dubin's curve for the thrust mode, and saw-tooth trajectory for the gliding mode. The linear feedback controller shows satisfactory results when applied to the nonlinear model. The robustness of the designed controller is investigated by injecting an unknown disturbance to the nonlinear model. Simulation shows satisfactory tracking performance in the presence of disturbance for the thrust mode. However, the tracking performance in gliding mode was poor. A disturbance observer is designed and applied to the nonlinear model in order to enhance the tracking performance in gliding mode. Although the tracking performance of the controller is improved.

In the future work, the control law need to be enhanced to give better tracking performance for the gliding mode in the presence of disturbance. Also in this work, the dynamics of the propeller and the fins were not included, so in the future the dynamics of the actuators should be included. And finally, test the controller on the actual prototype when it is complete.

Bibliography

[1] J. N. Newman, *Marine hydrodynamics*. MIT press, 1977.

[2] R. D. Blevins, *Formulas for natural frequency and mode shape*. Van Nostrand Reinhold Co., 1979.

[3] T. T. J. Prestero, *Verification of a six-degree of freedom simulation model for the REMUS autonomous underwater vehicle*. PhD thesis, Massachusetts institute of technology, 2001.

[4] D. R. Yoerger, M. Jakuba, A. M. Bradley, and B. Bingham, "Techniques for deep sea near bottom survey using an autonomous underwater vehicle," *The International Journal of Robotics Research*, vol. 26, no. 1, pp. 41–54, 2007.

[5] P. E. Hagen, N. Størkersen, B.-E. Marthinsen, G. Sten, and K. Vest-gård, "Rapid environmental assessment with autonomous underwater vehiclesâĂŤexamples from hugin operations," *Journal of Marine Systems*, vol. 69, no. 1, pp. 137–145, 2008.

[6] B.-H. Jun, J.-Y. Park, F.-Y. Lee, P.-M. Lee, C.-M. Lee, K. Kim, Y.-K. Lim, and J.-H. Oh, "Development of the auv 'isimi' and a free running test in an ocean engineering basin," *Ocean engineering*, vol. 36, no. 1, pp. 2–14, 2009.

[7] A. Alvarez, "Redesigning the slocum glider for torpedo tube launching," *IEEE Journal of Oceanic Engineering*, vol. 35, no. 4, pp. 984–991, 2010.

[8] D. C. Webb, P. J. Simonetti, and C. P. Jones, "Slocum: An underwater glider propelled by environmental energy," *IEEE Journal of Oceanic Engineering*, vol. 26, no. 4, pp. 447–452, 2001.

[9] C. C. Eriksen, T. J. Osse, R. D. Light, T. Wen, T. W. Lehman, P. L. Sabin, J. W. Ballard, and A. M. Chiodi, "Seaglider: A long-range autonomous underwater vehicle for oceanographic research," *IEEE Journal of oceanic Engineering*, vol. 26, no. 4, pp. 424–436, 2001.

[10] J. Sherman, R. E. Davis, W. Owens, and J. Valdes, "The autonomous underwater glider" spray"," *IEEE Journal of oceanic Engineering*, vol. 26, no. 4, pp. 437–446, 2001.

[11] W. P. Barker, *An Analysis of Undersea Glider Architectures and an Assessment of Undersea Glider Integration into Undersea Applications*. PhD thesis, Monterey, California. Naval Postgraduate School, 2012.

[12] A. J. Healey and D. Lienard, "Multivariable sliding mode control for autonomous diving and steering of unmanned underwater vehicles," *Oceanic Engineering, IEEE Journal of*, vol. 18, no. 3, pp. 327–339, 1993.

[13] D. Fryxell, "Modeling, identification, guidance and control of an autonomous underwater vehicle," *Master's thesis. Department of Electrical Engineering, Instituto Superior Tecnico. Lisboa, Portugal*, 1994.

[14] C. Samson, "Path following and time-varying feedback stabilization of a wheeled mobile robot," in *Proceedings of ICARV*, pp. RO–13.1, 1992.

[15] P. Encarnaçao, A. Pascoal, and M. Arcak, "Path following for marine vehicles in the presence of unknown currents," in *Proceedings of SYROCO*, vol. 2, pp. 469–474, 2000.

[16] P. Encarnacao and A. Pascoal, "3d path following for autonomous underwater vehicle," in *Decision and Control, 2000. Proceedings of the 39th IEEE Conference on*, vol. 3, pp. 2977–2982 vol.3, 2000.

[17] G. Casalino, M. Aicardi, A. Bicchi, and A. Balestrino, "Closed loop steering and path following for unicycle-like vehicles: a simple lyapunov function based approach," *IEEE Robotics and Automation Magazine*, vol. 2, no. 1, pp. 27–35, 1995.

[18] M. Aicardi, G. Casalino, G. Indiveri, A. Aguiar, P. Encarnaçao, and A. Pascoal, "A planar path following controller for underactuated marine vehicles," in *Ninth IEEE Mediterranean Conference on Control and Automation, Dubrovnik, Croatia*, 2001.

[19] L. Lapierre and D. Soetanto, "Nonlinear path-following control of an auv," *Ocean engineering*, vol. 34, no. 11, pp. 1734–1744, 2007.

[20] T. I. Fossen, *Handbook of marine craft hydrodynamics and motion control*. John Wiley & Sons, 2011.

[21] A. W. Divelbiss and J. T. Wen, "Trajectory tracking control of a car-trailer system," *IEEE Transactions on Control Systems Technology*, vol. 5, no. 3, pp. 269–278, 1997.

[22] M. G. Joo and Z. Qu, "An autonomous underwater vehicle as an underwater glider and its depth control," *International Journal of Control, Automation and Systems*, vol. 13, no. 5, pp. 1212–1220, 2015.

[23] B. Wehbe, E. Shammas, and D. Asmar, "A novel method to generate three-dimensional paths for vehicles with bounded pitch and yaw," in *Advanced Intelligent Mechatronics (AIM), 2015 IEEE International Conference on*, pp. 1701–1706, IEEE, 2015.

[24] B. Wehbe, E. Shammas, J. Zeaiter, and D. Asmar, "Dynamic modeling and path planning of a hybrid autonomous underwater vehicle," in *Robotics and Biomimetics (ROBIO), 2014 IEEE International Conference on*, pp. 729–734, IEEE, 2014.

[25] E. SNAM, "Nomenclature for treating the motion of a submerged body through a fluid jr," *New York: Technical and Research Bulletin*, pp. 1–5, 1952.

[26] T. I. Fossen, *Guidance and control of ocean vehicles*. John Wiley & Sons Inc, 1994.

[27] S. F. Hoerner and H. V. Borst, *Fluid-dynamic lift: practical information on aerodynamic and hydrodynamic lift*. Hoerner Fluid Dynamics Brick Town, NJ, 1985.

[28] T. Prestero, *Verification of a Six-Degree of Freedom Simulation Model for the REMUS Autonomous Underwater Vehicle*. PhD thesis, Massachusetts Institute of Technology and Woods Hole Oceanographic Institution, 2001.

[29] M. S. Triantafyllou, "Maneuvering and control of surface and underwater vehicles," 2004.

[30] E. V. Lewis, *Principles of naval architecture*. Society of Naval Architects and Marine Engineers, 1988.

[31] L. F. Whicker and L. F. Fehlner, "Free-stream characteristics of a family of low-aspect-ratio, all-movable control surfaces for application to ship design," tech. rep., DTIC Document, 1958.

[32] M. W. Spong, S. Hutchinson, and M. Vidyasagar, *Robot modeling and control*. John Wiley & Sons, 2006.

[33] M. P. Do Carmo and M. P. Do Carmo, *Differential geometry of curves and surfaces*, vol. 2. Prentice-hall Englewood Cliffs, 1976.

[34] M. C. de Oliveira, *Fundamentals of Linear Control.* preprint, 2015, http://control.ucsd.edu/mauricio/.